Université catholique de Louvain
École polytechnique de Louvain (EPL)

Stochastic geometry-based analysis of wireless device-to-device networks

Dissertation presented by
Simon Demey

for obtaining the Master's degree in
Electrical Engineering

Supervisors
Claude Oestges, Luc Vandendorpe

Readers
Jérôme Louveaux, Charles Wiame

Academic year 2017-2018

Aknowledgements

The completion of this document could not have been possible without the assistance and advice of several people.

First, I express my deepest appreciation to my supervisors, Prof. Claude Oestges and Prof. Luc Vandendorpe for their valuable suggestions, their expertise and their availability all along the academic year.

Then, a debt of gratitude is owed to Mr. Charles Wiame for supporting me as friend, for guiding me and for giving me such thoughtful feedback.

I also would like to thank Prof. Jérôme Louveaux for accepting to read this document and for devoting time to assess my work.

Last but not least, I would like to thank my friends for encouraging me and my family for their unceasing support.

Abstract

The main objective of this master thesis is to set up analytical models enabling to evaluate the evolution in terms of perfomance of conventional cellular networks after the integration of promising technologies. Therefore, device-to-device communications as well as energy harvesting-aided device-to-device communications are consecutively analyzed. The proposed approach is based on mathematical expressions derived from the stochastic geometry theory. The presented model mainly focusses on underlaid device-to-device communications and gives indications to carefully choose between the uplink and downlink band. A new and more general mathematical framework accounting for strong line-of-sight components is also established using Rician fading. Based on that model, the limits of stochastic geometry are demonstrated. Finally, the replacement of conventional batteries by rechargeable batteries powered using microwave power transfer at the device-to-device user is studied.

L'objectif principal de ce travail de fin d'études est de mettre en place des modèles analytiques permettant d'évaluer l'évolution de la performance des réseaux cellulaires conventionnels après l'intégration de plusieurs nouvelles technologies. Pour ce faire, les communications dispositif à dispositif ainsi que les communications dispositif à dispositif alimentées par collecte de la puissance environnante sont consécutivement analysées. La méthode proposée est fondée sur des expressions mathématiques basées sur la géométrie stochastique. Le modèle présenté se focalise principalement sur les communications dispositif à dispositif réutilisant les fréquences normalement dédiées aux communications cellulaires. Grâce à celui-ci, des indications concernant le choix de la bande de fréquence sont révélées. Un nouveau cadre mathématique est également établi pour plus fidèlement modéliser une forte composante en ligne directe à la réception du signal. Pour ce faire, une distribution dite de Rice a été utilisée. A travers l'étude proposée, les limites de la géométrie stochastique en terme de complexité mathématique et de temps d'exécution du programme ont été démontrées. Finalement, le remplacement des batteries conventionnelles par des batteries rechargeables au niveau de l'émetteur impliqué dans le lien dispositif à dispositif est étudié. Ces batteries sont rechargées à l'aide d'une technologie de tranfert de puissance basée sur les micro-ondes.

Contents

Aknowledgements **i**

Abstract **ii**

Nomenclature **v**

1 Introduction **1**

2 State of Art **3**
2.1 Basics of stochastic geometry . . . 3
2.1.1 Point processes . . . 3
2.1.2 Model fundamentals . . . 6
2.2 Device-to-device communications . . . 9
2.2.1 Inband underlaying device-to-device communications . . . 10
2.2.2 Inband overlaying device-to-device communications . . . 12
2.2.3 Comparison of the underlaid and the overlaid scheme . . . 14
2.2.4 Outband device-to-device communications . . . 14
2.3 Energy harvesting and energy harvesting-aided device-to-device communications . . . 15

3 Inband underlaying device-to-device communications under Rician fading **17**
3.1 System model . . . 17
3.2 General computations . . . 19
3.3 Conventional cellular outage probability . . . 24
3.4 Integration of device-to-device communications . . . 25
3.4.1 Device-to-device outage probability . . . 27
3.4.2 Impact on the conventional cellular outage probability . . . 27
3.5 Numerical results . . . 27
3.5.1 Cellular outage probability without device-to-device communications . . . 29
3.5.2 Integration of device-to-device communications . . . 30
3.5.3 Performance dependencies on different parameters . . . 31
3.5.4 Further improvements and analyses of the studied network . . . 35
3.5.5 Computation time . . . 38
3.6 Model weaknesses . . . 39
3.6.1 Interferers fading model . . . 39
3.6.2 Mathematical complexity . . . 40
3.7 Chapter summary . . . 41

4 Energy harvesting-aided device-to-device communications **42**
4.1 System model . . . 43
4.1.1 Mathematical modifications . . . 43
4.1.2 Energy harvesting model . . . 44
4.1.3 Power harvesting from all power beacons . . . 45
4.1.4 Power harvesting from the nearest power beacon . . . 48
4.2 Numerical results . . . 51

4.2.1 Model validation . . . 51
4.2.2 Trade-off between the transmission probability and the maximum D2D link distance 54
4.2.3 Model innaccuracies . . . 57
4.3 Introduction to another strategy using energy harvesting . . . 58
4.4 Chapter summary . . . 58

5 Conclusions **59**
5.1 Summary of contributions . . . 59
5.2 Further research directions . . . 59
5.2.1 Analytical models . . . 59
5.2.2 Beyond the framework of this document . . . 60

Bibliography **61**

Nomenclature

Acronyms

Symbol	Description
ABG	Alpha-beta-gamma
AP	Access point
ASE	Area spectral efficiency
BPP	Binomial point process
BS	Base station
CC	Conventional cellular
CDF	Cumulative distribution function
CI	Close-in
D2D	Device-to-device
DL	Downlink
EH	Energy harvesting
FS	Free space
GZ	Guard zones
HPPP	Homogeneous poisson point process
IAR	Interference aware routine
ISM	Industrial, scientific and medical (radio bands)
LOS	Line-of-sight
LT	Laplace transform
MC	Monte-Carlo
MHCPP	Matérn Hard core point process
MIMO	Multiple inputs multiple outputs
MPT	Microwave power transfer
PB	Power beacon
PCPP	Poisson cluster point process
PDF	Probability density function

PGFL	Probability generating functional
PL	Path loss
PP	Point process
PPP	Poisson point process
RV	Random variable
RX	Receiver
SG	Stochastic geometry
SPR	Shortest path routine
TX	Transmitter
UE	User equipment
UL	Uplink

Special Functions

Symbol	Description	Definition
$(\cdot)_k$	Pochhammer symbol:	$(x)_k = x(x+1)\dots(x+k-1)$
$1_A(\cdot)$	Indicator function:	$1_A(x) = \begin{cases} 1 & \text{if x} \in \text{A} \\ 0 & \text{if x} \notin \text{A} \end{cases}$
$\binom{\cdot}{\cdot}$	Binomial coefficient:	$\binom{n}{k} = \frac{n!}{k!(n-k)!}$
$\Gamma(\cdot)$	Gamma function:	$\Gamma(z) = \int_0^\infty x^{z-1}e^{-x}dx$
$\Gamma(\cdot,\cdot)$	Upper incomplete gamma function:	$\Gamma(a,z) = \int_a^\infty x^{z-1}e^{-x}dx$
${}_2F_1(\cdot,\cdot;\cdot;\cdot)$	Hypergeometric function:	${}_2F_1(a,b;c;z) = \sum_{n=0}^{\infty} \frac{(a)_n(b)_n}{(c)_n}\frac{z^n}{n!}$
$\mathcal{L}_X(\cdot)$	Laplace transform:	$\mathcal{L}_X(s) = \mathbb{E}\left[e^{-sX}\right]$
$I_0(\cdot)$	Zeroth order modified Bessel function of the first kind:	$I_0(x) = \frac{1}{2\pi i}\oint \frac{1}{t}e^{\frac{x}{2}\frac{t+1}{t}}dt$
$sinc(\cdot)$	Cardinal sine:	$sinc(x) = \frac{sin(x)}{x}$

Posed Functions

Symbol	Definition
$\mathcal{A}_{jk}$	$\frac{K^k}{(k!)^2}e^{-K}j!\binom{k}{j}$
$\mathcal{B}(\text{int})$	$\pi\Lambda_{int}\sqrt{P_{\text{int}}\lambda}$
$\mathcal{C}(\text{int})$	$\frac{1}{\sqrt{P_{\text{int}}\lambda}}$
$\mathcal{D}_{iljk}(\text{int},\text{link})$	$\mathcal{A}_{jk}(-1)^{k-j+i}\frac{\left(-\pi\Lambda_{\text{int}}\sqrt{\lambda P_{\text{int}}}\arctan\left(\sqrt{\frac{\xi(K+1)P_{\text{int}}}{P_{\text{link}}}}\right)\right)^i}{i!(l-i)!}\left(\frac{\xi(K+1)}{\lambda P_{\text{link}}}\right)^{\frac{i}{2}+k-j}$
$\mathcal{E}(\text{int},\text{link})$	$\Lambda_{\text{int}}\sqrt{\frac{\xi(K+1)P_{\text{int}}}{P_{\text{link}}}}\arctan\left(\sqrt{\frac{\xi(K+1)P_{\text{int}}}{P_{\text{link}}}}\right)$
$\mathcal{F}_{li}(\text{int},\text{link},x,y,n)$	$\frac{\partial^n\left(-\mathcal{B}(\text{int})\sqrt{s}\arctan\left(\frac{\sqrt{s}}{\mathcal{C}(\text{int})r_{x,y}^2}\right)\right)^{l-i}}{\partial^n s}$ evaluated in $s = \frac{\xi(K+1)}{\lambda P_{\text{link}}}r_{x,y}^4$
$\mathcal{G}(\text{int})$	$\Lambda_{\text{int}}\pi\lambda^\delta P_{\text{int}}^\delta sinc^{-1}(\pi\delta)$
$\mathcal{H}_{iljk}(\text{link})$	$\mathcal{A}_{jk}(-1)^{k-j+i}\left(\frac{\xi(K+1)}{\lambda P_{\text{link}}}\right)^{\frac{l}{2}}(-\mathcal{G}(\text{int}))^l\frac{\left(1-\frac{i}{2}+\frac{l}{2}-(k-j)\right)_{k-j}}{i!(l-i)!}$
$\mathcal{I}_{iljk}(\text{int},\text{link},x,y)$	$\int_0^\infty \mathcal{F}_{li}(\text{int},\text{link},x,y,a)\exp\left(-\pi(\mathcal{E}(\text{int},\text{link})+\Lambda_b)r_{x,y}^2\right)r_{x,y}^{2i+4(k-j)+1}dr_{x,y}$
$\mathcal{J}_{i'l'ilpjk}(v,\text{int}_1,\text{int}_2)$	$\mathcal{A}_{jk}\binom{k-j}{p}(-1)^{k-j+i+i'}\frac{(-\mathcal{G}(\text{int}_1))^l\left(1-\frac{i}{2}+\frac{l}{2}-p\right)_p}{i!(l-i)!i'l'-i')!}\times \left(\frac{\xi(K+1)}{\lambda P_v}\right)^{k-j+\frac{l}{2}-p+\frac{i'}{2}}\left(-\pi\Lambda_{\text{int}_2}\arctan\left(\sqrt{\frac{\xi(K+1)P_{int_2}}{P_v}}\right)\right)^{i'}$
$\mathcal{K}(\alpha,\xi,\text{int},\text{link})$	$\int_{\left(\frac{\xi P_{\text{int}}}{P_{\text{link}}}\right)^{-\frac{2}{\alpha}}}^\infty \frac{\left(\frac{\xi P_{\text{int}}}{P_{\text{link}}}\right)^{\frac{2}{\alpha}}}{1+u^{\frac{\alpha}{2}}}du$

Variables

Symbol	Description
α	Path loss coefficient on D2D and CC communications
ϵ	RF-to-DC power conversion efficiency factor
γ	Path loss coefficient on power transfer links
$\gamma_{x,y}^{s}$	SINR on the s-link (s $\in$ {UL,DL,D2D}) between elements x and y
λ	frequency dependent pathloss
Λ_k	Density of the PPP of element k
Φ_k	PP of element k
ξ	SINR threshold
P_k	Transmit power of element k
R_g	Circular guard zone radius
$r_{x,y}$	distance between elements x and y
$\mathrm{g}_{x,y}$	fading power gain of the link between elements x and y
I	Interference
K	Rice K-factor
W	Noise power

Chapter 1

Introduction

Decades ago, the interest in modeling wireless networks started growing up and triggered the appearance of many questions in the scientific world. Ever since that moment, researchers have proposed from very simple to more complex models. Some of them were considered for a long time as close enough to the reality [SG4]:

- The Wyner model originally proposed by Aaron D. Wyner in [Misc71] whose accuracy has been contested in [Misc72].
- Grid-based models like the hexagonal grid depicted in Figure 1.1 that have been extensively used by the scientific community.

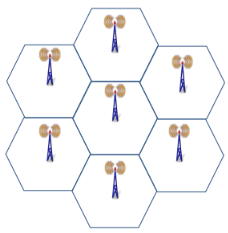

Figure 1.1: Hexagonal grid (Source: [SG4]).

However, those models fail to take into account the network topology by making too simple or idealistic assumptions. Besides the difficult analytical modeling, grid-based models, which were widely accepted to model large-scale wireless networks, are not anymore capturing the various aspects of nowadays networks especially with the arrival of multi-tier networks. Also, in some cases like ad hoc networks[1], the worst case scenario is generally assumed resulting in too restrictive conclusions. Finally, loads of simple models are considering the SNR as the metric of interest while the SINR, which is moreover geometry-dependent, become more important for analyzing current networks.

In order to tackle the problem of network geometry randomness, a simple way could be to try every single spatial realization for a complete analysis of the studied network. This approach, more commonly known as Monte Carlo (MC) simulation, is however time-consuming and lacks mathematical insight. For those reasons, MC simulations are generally avoided and used for validation instead.

This is where stochastic geometry (SG) jumped in as one of the most promising tools for the set up of closed-form expressions. This powerful tool enabled researchers to capture the randomness of emerging networks by averaging over all possible geometrical patterns and to define and compute macroscopic properties of large-scale networks. More precisely, SG relies on the principle of point process (PP) whose realization can represent base stations (BS) or user equipments (UE) locations in the Euclidian space. The ability to establish analytical models by means of SG makes it possible to highlight network performance

[1] An ad hoc network is an infrastructure-less network where two nodes can directly communicate with each other

dependencies on a few parameters, typically the PP densities. An introduction to basic concepts used in SG is proposed in Chapter 2.

Throughout this document, a particular interest will successively be dedicated to two promising topics: device-to-device (D2D) communications and energy harvesting (EH).

Chapter 3 focusses on the introduction of D2D communications into conventional cellular (CC) networks, a technology that has generated a lot of interest inside the scientific community during the last years. Its main goal is to meet today's increasing needs for local-area services and thus for short range services as depicted in Figure 1.2. In fact, it offers the possibility for higher throughputs (up to 1Gb/s), lower latencies, lower power consumptions and single hop links. In addition, it seems to be particularly interersting to handle poor coverage conditions as shown in Figure 1.3 and to serve as a backup solution in case of a congested cellular network [D2D14, D2D42, D2D47].
By resorting to this kind of technology, many challenges for an implementation in the real world arise like interference management, power allocation, ressource allocation, etc [D2D18]. In the particular case of underlaying inband D2D communications (explained in Chapter 2), a trade-off between CC and D2D communications has to be found. This problem will also be adressed in the Chapter 3. In addition, Rician fading will be assumed for the link of interest. This last assumption is the source of an increased mathematical complexity sometimes leading to non closed-form expressions and showing the limits of SG regarding the time consumption.

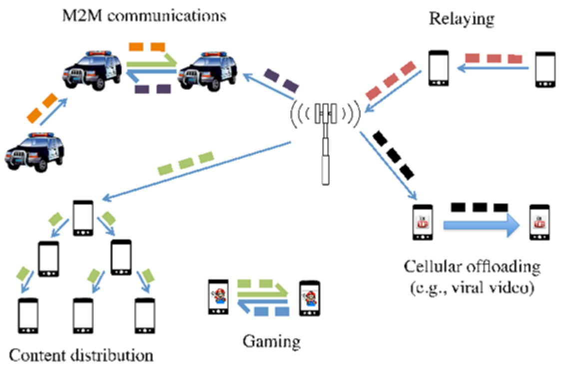

Figure 1.2: Different applications requiring D2D communications (Source: [D2D18]).

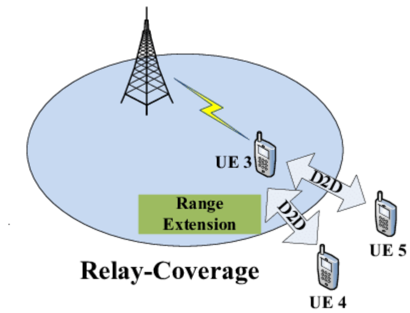

Figure 1.3: Extension of the coverage zone using D2D communications (Source: [D2D44]).

Chapter 4 studies the introduction of EH into the networks studied in Chapter 3. More specifically, energy harvesting-based D2D communications relying on idealistic infinite capacity batteries will be investigated. This principle of EH has drawn increasing interest in recent years especially for SWIPT (simultaneaous wireless information and power transfer) networks. In addition, the need for a battery is potentially eliminated for low-powered devices. As a consequence, the system reliability increases and severe inconvenience (financial loss, threats to health and public safety) due to dead batteries can be avoided [EH57].
In contrast to its harmfull impact on usual communications, interference is in the particular case of EH beneficial. Indeed, harvesters are able to extract power from their surrounding environment. However, this last observation often leads to a trade-off between the achievable information rate and the harvested power.
Wireless power transfer can rely on non-radiative technologies such as inductive coupling and magnetic resonance coupling as well as radiative technologies like microwave power transfer (MPT). Due to their extremely short transfer distances and their lack of support for mobility, the first two options will not be discussed in this document and our interest will be turned to the third technology. Thanks to a frequency carrier around 2.45GHz, MPT can be complemented by a sharp beamforming using only a small antenna array. Chapter 4 will moreover compare the addition of beamforming to the isotropic case.

Chapter 2

State of Art

This chapter is structured as follows: the basics of stochastic geometry are presented in section 2.1. The literature on the D2D communications and EH technologies is then respectively detailed in sections 2.2 and 2.3

2.1 Basics of stochastic geometry

Stochastic geometry is a mathematical discipline in which one studies the relations between geometry and probabilities theory (i.e. random spatial patterns). Interestingly, this tool was first used in fields like signal procesing, astronomy or even forestry before being used for modeling wireless networks.

One of the basic concepts of SG is the process of geometric elements in a fundamental space A. The main difference it has with the theory of random sets is the interest it has for processes with distribution that are invariant relative to certain operations acting on the fundamental A like rotation. In other words, as the network users are constantly moving and going through completely different environments, a good model should be able to represent any spatial configuration of the users at any given time. Given the number of successful publications already related to stochastic geometry-based analysis of wireless networks, this tool seems to have proven itself as an instrument tackling fruitfully the problem of network geometry randomness.
A general approach using SG often relies on the theory of point processes presented in Section 2.1.1. Most of the following results were based on articles [SG1],[SG3] and [SG5].

2.1.1 Point processes

As already mentioned, PPs are generally used to account for the random network geometry. They are essentially useful for the computation of certain geometry-dependent metrics like the coverage probability which is founded on the distribution of the SINR. This represents a non-negligible advance in modeling as the network topology was usually ignored either by *incorporating the distance path loss into the chanel fading (Wyner model) or by assuming a simple and deterministic spatial configuration (grid-based models)* [SG4].

Definition 2.1.1 (Point process)**.** A point process (PP) $\Phi = \{ \overline{X_i},\, i \in \mathbb{N}\}$ is a random collection of points in a measure space A.

In the framework of cellular networks, A is generally considered as $\mathbb{R}^d$ with d $\in \{1, 2, 3\}$ for an easy physical interpretation and mostly as $\mathbb{R}^2$. A PP can also be marked as every point of a realization can be given an additional label (e.g. the transmit power). Also, any realization of a PP generally comes together with a random counting measure like the following one:

Example (Random counting measure)**.**

$$\Psi : A \subset \mathbb{R}^d \to \mathbb{N} : \Psi(A) = \sum_{\overline{X_i} \in \Phi} 1_A(\overline{X_i})$$

where $1_A(\cdot)$ is the indicator function

The distribution of the random counting measure is clearly dependent on the PP Φ itself and its expectation is an alternative way to characterize the PP as it will be seen later in this section.
Another notion that needs to be defined is the notion of thinning.

Definition 2.1.2 (p-thinning)**.** p-thinning a PP remounts to consider every point of the realization and respectively keep/remove it with a probability p/1-p resulting in a new PP.

Properties of point processes

Different properties can be assigned to each of the PPs. A PP is said to be:

- **simple** if the multiplicity of each point in a given realization is one;
- **stationary** if its law is invariant by translation;
- **isotropic** if its law is invariant to rotation;
- **motion-invariant** if it is both stationary and isotropic;

Other properties are there to capture the interactions among points of the PP to see if they are more (PP with **attraction**) or less (PP with **repulsion**) likely to be separated by a distance r than expected under a null, no interaction scenario.

Poisson point process (PPP)

The homogeneous Poisson point process (HPPP) is undoubtedly the most popular PP so far. The vast majority of the available articles are indeed using this PP for several reasons:

- It is the basic model for complete spatial randomness (see Chapter 3, figure 3.5). It is often considered as the "Gaussian of point processes".
- It has interesting properties: (1) p-thinning of a PPP with intensity Λ results in PPP with intensity $p\Lambda$ (2) Superposition of independent PPPs results in a PPP (3) Displacement of a PPP results in a different PPP (motion-invariant).
- It leads to tractable results. Actually, several of the theorems presented later in this section are only valid for PPPs.

The PPP and the HPPP are further defined as follows:

Definition 2.1.3 (PPP)**.** A Poisson point process is a simple motion-invariant point process with expectation measure $\mu(\cdot)$ if:

- The random counting measure $\Psi(A)$ is Poisson distributed with mean $\mu(A)$ for every A $\subset \mathbb{R}^d$.
- For any disjoint sets $A_1, ..., A_m$, the random variables $\Psi(A_1), ..., \Psi(A_m)$ are independent.

In reality, knowing $\Psi(A) = N$, those N points are uniformly distributed inside A. This last remark is important as it will be used to generate random networks for the validation with MC simulations. In addition, one can observe that:

$$\mathbb{P}\left(\Psi(A_1) = n_1, ..., \Psi(A_m) = n_m\right) = \prod_{i=1}^{k} e^{-\mu(A_i)} \frac{\mu(A_i)^{n_i}}{n_i!} \quad \text{(product of m Poisson distributions)}$$

Definition 2.1.4 (HPPP)**.** A homogeneous Poisson point process is a PPP with uniform intensity Λ s.t. $\mu(A) = \Lambda l(A)$ where $l(A)$ is the Lebesgue measure.

More specifically, the Lebesgue measure of A represents respectively the length, the area or the volume of A for A $\subset \mathbb{R}$,$\mathbb{R}^2$ or $\mathbb{R}^3$.

Before mentioning three theorems specific to the PPP, an important instrument has to be introduced.

Definition 2.1.5 (PGFL)**.** Let f : $\mathbb{R}^d \to \mathbb{R}^+$. The probability generating functional of the PP with respect to function f is defined as follows:

$$P_\Phi(f) = \mathbb{E}\left[\prod_{\overline{X_i}\in\Phi} f\left(\overline{X_i}\right)\right]$$

Let F be of the type $F = \sum_{\overline{X_i}\in\Phi} g(\overline{X_i})$ in the following results. The PGFL can be used to compute the Laplace transform (LT) of the random variable (RV) F. This last tool is especially used to characterize metrics like the coverage probability as the interference has an expression comparable to the RV F defined above.
The LT of F is then computed as follows:

$$\mathcal{L}_F(s) = \mathbb{E}\left[\exp\left(-\sum_{\overline{X_i}\in\Phi} sg(\overline{X_i})\right)\right] = \mathbb{E}\left[\prod_{\overline{X_i}\in\Phi} e^{-sg(\overline{X_i})}\right]$$

where we indeed find an expression similar to definition 2.1.5.
The following theorems are three broadly used theorems in SG that we will refer to throughout this document.

Theorem 2.1.1. If the PP points X_i are derived from a PPP of intensity Λ defined on $\mathbb{R}^d$, for any non-negative function $f(\overline{X_i})$:$\mathbb{R}^d \to \mathbb{R}^+$, the PGFL of $\exp\left(-f(\overline{X_i})\right)$ can be more easily written as:

$$\mathbb{E}\left[\exp\left(-\sum_{\overline{X_i}\in\Phi} f(\overline{X_i})\right)\right] = \exp\left(-\int_{\mathbb{R}^d}\left(1 - \exp\left(-f(x)\right)\right)\Lambda dx\right)$$

Theorem 2.1.2 (Campbell's theorem)**.** For any PPP Φ of intensity Λ defined on $\mathbb{R}^d$:

$$\mathbb{E}\left[F\right] = \mathbb{E}\left[\sum_{\overline{X_i}\in\Phi} g(\overline{X_i})\right] = \int_{\mathbb{R}^d} \Lambda g(x)dx \qquad Var\left[F\right] = Var\left[\sum_{\overline{X_i}\in\Phi} g(\overline{X_i})\right] = \int_{\mathbb{R}^d} \Lambda g^2(x)dx$$

Theorem 2.1.3 (Slivnyak's theorem)**.** For a PPP Φ, because all points are independent, conditioning on a point at x does not change the distribution of the rest of the process.

In other words, it enables us to add or remove a node to the PPP at any location we like without changing its statistical properties. For general PPs, it is not the case especially for PPs with repulsion/attraction as it would affect the overall behaviour of points within some finite distance of the conditioning. In the particular context of cellular downlink , it allows to treat interference as coming from a PPP despite removing the serving BS from the PPP [SG11].

Other point processes

Sometimes, the spatial location of the UEs or BSs are respecting additional conditions which are not compatible with the complete spatial randomness provided by PPPs. As a consequence, in order to propose more coherent models, researchers studied other PPs which disperses points in particular way which respects those conditions. Indicatively, the reader can find an already complete taxonomy of the available literature related to SG modeling for each of the following PPs on Table I of [SG3]. Therefore, this same table will be considered as sufficiently representative of the existing publications.

- The **binomial point process** (BPP) is the superposition of N independent and uniformly distributed points on the set B. It has the same properties as the PPP but this time:

$$\mathbb{P}\left(\Psi(A) = n\right) = \binom{N}{n} \left(\frac{|A|}{|B|}\right)^{n} \left(1 - \frac{|A|}{|B|}\right)^{N-n} \quad \text{(binomial distribution)}$$

- The **Matérn hard core point process** (MHCPP) is a simple stationary point process with repulsion that has been widely used to impose a certain distance r between the different points of a realization of the PP. Moreover, it is a suitable candidate for modeling carrier-sense multiple access (CSMA) ad hoc networks as well as macro BSs in cellular networks. Nevertheless, a well chosen PPP (i.e. a good choise of its density) can still provide a good approximation of the generated aggregate interference associated with a MHCPP and is thus often preferred to the MHCPP for its mathematical tractability

- Although rarely used, the **α-Ginibre point process** has also been investigated. It is a simple detrimental stationary PP for wich the interested reader can find a formal definition in [SG7].

- The **Poisson cluster point process** (PCPP) is simple stationary point process composed by two different PPs: the parent PP and the associated daughter PP. The parent PP is actually a PPP. Then, the same PDF is used to generate a random number of daughters for each parent. Those daughters are then placed around their parent following another given PDF forming a cluster centered on their parent. This last PP has been recently studied for replacing the famous PPP as the latter fails to correctly represent the spatial configuration of today's Hetnets [SG8].

An illustration of these PPs above in a square of dimension 10×10 can be found in Figure 2.1.

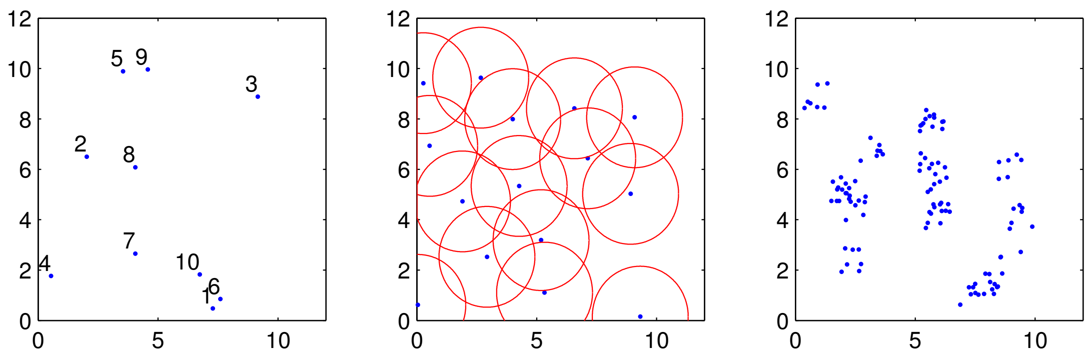

Figure 2.1: Left: 10-points BPP Middle: MHCPP of intensity 0.1 with a repulsion distance of 2 Right: PCPP of intensity 0.1 where (1) The number of daughters follows a Poisson distribution of mean 7 (2) The daughters are uniformly distributed around their parent in a square of area 1.

2.1.2 Model fundamentals

Most of the papers generally use the same steps to model wireless networks:

1. Choice of an appropriate propagation model.

2. Choice of an adequate node positionning model generally based on PPs in the framework of SG.
3. Choice of the critical metric(s) to analyze the performance of the studied network.

Additional considerations can be taken into account regarding the choice of the D2D communication policy, the energy harvesting technique as well as an eventual beamforming technique. Those considerations will be handled in the corresponding sections. Also, the considered user is usually taken at the origin without loss of generality thanks to the stationarity property of generally used PPs.

Propagation model

The propagation model typically consists of three different contributions:

(1) The **path loss** (PL) which models the loss of signal intensity due to distance. Two following models have been studied and compared for 5G urban micro and macro-cellular scenarios in [Misc70]: the alpha-beta-gamma (ABG) model and the close-in (CI) model. In the framework of this document, a slightly modified CI model will be assumed as the shadow fading term will be neglected. The same PL model is actually assumed in most of the papers. In addition, when analyzing the network performance based on the SIR, the frequency dependent term (called λ in the rest of the document) can be logically neglected. However, to allow the reader for further generalization to the SINR, this term will be kept in any case.

$$PL_{ABG}[dB] = \underbrace{10\alpha \log_{10}\left(\frac{d}{1m}\right)}_{\text{distance dependence}} + \underbrace{\beta}_{\text{offset}} + \underbrace{10\gamma \log_{10}\left(\frac{f}{1GHz}\right)}_{\text{frequency dependence}} + \underbrace{\chi_\sigma^{ABG}}_{\text{shadow fading}} \tag{2.1}$$

$$PL_{CI}[dB] = \underbrace{10\alpha \log_{10}\left(\frac{d}{1m}\right)}_{\text{distance dependence}} + \underbrace{20 \log_{10}\left(\frac{4\pi f}{c}\right)}_{\text{frequency dependence}} + \underbrace{\chi_\sigma^{CI}}_{\text{shadow fading}} \tag{2.2}$$

(2) The **fading** which models the multipath propagation of the wave. The most common fading model in the literature is definitely Rayleigh fading as it leads quite easily to closed-form expressions based on the LT of the interference. The computation of the coverage probability given in equation 2.4 illustrates this last observation. Nevertheless, Rayleigh fading is a suitable choice only if there is no line-of-sight (LOS) path. If it is not the case, a better choice would be the Rician fading. To the best of my knowledge, Rician fading was quite poorly investigated [D2D38]. The main reason for its unpopularity comes most likely from the increased computation complexity of the performance metrics due to its mathematical expression as seen in Chapter 3. However, for dense deployment of BSs in CC networks, ad hoc networks as well as D2D networks, the need to take short-range transmissions or equivalently LOS components into consideration is real.
Recently, a more general fading model has been proposed to account for the large number of signal propagation mechanisms: the $\kappa - \mu$ fading model. This last model encompasses all previously studied fading models as shown in Figure 2.2. The general approach adopted for the Rayleigh and Rican fading is adapted to the former model in [SG2] and for D2D communications in [D2D22].

	κ-μ fading	η-μ fading	κ-μ shadowed fading
Rayleigh	$\kappa \to 0, \mu = 1$	$\eta = 1, \mu = 0.5$	$\underline{\kappa} \to 0, \underline{\mu} = 1$ or $\underline{m} = 1, \underline{\mu} = 1$
Nakagami-m	$\kappa \to 0, \mu = m$	$\eta = 1, \mu = m/2$ or $\eta \to 0, \mu = m$	$\underline{\kappa} \to 0, \underline{\mu} = m$ or $\underline{m} \to m, \underline{\mu} = m$
Nakagami-n (Rice)	$\mu = 1$		$\underline{\kappa} = K, \underline{\mu} = 1, \underline{m} \to \infty$
Nakagami-q (Hoyt)		$\mu = 0.5$	$\underline{\kappa} = (1-q^2)/2q^2, \underline{\mu} = 1, \underline{m} = 0.5$
One-sided Gaussian	$\kappa \to 0, \mu = 0.5$	$\eta \to 0, \mu = 0.5$ or $\eta \to \infty, \mu = 0.5$	$\underline{\kappa} \to 0, \underline{\mu} = 0.5$ or $\underline{m} = 0.5, \underline{\mu} = 0.5$
κ-μ fading	κ, μ		$\underline{\kappa} \to \kappa, \underline{\mu} \to \mu, \underline{m} \to \infty$
η-μ fading		η, μ	$\underline{\kappa} = (1-\eta)/2\eta, \underline{\mu} = 2\mu, \underline{m} = \mu$
Rician shadowed			$\underline{\kappa} = K, \underline{\mu} = 1, \underline{m} = m$

Figure 2.2: Special cases of the $\kappa - \mu$ fading model (Source: [SG2]).

The $\eta - \mu$ constitutes another general fading model. Other fading models can be mentioned like Nakagami, Hoyt or even one-sided Gaussian.

(3) The **shadowing** which models the obstacles obstructing the wave. This last contribution will not be discussed in this document. The interested reader can still find related discussions in [SG2, SG11].

Performance metrics

Again, Table I of [SG3] will be considered as sufficiently representative of the existing literature. The commonly studied performance metrics are:

- The **coverage probability** or reciprocally the **outage probability** which represents the probability of a transmission to be respectively successful or unsuccessful. It is generally defined as the probability of the SINR to be respectively above or below a certain treshold ξ.

  Assuming a modified CI model and fading effects, the SINR of the link between elements x and y is defined as:

$$\gamma_{x,y} = \frac{g_{x,y} P_x \lambda r_{x,y}^{-\alpha}}{W + \sum_{\substack{\text{int} \in \Phi_{\text{int}} \\ \text{int} \neq x}} g_{\text{int},y} P_{\text{int}} \lambda r_{\text{int},y}^{-\alpha}} = \frac{g_{x,y} P_x \lambda r_{x,y}^{-\alpha}}{W + I} \tag{2.3}$$

  where $g_{x,y}$ is the fading power gain between the elements x and y , $r_{x,y}$ is the distance between the elements x and y, P_x is the transmitted power of element x, Φ_{int} is the PP of the interferers (int), λ is the frequency dependent pathloss and W is the noise power.

  Furthermore, the definition of the SINR above will be used as the general definition along the entire document. Ideally, the PDF of the interference would be required. This is not possible as shown in [SG3] where the interference is said to be related to both Gaussian and α-stable distributions. Instead, the following approach will be used in this document.
  The coverage probability defined as P(SINR>ξ) assuming Rayleigh fading is given by:

$$\begin{aligned}
P(\gamma_{x,y} > \xi, \alpha) &= P\left(\frac{g_{x,y} P_{\text{link}} \lambda r_{x,y}^{-\alpha}}{W + I} > \xi\right) \\
&= 1 - P\left(g_{x,y} < \frac{\xi (W+I) r_{x,y}^{\alpha}}{P_{\text{link}} \lambda}\right) \\
&= 1 - \int_i F_G(g)|_{\frac{(W+i)\xi r_{x,y}^{\alpha}}{\lambda P_{\text{link}}}} f_I(i) di \\
&\overset{(1)}{=} 1 - \int_i f_I(i) di + \int_i e^{-g}\Big|_{g=(W+i)\frac{\xi r_{x,y}^{\alpha}}{\lambda P_{\text{link}}}} f_I(i) di \\
&\overset{(2)}{=} \int_i e^{-g}\Big|_{g=(W+i)\frac{\xi r_{x,y}^{\alpha}}{\lambda P_{\text{link}}}} f_I(i) di \\
&\overset{(3)}{=} e^{-W\frac{\xi r_{x,y}^{\alpha}}{\lambda P_{\text{link}}}} \mathbb{E}\left[\exp\left(-\frac{\xi r_{x,y}^{\alpha}}{\lambda P_{\text{link}}} I\right)\right] \\
&\overset{(4)}{=} e^{-W\frac{\xi r_{x,y}^{\alpha}}{\lambda P_{\text{link}}}} \mathcal{L}_I(s,\alpha)\Big|_{s=\frac{\xi r_{x,y}^{\alpha}}{\lambda P_{\text{link}}}}
\end{aligned} \tag{2.4}$$

  where (1) comes from the fact that the fading power gain g=$|h|^2$ ~exp(1) thus $F_G(g) = 1 - e^{-g}$, (2) results from the fact that the integral over all possible values of a PDF is always equal to 1, (3) arises from the definition of the expectation and (4) follows from the definition of the Laplace transform.

- The **ergodic rate** or equivalently the ergodic capacity defined as $\mathbb{E}[\log(1 + \text{SINR})]$. It measures the average achievable rate over all possible network realizations.

- The **error rate** defined as the probability that a bit/symbol is wrongly detected.

2.2 Device-to-device communications

D2D communications are seen as one of most promising additional technological features of the 5G release especially for improving spectral efficicency. The main idea behind them is to exploit spatial proximity between CC UEs to enable them to speak directly with each other without passing through the serving BS. This results in increased throughputs and reduced latencies and provide the D2D UEs with guaranteed quality of service. They generally consists of single-hop links as the transmissions distances are very short. Another advantage of D2D communications is the fact that they can enhance bad coverage conditions and even serve as a backup solution when the network is congested or when the CC infrastructure shuts down. As the goal is in this case to offer an alternative to the CC networks, transmissions distances may be more important, hence the need for multi-hop links.

Before even entering in the available literature, a few useful notions that will be used along this document have to be fixed. The main point to clarify concerns the different types of D2D communication policies. First of all, the D2D communications are either inband or outband depending on whether they are done in the licensed band or unlicensed band. In addition, when talking about inband D2D communications, a further overlaying or underlaying policy can be assumed. In the overlaying case, D2D and CC communications are given respective bands inside the licensed band. On the contrary, in the underlaying case, the D2D and CC communications are sharing the same ressources. Finally, when going for outband D2D communications, two different cases arise as the D2D communications control can be handled by the CC network (controlled) or by the users themselves (autonomous). Figure 2.3 summarizes the latest discussion in a more visual manner.

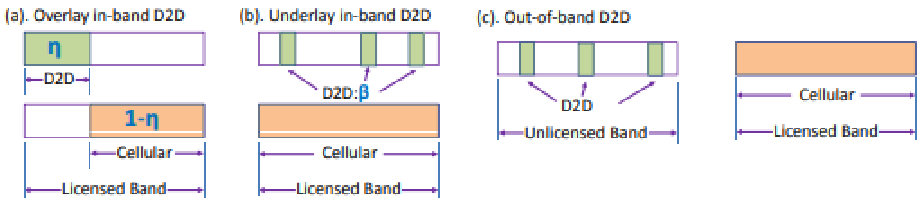

Figure 2.3: Different D2D communications policies (Source: [D2D30]).

Next, according to the chosen policy, several challenges arise and require to be tackled [D2D23, D2D46]. Among them, the interference mangement, the multihop D2D communications and the D2D communications are of particular interest. In addition, the different drawbacks and advantages of each D2D communications scheme are listed in [D2D18, D2D27, D2D39] and summarized in Figure 2.4.

Criteria	**Inband**		**Outband**	
	Overlay	**Underlay**	**Network-assisted**	**Autonomous**
Spectral efficiency	Medium	Very High	Low	Low
Interference between cellular and D2D users	Very Low	High	Negligible	Negligible
Interference among D2D users	Medium	Medium	High	High
Controlled interference environment	Yes	Yes	No	No
Implementation complexity	Medium	Low	High	High
Extra signalling overhead to network	Medium	High	High	Very low
Inter – platform coordination	No	No	Yes	Yes
Network controlled	Full/Hybrid	Full/Hybrid	Full	Loose
Cell coverage	In coverage/partial coverage	In coverage/partial coverage	In coverage	In coverage and out of coverage
Simultaneous D2D and Cellular transmission	No	No	Yes	Yes
Energy efficiency	High	High	Low	Low

Figure 2.4: Comparison of the different D2D communication policies (Source: [D2D39]).

Furthermore, most of the papers so far are focussing on three main topics: mode selection, bandwidth allocation and power control that constitute real challenges in the particular case of inband D2D communications. At what time rate do we perform mode selection? What measurements, reporting mechanisms and algorithms need to be used in order to select between a CC or a D2D link? What is the optimal bandwidth allocation? Which power algorithms could be implemented to enhance the network performance? Those are all questions that needed to be handled when D2D communications were firstly introduced and that were already partially answered.

2.2.1 Inband underlaying device-to-device communications

A particular interest will be dedicated to inband underlaying D2D communications in the framework of this document as this scheme provides an improved spectral efficiency. The underlaying inband scheme is actually the most studied policy until now. Moreover, in the vast majority of cases, D2D communications are said to use the UL ressources. Several reasons are put forward for explaining such a choice: lower congestion [D2D26], potentially better energy efficiency or hardware constraints [D2D40] or ultimately a stronger ability to process interference at the BS when compared to the CC UE [D2D43].

Interestingly, some of the available approaches are not using SG as a tool [D2D43] where others are still focussing on partially SG-based analysis of the studied networks. In some cases, the BSs are indeed distributed in a deterministic way. This kind of approach may fail to correctly represent today's networks as it is unlikely that the network elements are given a fixed organized position.
For example, in [D2D26], a single circular cell scenario is studied where only intra-cell interference is considered as inter-cell interference is supposed correctly handled by the inter-cell interference coordination (ICIC) mechanism. The single BS is then placed a the center of this circular cell and the single CC UE included in the analysis is randomly and uniformly place inside the cell.
In [D2D34, D2D40], the BSs are rather placed following a grid-based model with hexagonal pattern as shown in Figure 1.1. In both cases, the area of an hexagonal cell is fixed to $\frac{1}{\Lambda_b}$ in order for the BSs density to be Λ_b per unit area.

Another interesting point is certainly the choice of the fading model that has to be carefuly chosen to account for a strong LOS component which is specific to the D2D communications. While many publications go for Rayleigh fading for its mathematical tractability, some of them have already made a good start in that direction. In fact, [D2D26, D2D40] have opted for Nakagami fading distribution while [D2D38] has adopted Rician fading distribution.

For an efficient introduction of the D2D technology inside the already existing CC network, researchers were also concerned about how to decide when two CC UEs are eligible for a faster D2D link, hence the need for a proper mode selection scheme. This is the reason why most papers talk about "potential D2D UEs" as they are not sure to talk via a D2D link. In some conditions, the CC link is in fact preferable. For this purpose, [D2D34] has decided to compare three different mode selection schemes:

1. The **distance cut-off** scheme where the D2D mode is activated if the D2D link distance r_d is lower than a given treshold γ.

2. The **link gain** scheme where the D2D mode is chosen if the biased D2D link quality is at least as good as the cellular UL link quality. This is translated by $r_c^{-\alpha} < T_d r_d^{-\beta}$ where r_c is the distance between the D2D transmitter (TX) and its serving BS, r_d is the distance between the D2D TX and the D2D receiver (RX), α and β are respectively the path loss coefficients on the CC and D2D links and T_d is the bias factor.

3. The **guard zone scheme** where the D2D mode is selected if the UL distance r_c defined above is bigger than the guard zone radius R_g.

Closed-form expressions for the success probabilities at the BS and at the D2D RX have been derived for the three different schemes. Those expressions have been proven to be pretty accurate except for the

D2D RX success probability which seems to be a good approximation only for D2D RX on the edge of the cell. Based on this analysis, the first scheme is shown to outperfom the two other schemes as shown in Figure 2.5. The main reason for this is that less potential D2D UEs are actually in D2D mode.

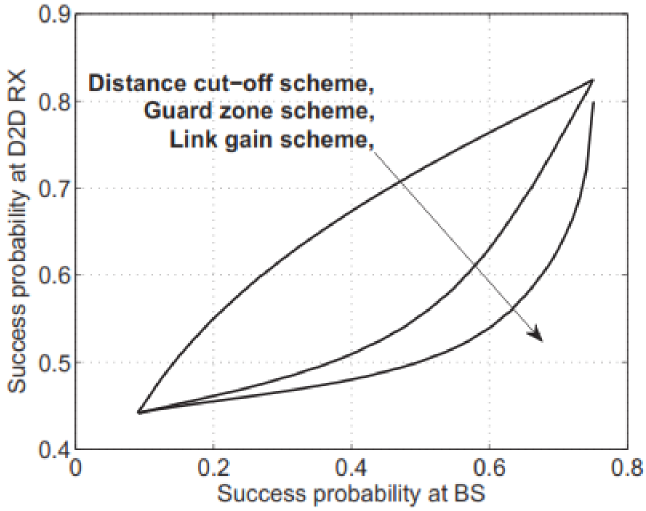

Figure 2.5: Comparison of the different mode selection schemes (Source: [D2D34]).

The general guard zone principle is well known in the scientific community as it can be encountered in several papers. In [D2D20], the authors have combined a SIR-aware D2D link activation with guard zones around the BSs for a network under UL underlaid policy to ensure low interference at the BS. In addition, they have shown the impact of the guard zone radius R_g and SIR treshold ξ (based on which the D2D link is permitted or not) on the D2D area spectral efficiency (ASE) and cellular coverage. They further derived optimal values of R_g and ξ for an optimal ASE under sufficient cellular coverage. [D2D19] also used guard zones this time around the D2D Tx for a network under DL underlaid policy to avoid nearby interference from BSs and other D2D UEs. The optimal guard zone radius was then computed in order to maximize the D2D network throughput.
Regarding the mode selection scheme or the link activation policy, other approaches that will not be developed here can be found in [D2D26, D2D37, D2D38].

As the choice of the underlaid ressources (either UL or DL) was quite unclear, the authors of [D2D40] decided to provide us with a comparison between the two cases. They defined their performance metric as the probability to correctly decode two consecutive messages at the D2D RX in order to capture the change of network topology over time. It was then found out that the interference from CC network in the DL case, which is correlated over different time slots, promotes the D2D link and permits a lower outage probability. This conclusion was drawn for equivalent BS (P_{bs}) and CC (P_{cc}) transmit powers as P_{bs} was fixed to $\overline{P_{cc}}$ (average value). [D2D45] also provides a simultaneous analysis of the two different cases.

As already explained, in some applications where the D2D communications are desired to be involved, the need for multi-hop communications appears. The authors of [D2D45] tried to tackle this problem by providing a new model based on the shortest path routine (SPR) algorithm. The main idea behind the algorithm is to minimize the number of hops by taking each time the D2D UE providing sufficiently good transmission conditions which is closer to the target D2D UE as a relay. This procedure is then repeated until we reach this same target user. They provided closed-form expressions for the CC and D2D outage probabilities under both the UL and DL underlaid policy as well as an expression of the number of hops depending on the intended link distance.
The same authors provided in [D2D47] a comparison between the SPR algorithm and other multihop algorithms that were implemented over a modeled version of a neighbourhood in Ottawa. One of them is the interference aware routine (IAR) which consists on doing the biggest part of the multihop path on the edge of the cell to limit the interference at the BS. As a consequence, the cell edge has to be reached

as quickly as possible before converging back to the targeted user. Each intermediate step on the cell edge is actually done following a SPR step.

Finally, the main conclusion of [D2D26] is that increasing D2D communications can be beneficial for future networks. This observation is based on the analysis of the CC and D2D outage probabilities as well as the spectrum reuse ratio.

2.2.2 Inband overlaying device-to-device communications

Other authors decided to opt for an overlaid scheme instead. Again, several papers decided to place the BS following an hexagonal grid-based model as explained in the previous section [D2D13, D2D22, D2D24]. The authors of [D2D48] even decided to propose a first step into multi-tier networks as depicted in Figure 2.7. In fact, when a given potential D2D UE can not establish a D2D link, it can either communicate with a macro BS or a pico BS. As shown in the picture, the hexagonal cell has 6 pico BSs on each of its corner and each of them is equipped with three directional antennas in order to achieve a general frequency reuse of $\frac{1}{3}$. They further demonstrated that different choices of the frequency allocation for the D2D pairs for given networks settings may lead to completely different behaviours regarding the user average rate.

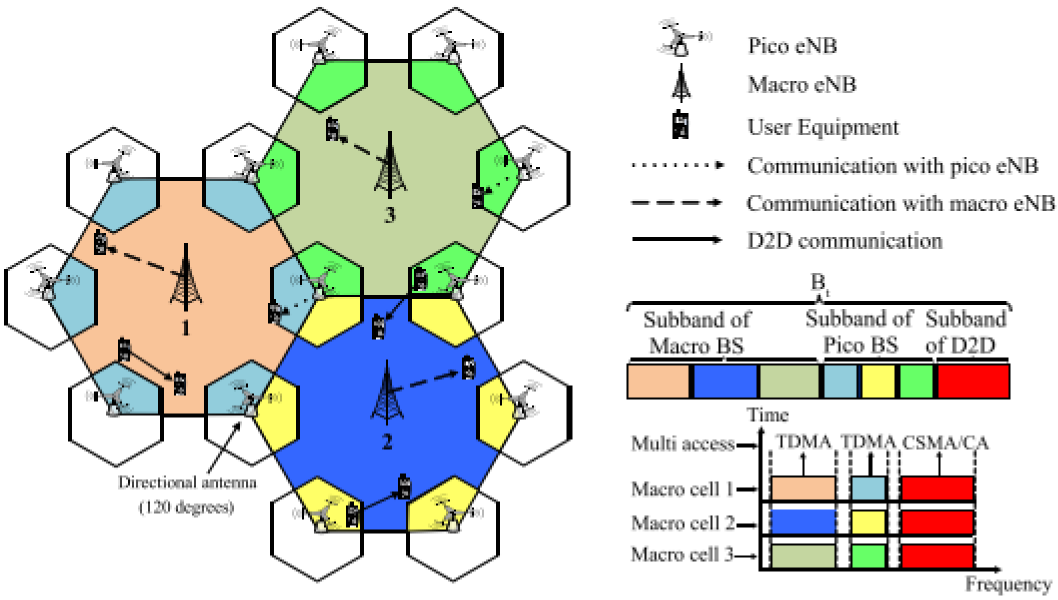

Figure 2.6: Two-tier cellular network including overlaid D2D communications (Source: [D2D48]).

As for the underlaid policy, several contributions also decided to account for a LOS component by opting for non-Rayleigh fading models.
[D2D22] proposed an analysis under generalized fading channels, namely $\kappa - \mu$ and $\eta - \mu$ models. In this article, the BS were placed following PPP Φ_{bs} of intensity Λ_{bs} and the potential D2D UEs following a marked PPP $\widetilde{\Phi}_{bs}$ of intensity Λ_u as follows

$$\widetilde{\Phi}_{bs} = \{X_i, \rho_i, L_i, P_i\}$$

where $X_i \in \mathbb{R}^2$ are the coordinates of D2D UE i, $\rho_i \in \{0, 1\}$ indicates respectively whether D2D UE i is in D2D mode or in CC mode, L_i is the distance of the link intended by D2D UE i and P_i is the transmit power of D2D UE i. This kind of marked point process was used in other articles [D2D30, D2D31]. Also, a distance cut-off mode selection scheme was adopted as for most of the reviewed articles related to the underlaid scheme. The D2D link rate was then proven to be higher than the CC link rate if the spectrum factor η (see figure 2.3) is chosen carefuly. Also, it was shown that increasing the threshold for mode selection increases the number of D2D links and thus the average UE rate but at the cost of an increased

bit error probability. Finally, it was shown that for small values of the spectrum factor η the D2D rate can become lower than the CC rate.
In an easier and quite simplistic way, [D2D32, D2D33] decided to distinguish the D2D link and the CC link by supposing $g_{d2d} \sim \exp(\mu_{d2d})$ and $g_{cc} \sim \exp(\mu_{cc})$ where g_{d2d} and g_{cc} are respectively the power fading gain on the D2D link and the CC link.
Finaly, the authors of [D2D13] have chosen to follow the 3GPP propagation model to account for potential line-of-sight (LOS), non line-of-sight (NLOS) and free space (FS) links of lentgh x as seen on equations 2.5 and 2.6.

$$PL_{cc}(x) = \begin{cases} A_{cc,LOS}x^{-\alpha_{cc,LOS}} & \text{with prob. } P^{LOS}_{r_{cc}}(x) \text{ if } 0 \leq x \leq r_{cc} \\ A_{cc,NLOS}x^{-\alpha_{cc,NLOS}} & \text{with prob. 1-}P^{LOS}_{r_{cc}}(x) \text{ if } 0 \leq x \leq r_{cc} \\ A_{cc,NLOS}x^{-\alpha_{cc,NLOS}} & \text{if } x > r_{cc} \end{cases} \tag{2.5}$$

$$PL_{d2d}(x) = \begin{cases} A_{FS}x^{-\alpha_{FS}} & \text{if } 0 \leq x \leq r_{FS} \\ A_{d2d,LOS}x^{-\alpha_{d2d,LOS}} & \text{if } r_{FS} \leq x \leq r_{d2d} \\ A_{d2d,LOS}x^{-\alpha_{d2d,LOS}} & \text{with prob. } P^{LOS}_{r_{d2d}}(x) \text{ if } x > r_{d2d} \\ A_{d2d,NLOS}x^{-\alpha_{d2d,NLOS}} & \text{with prob. 1-}P^{LOS}_{r_{d2d}}(x) \text{ if } x > r_{d2d} \end{cases} \tag{2.6}$$

where $A_{cc,LOS}$,$A_{cc,NLOS}$,$A_{d2d,LOS}$,$A_{d2d,NLOS}$ and A_{FS} are respectively the CC LOS, CC NLOS, D2D LOS, D2D NLOS and free space reference path losses. Furthermore, $\alpha_{cc,LOS}$,$\alpha_{cc,NLOS}$,$\alpha_{d2d,LOS}$,$\alpha_{d2d,NLOS}$ and α_{FS} are respectively the CC LOS, CC NLOS, D2D LOS, D2D NLOS and free space path loss exponents. Finaly, r_{cc} and r_{d2d} are the CC and D2D distance treshold fixed by measurements and $r_f = qf_c$ where f_c is the carrier frequency and $q = \frac{2.56}{c}[m/Hz]$. The interested reader can find an expression for $P^{LOS}_{r_{cc}}(x)$ and $P^{LOS}_{r_{d2d}}(x)$ in the article in question. This 3GPP PL model is subject to some surprising results. In fact, while using the general PL reference model makes the normalized throughput saturates after a certain BS density threshold, using the 3GPP PL model makes it possible to find a value for the BS density that maximizes the throughput.This represents a very interesting result as the PL reference model was widely used in the literature.

Other approaches of spectrum sharing were further proposed. In [D2D41], a comparison between a coordinated and uncoordinated scheduling is suggested. The bandwidth dedicated to the D2D communications is then separated into N equal subparts. Each D2D TX can only communicate in one of them with, however, the possibility of multiple D2D transmissions on one single subpart. Each D2D TX is then scheduled either in an uncoordinated or in a coordinated manner. In the uncoordinated case, each of them is randomly given a subpart risking to have close D2D TX using the same subpart. In the coordinated case, each cell allocates a subpart to its associated K D2D TX following the steps below:

1. The K D2D UEs are partitionned into $\lfloor \frac{K}{N} \rfloor$ of size N and one group of size $K - \lfloor \frac{K}{N} \rfloor N$. They are then randomly ordered inside each group.

2. Each cell then allocates the k^{th} subpart to the k^{th} UE inside each group.

This scheme still makes it possible to have several close interfering D2D TX . The coordinated case is however proven to outperform the uncoordinated case in terms of UE average rate.

In [D2D36], the perfomances of the two most popular schemes to separate D2D transmissions into non-interfering sets to be allocated to separate channels, namely ITLinQ and FlashLinQ, are compared. ITLinQ is a peer-to-peer scheduler mechanism which is based on a given information-theoretic optimality notion. It selects a group of links for which the mutual interference is assumed negligible while still achieving the capacity region for that group within a certain error margin. On the contrary, FlashLinq is principally based on heuristical approaches. The main parameters of the two methods were optimized in order to propose a fair comparison. Both of them manage to avoid situations of excessive interference. Even if FlashLinq is essentially based on heuristical methods, the difference in terms of performance between the two schemes is very small but a slight preference is still given to ITLinQ.

Regarding multi-hop routines, the authors of [D2D32] proposed an extension of the conventional CC link in the UL via a D2D relay in a two-hop fashion. As a consequence, a normal CC link providing an unsufficient SIR value at the BS is replaced by another CC hop complemented by a D2D hop. The gains of using an intermediate D2D hop are shown in the article but will not be discussed here. The same authors proposed in [D2D33] this same approach for the DL extension analysis.

Many articles also use different embodiments of the channel inversion power control in the UL. In [D2D32], a fractional channel inversion power control with maximum transmit power is used. Similar approaches are used in [D2D13, D2D30, D2D31] where the path loss $L^{-\alpha}$ is cancelled by multiplying the transmit power by L^{α}. The fading is not included in that power control to avoid an estimation of it at each time slot.

Different subjects were also treated in [D2D21, D2D49]. In [D2D21], an optimization of the cache-aided throughput is proposed and shown to be better than the cache-hit optimal case in terms of density of succesfully served UE file requests. Caching enabled networks are networks were the UEs can store several files themselves. When another UE needs a particular file, he can ask its neighbouring UEs if they have it before asking the nearest BS. Several approaches were initially based on the maximization of the cache hit probability which represents the probability for a user to get the requested file. In that article, the authors rather proposed a method built on the maximization of the cache-aided througput based on which the critical role of D2D communications reliability has been proven.

In [D2D49], the authors proposed a pricing-based Stackelberg game approach for an optimal mode selection and spectrum partitionning. In this scheme, the goal of each BS (leader) is to partition the spectrum among potential D2D UEs in order to maximize the overal network utility while each of the potential D2D UEs (followers) then select their mode to maximize their own utility. The divided and shared schemes are also analyzed. In the divided case, each D2D UE is given an orthogonal ressource while they can use the entire bandwidth in the shared scheme.

2.2.3 Comparison of the underlaid and the overlaid scheme

Another concern about D2D communications is whether to choose the underlaid or overlaid policy. In [D2D30, D2D31], the authors tried to answer that question. In both cases, the rate for the potential D2D UEs that opted for the D2D mode is increased. Nevertheless, the CC UEs rate is also improved in the overlaid scheme thanks to the offloading capability of D2D communications while it does not change or even slightly degrades in the underlaid scheme due to extra interference caused by D2D communications. The spectrum partitionning (η,β) is made as shown in Figure 2.3 except that frequency hoping is used in the underlaid case to randomize the interference caused by each UE to other links. It is shown that even with only 16% of D2D links, the overall rate is already significantly and positively impacted. It can also be observed that equivalent performances are achieved with $\eta = 0.3$ in the overlaid scheme and $\beta = 0.9$ in the underlaid scheme due to inter-mode interference in the second case. In addition, it is demonstrated that a stricter network control is needed in the underlaid case. In fact, the ressource portion β and mode selection treshold (cut-off distance) γ in the underlaid case need to be updated fairly regularly to keep the link outage within an acceptable level. More precisely, an increased number of D2D links should result in a lower value of β. On the contrary, they can be tuned slowlier in the overlaid case.
The authors of [D2D25] also did a parallel study of both cases by providing different examples but using a completely different approach that will not be discussed here.

2.2.4 Outband device-to-device communications

Articles on different topics related to out of band D2D communications can be found in [D2D12, D2D16, D2D17, D2D28]. They will not be discussed here as they are not of particular interest in the framework of this document.

2.3 Energy harvesting and energy harvesting-aided device-to-device communications

The main principle behind energy harvesting technologies is the ability of a given system to take advantage of its surrounding environment by extracting power from it. This is actually achieved by a device called the energy harvester that manages to convert RF ambient power into DC power for the system's use. Those technologies have drawn increasing interest in the past few years. The reasons why they became so popular are the following:

- It reduces installations as there is no need for power lines. This has three main benefits: it provides the ability to reach hazardous places, it reduces the operating costs and it increases the possible mobility.
- The need for a battery is deleted or, at least, rechargeable batteries can be used. Therefore, it is maintenance-free, available on demand and it increases the batteries lifetime.
- It enhances the system reliability, thereby suppressing the risk for severe consequences. In fact, it eliminates the risk of service shutdown caused by dead batteries.

Three alternatives for power harvesting in the framework of wireless networks are generally proposed, namely microwave power transfer (MPT) [EH52], magnetic resonance coupling [EH58] and inductive coupling [EH62]. Those technologies are respectively made for long (up to tens of km), medium (several meters), and short (< 1m) range power transfer distances [EH56]. Based on this last factor, a particular interest will be devoted to MPT in this document. The frequencies traditionally used for MPT are 2.4/2.45GHz and 5.8GHz in the ISM band. However, thanks to recent technological advances, the 60GHz bandwidth coul be used in a near future [EH57]. Such high frequencies should enable sharp beamforming with a very small number of antennas. Different beamforming techniques will be proposed in Chapter 4.

In [EH54], the authors proposed upper bound expressions for the power outage and transmission outage probabilities of a single sensor node trying to communicate. This node harvests energy from RF sources deployed following an α-Ginibre PP that can be generalized to a PPP if α=0. The node power equation is given by

$$P_T = P_H - P_C$$

where P_T,P_H and P_C are respectively the transmit power, the harvested power and the power consumption of the node circuit. The mathematical expressions even if they are upper bounds were proven to be quite accurate.

In [EH56], an already more complete approach is proposed. CC UEs are harvesting power from power beacons (PB) deployed following a PPP and transmitting in an orthogonal band. Those CC UEs try to communicate with their associated BS and the interference from the K closer interferers is supposed correctly handled and cancelled at the BS. Feasible regions are defined as the combinations of several parameters providing results that satisfy a certain number of constraints (i.e. the outage probability has to be lower than a fixed threshold). The feasible regions over parameters P_{cc} (CC transmit power), P_{pb} (PB transmit power),Λ_{bs} (BS density) and Λ_{pb} (power beacon density) under three constraints are derived. This is done for both infinite and finite battery storage. In addition, two different schemes are compared: the isotropic scheme and the directed scheme. In the isotropic case , each UE receives power from every PB that transmits isotropically. In the directed scheme, each CC UE is charged by its nearest PB thanks to beamforming and further receives the secondary lobes contributions of the remaining PBs. The directed case is shown to loose its efficiency when compared to the isotropic case when the density of PB is increased.

One step further, the combination of D2D communications and energy harvesting techniques seems very interesting and was already proposed in several papers [EH51, EH53, EH59, EH60, EH63]. In some cases, a D2D UE is requested as a relay for another user information in order to improve the probability of successful transmission. In that situation, the relay D2D UE is constrained to use its own power which is certainly not desirable. This is where combining those two recent technologies became interesting.

In [EH63], a completely new model called D2D-EHHN is proposed for heterogeneous cellular networks with energy harvesting-based D2D communications. In this model, the access points (AP) of each tier i are deployed following a PPP. Each potential D2D user harvests energy from its associated strongest AP defined as the one delivering the highest bias power. A potential D2D UE can play the role of a relay between the AP and an intended user if he has harvested sufficient power. They suppose in a simplistic way that each UE harvests C Watts at each time slot. They also defined zones (EHR) were we can actually harvest energy leaving certain spatial locations were no energy can be harvested. As the users are supposed to move, this does not represent a problem. The required power to be a relay is then assumed to be $P_{d2d} = NC$ such that the UE states follow the next finite state machine (FSM):

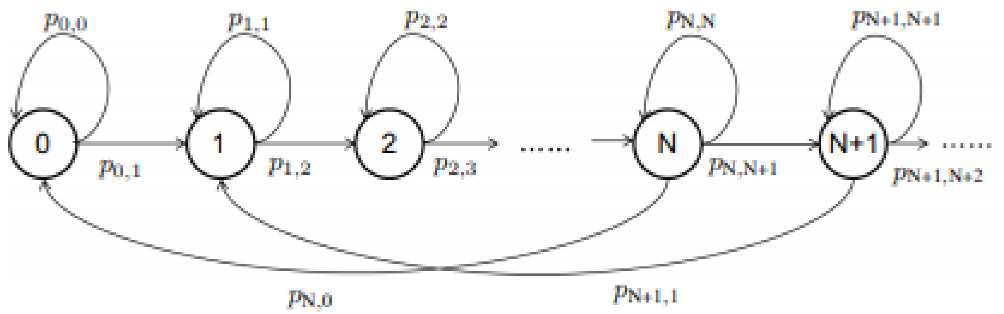

Figure 2.7: FSM : each user goes to next state if he is in the EHR and if he does not need to receive information itself. From the N^{th} state, he has acquired enough energy to be a relay and if he does, he steps N states back (Source: [EH63]).

They also established a new transmission mode selection based on a computed optimal D2D relay position and its associated feasible region defined as a circle centered on that same optimal position. The relay is then defined as the closest potential D2D UE to the optimal position inside the feasible region having harvested enough energy. If no such a UE can be found, the AP goes for a simple CC link with the targeted UE. Interestingly, the optimal position is shown to converge to the targeted UE and the radius of the feasible region to decrease when the density of AP increases. This is logical since the CC link becomes more and more interesting. The D2D-EHHN model involving all those new features is shown to significantly outperform the benchmark model in terms of outage probability.

[EH53] proposes EH-based D2D communication based on a time-splitting protocol: τT seconds dedicated to harvesting and (1-τ)T seconds to information transfer where T is the time needed to transfer one information block and $\tau \in$ [0,1]. The potential D2D UE harvests energy from PBs. Supposing multiple antennas at the PB and at the potential D2D, two different beamforming techniques are proposed to improve the wireless power transfer: the best antenna based beamforming technique and the optimal beamforming vector technique that will be presented in Chapter 4.

[EH59] evaluates the security of underlaid (DL) D2D communications in large-scale cognitive CC networks where the potential D2D UEs harvest from PBs under three different power transfer policies and two different information signal models. The interested reader will be redirected to the abstract of the paper that already gives a precise and complete idea of the paper contents.

Chapter 3

Inband underlaying device-to-device communications under Rician fading

D2D communications represent a new technological paradigm that is intended to revolutionize the traditional communications methods. Its goal is to exploit the proximity of network users and enable them to communicate directly with each other. Due to the mathematical tractability provided by Rayleigh fading, the most important part of the work related to D2D communications is using that fading model. However, as the D2D technology mainly concerns short-range transmissions, the need to account for LOS components is meaningful. This chapter tries to fill this gap by providing a D2D network analysis under Rician fading. The contributions of this chapter are the following:

- Partly closed-form expressions are derived under Rician fading. A similar approach was already done in a slightly different way in [D2D38]. For this reason, the computations specific to Rician fading are mainly inspired by this same article. However, the proposed model is more general as it also includes expressions for interferers that are known to be further than the source of a given link. This enables us to model more accurately networks where the interference comes from other cells.

- The trade-off between CC and D2D communications under an inband underlaying policy is analyzed. As for [D2D40], this model intends to provide sufficient tools to decide whether to use the UL or DL band for D2D communications and under what conditions. It also includes additional features to further improve the network perfomances in both cases.

- The limits of SG regarding the computation time are shown by comparing the model computation time to the MC simulations computation time. A more critical point of view is adopted about SG based on this time analysis and on the obtained mathematical expressions complexity.

The model under review draws heavily on [D2D45] in which a similar work was done for Rayleigh fading. This chapter is about adapting this model to the case where the useful link is instead affected by Rician fading.

3.1 System model

In this model, a CC UE m tries to communicate with a CC UE m' of the same cell via their closest base station n. All BSs, CC UEs and D2D UEs are respectively distibuted following three independent PPPs of intensities Λ_b,Λ_c and Λ_d defined in $\mathbb{R}^2$. They also respectively use transmit powers P_{bs}, P_{cc} and P_{d2d}. The interferers PPs will be described in the corresponding sections and randomly chosen among the overall BSs, CC UEs and D2D UEs. The frequencies of the UL and the DL are considered to be separate bands and each UL or DL frequency can be used once in each cell.

The D2D communications follow an underlay policy. D2D communications are then supposed to be done either in the UL band or in the DL band while the cellular communications use both bands as depicted in Figures 3.1 and 3.2. Also, the D2D receiver is uniformly located in a circle of radius R_{max}

around the D2D transmitter. This relies on the same idea as the cut-off frequency mode selection method presented in Chapter 2. Unlike the authors of [D2D45], we will focuss here on single-hop D2D communications. Nevertheless, this work could be easily adapted to take multi-hop D2D communications into account.

The following PDFs will be used along this document. [SG9] shows that the PDF of the distance between a UE and its nearest BS when the BSs are distributed following a HPPP of density Λ_b in $\mathbb{R}^2$ is given by:

$$f_R(r) = 2\Lambda_b \pi r \exp\left(-\Lambda_b \pi r^2\right) \tag{3.1}$$

[D2D15] shows that the PDF of the distance between two D2D UEs involved in a single-hop D2D link is:

$$f_R(r) = \frac{2r}{R_{max}^2} \quad \text{for} \quad 0 \leq r \leq R_{max} \tag{3.2}$$

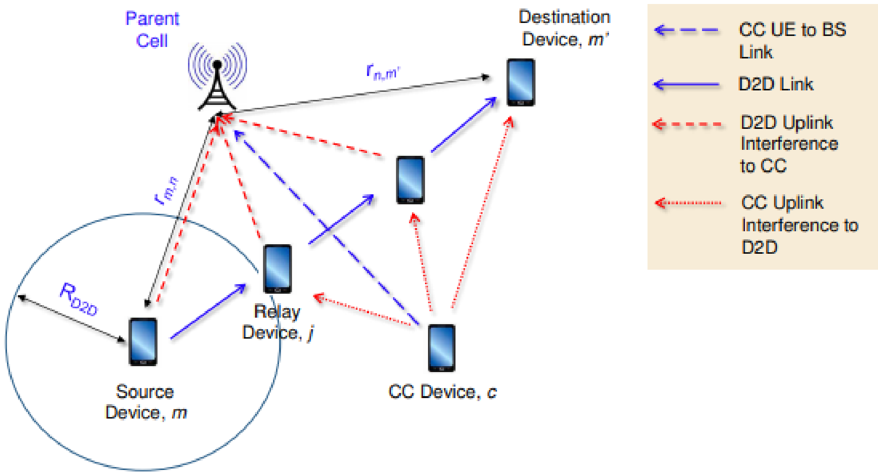

Figure 3.1: Case 1: D2D transmissions in the UL band (Source: [D2D45]).

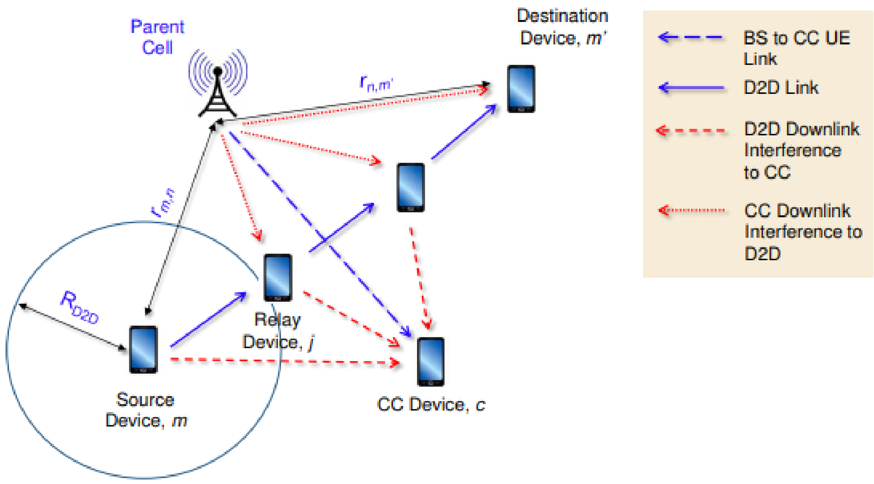

Figure 3.2: Case 2: D2D transmissions in the DL band (Source: [D2D45]).

Also, α and λ respectively represent the pathloss coefficient on both types of links and the frequency dependent pathoss. Finally, a summary of the interference scheme can be seen on Table 3.1 for single-hop D2D communications. The proposition (see Section 3.2) that best matches a given source of interference is highlighted if it is indeed a source of interference and left empty otherwise.

			Interferers					
			CC UEs		D2D UEs		BSs	
			Intra-cell	Inter-cell	Intra-cell	Inter-cell	Intra-cell	Inter-cell
Case 1	CC comm.	UL		3.2.2	3.2.3			
		DL						3.2.2
	D2D comm.		3.2.3			3.2.2		
Case 2	CC comm.	UL		3.2.2				
		DL			3.2.3			3.2.2
	D2D comm.					3.2.2	3.2.3	

Table 3.1: Interference scheme.

3.2 General computations

As already mentioned, the useful link is here assumed to be affected by Rician fading h which is usually described by the K factor. It is worth mentioning that this factor is the ratio between the power in the direct path and the power in the other, scattered, paths. Knowing $|h| \sim$ Rice(K) and supposing q = $|h|^2$, it can be shown that q $\sim$ non-central χ^2 and its PDF is given by:

$$f_Q(q) = \frac{(K+1)e^{-K}}{\overline{q}} \exp\left(\frac{-(K+1)q}{\overline{q}}\right) I_0\left(\sqrt{\frac{4K(K+1)q}{\overline{q}}}\right) \tag{3.3}$$

where $I_0(\cdot)$ is the zeroth order modified Bessel function of the first kind.

Assuming $\overline{q} = K+1$ and using a series expansion for $I_0(\cdot)$ given in [Misc67], it can be rewritten as

$$f_Q(q) = \exp\left(-K-q\right) \sum_{k=0}^{\infty} \frac{(Kq)^k}{(k!)^2} \tag{3.4}$$

However, this last expression has no physical sense as the fading power gain would shift with an higher value of K as it can be seen in Figure 3.4. Therefore, the PDF of $g = \frac{q}{K+1}$ is used instead. As g is a monotonic function of q, a simple change of variable can be used to provide the following expression:

$$f_G(g) = (K+1)\exp\left(-K-(K+1)g\right) \sum_{k=0}^{\infty} \frac{\left(K(K+1)g\right)^k}{(k!)^2} \tag{3.5}$$

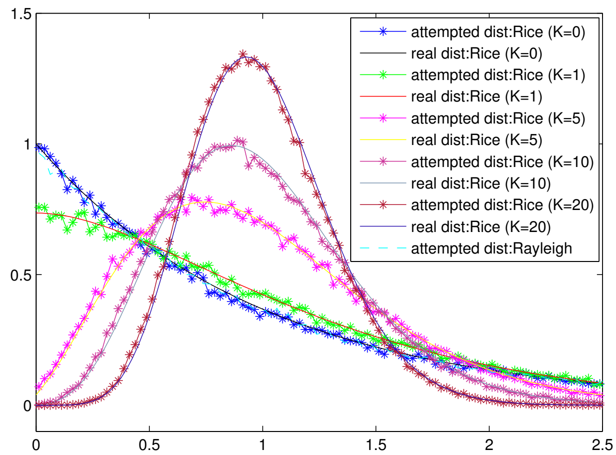

Figure 3.3: PDF of q: attempted dist. based on 100000 randomly generated channels.

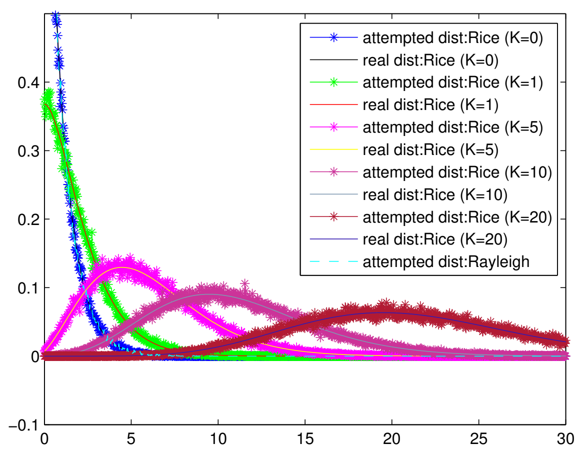

Figure 3.4: PDF of g: attempted dist. based on 100000 randomly generated channels.

The attempted distributions were drawn knowing $G = \frac{X^2+Y^2}{K+1}$ where $X \sim N\left(\sqrt{K}cos(C), \sqrt{1/2}\right)$ and $X \sim N\left(\sqrt{K}sin(C), \sqrt{1/2}\right)$,$\forall C \in \mathbb{R}$.
[Misc67] also shows that:

$$B\int x^n \exp(ax)dx = B\exp(ax)\left(\frac{x^n}{a} + \sum_{k=1}^{n}(-1)^k \frac{n(n-1)\dots(n-k+1)}{a^{k+1}}x^{n-k}\right) \tag{3.6}$$

Using equation 3.6, it can then be shown that the CDF is as follows:

$$F_G(g) = 1 - \sum_{k=0}^{\infty}\sum_{j=0}^{k}\mathcal{A}_{jk}\left((K+1)g\right)^{k-j} e^{-(K+1)g} \tag{3.7}$$

where

$$\mathcal{A}_{jk} = \frac{K^k}{(k!)^2}e^{-K}j!\binom{k}{j}$$

In the following mathematical developments, the following notations will be used: "link" refers to the link of interest and "int" to the interferers. Also, link and int ∈ {CC,D2D,BS}.

Proposition 3.2.1. Under Rician fading on the studied link, the coverage probability in the t-link (t ∈ {UL,DL}) is given by:

$$P\left(\gamma_{x,y}^t > \xi, \alpha\right) = \sum_{k=0}^{\infty}\sum_{j=0}^{k}\mathcal{A}_{jk}\left(Tr_{x,y}^{\alpha}\right)^{k-j}(-1)^{k-j}\left.\frac{\partial^{k-j}\mathcal{L}_I(s,\alpha)}{\partial^{k-j}s}\right|_{s=Tr_{x,y}^{\alpha}}$$

where

$$T = \frac{\xi(K+1)}{\lambda P_{\text{link}}} \tag{3.8}$$

Proof. As for equation 2.4, it can be computed by means of the following equalities:

$$\begin{aligned}
P\left(\gamma_{x,y}^t > \xi, \alpha\right) &= P\left(\frac{g_{x,y}P_{\text{link}}\lambda r_{x,y}^{-\alpha}}{W+I} > \xi\right)\\
&\overset{(1)}{=} P\left(\frac{g_{x,y}P_{\text{link}}\lambda r_{x,y}^{-\alpha}}{I} > \xi\right)\\
&= 1 - P\left(g_{x,y} < \frac{\xi I r_{x,y}^{\alpha}}{P_{\text{link}}\lambda}\right)\\
&= 1 - \int_i F_G(g)|_{\frac{i\xi r_{x,y}^{\alpha}}{\lambda P_{\text{link}}}} f_I(i)di\\
&= 1 - \int_i f_I(i)di + \int_i \left[\sum_{k=0}^{\infty}\sum_{j=0}^{k}\mathcal{A}_{jk}\left((K+1)g\right)^{k-j}e^{-(K+1)g}\right]\Bigg|_{g=i\frac{\xi r_{x,y}^{\alpha}}{\lambda P_{\text{link}}}} f_I(i)di\\
&\overset{(2)}{=} \int_i \left[\sum_{k=0}^{\infty}\sum_{j=0}^{k}\mathcal{A}_{jk}\left((K+1)g\right)^{k-j}e^{-(K+1)g}\right]\Bigg|_{g=i\frac{\xi r_{x,y}^{\alpha}}{\lambda P_{\text{link}}}} f_I(i)di\\
&\overset{(3)}{=} \sum_{k=0}^{\infty}\sum_{j=0}^{k}\mathcal{A}_{jk}\left(Tr_{x,y}^{\alpha}\right)^{k-j}\mathbb{E}\left[I^{k-j}\exp(-Tr_{x,y}^{\alpha}I)\right]\\
&\overset{(4)}{=} \sum_{k=0}^{\infty}\sum_{j=0}^{k}\mathcal{A}_{jk}\left(Tr_{x,y}^{\alpha}\right)^{k-j}(-1)^{k-j}\left.\frac{\partial^{k-j}\mathcal{L}_I(s,\alpha)}{\partial^{k-j}s}\right|_{s=Tr_{x,y}^{\alpha}}
\end{aligned} \tag{3.9}$$

(1) is obtained by neglecting the noise, (2) comes from the fact that the integral over all possible values of a PDF is always equal to 1, (3) is achieved by supposing $T = \frac{\xi(K+1)}{\lambda P_{\text{link}}}$ and by using the definition of the expectation and (4) follows from the definition of the Laplace transform. □

Two different hypotheses that are depicted in Figure 3.24 are considered in this document to match as much as possible the different types of communications:

- **Hypothesis 1**: interferers are at least at the same distance from the receiver than the transmitter.
- **Hypothesis 2**: interferers can be at any distance from the receiver.

The computations specific to the Laplacian of the interference for hypothesis 1 are inspired by [SG10] and for hypothesis 2 by [SG5]. Interferers are here supposed to follow a PPP Φ_{int} of intensity Λ_{int}.

Proposition 3.2.2 (Laplacian transform under hypothesis 1)**.** Let w be the integration variable. Under Rician fading on the studied link, the Laplacian transform of the interference is given by:

$$\mathcal{L}_I(s,\alpha) = \exp\left(-2\pi\Lambda_{\text{int}}\left[\frac{1}{2}t^2{}_2F_1\left(1,\frac{2}{\alpha};\frac{\alpha+2}{\alpha};\frac{-w^\alpha}{sP_{\text{int}}\lambda}\right)\right]_{w=r_{x,y}}^{w=\infty}\right) \tag{3.10}$$

where ${}_2F_1(\cdot)$ is the hypergeometric function.

Proof. It can be computed by means of the following equalities:

$$\begin{aligned}
\mathcal{L}_I(s,\alpha) &= \int_0^\infty \exp(-sI) f_I(I|r_{x,y}) dI \\
&\overset{(1)}{=} \int_{r_{x,y}}^\infty \int_0^\infty \exp\left(-s\sum_{\substack{\text{int}\in\Phi_{\text{int}}\\ \text{int}\neq x}} g_i P_{\text{int}}\lambda r_i^{-\alpha}\right) f_G(g_i) f_R(r_i) dg_i dr_i \\
&\overset{(2)}{=} \int_{r_{x,y}}^\infty \prod_{\substack{\text{int}\in\Phi_{\text{int}}\\ \text{int}\neq x}} \int_0^\infty \exp\left(-sg_i P_{\text{int}}\lambda r_i^{-\alpha}\right)\exp(-g_i) dg_i f_R(r_i) dr_i \\
&= \int_{r_{x,y}}^\infty \prod_{\substack{\text{int}\in\Phi_{\text{int}}\\ \text{int}\neq x}} \frac{1}{1+sP_{\text{int}}\lambda r_i^{-\alpha}} f_R(r_i) dr_i \\
&\overset{(3)}{=} \exp\left(\int_{\mathbb{R}^2} \Lambda_{\text{int}}\left[\frac{1}{1+sP_{\text{int}}\lambda r_i^{-\alpha}} - 1\right] dr_i\right) \\
&\overset{(4)}{=} \exp\left(\int_{r_{x,y}}^\infty -2\pi\Lambda_{\text{int}} \frac{sP_{\text{int}}\lambda w^{-\alpha}}{1+sP_{\text{int}}\lambda w^{-\alpha}} ldl\right) \\
&= \exp\left(-2\pi\Lambda_{\text{int}}\left[\frac{1}{2}t^2{}_2F_1\left(1,\frac{2}{\alpha};\frac{\alpha+2}{\alpha};\frac{-w^\alpha}{sP_{\text{int}}\lambda}\right)\right]_{w=r_{x,y}}^{w=\infty}\right)
\end{aligned} \tag{3.11}$$

(1) follows from hypothesis 1, (2) is obtained by supposing Rayleigh-affected interferers, (3) comes from Theorem 2.1.1, (4) comes from the conversion from cartesian to polar coordinates as mentioned in [SG10]. □

Note that if $\alpha = 2$, the integral in Proposition 3.2.2 is divergent. For sake of mathematical tractability, the special case $\alpha = 4$ will be considered in the rest of computations:

$$\alpha = 4 \rightarrow \quad w^2{}_2F_1\left(1,\frac{1}{2};\frac{3}{2};\frac{-w^4}{sP_{\text{int}}\lambda}\right) \quad = \quad \sqrt{sP_{\text{int}}\lambda}\arctan\left(\frac{w^2}{\sqrt{sP_{\text{int}}\lambda}}\right) \tag{3.12}$$

However, a more complex case that will not be analyzed in this document could be:

$$\begin{aligned}
\alpha = 3 \rightarrow \quad l^2{}_2F_1\left(1,\frac{1}{2};\frac{3}{2};\frac{-w^4}{sP_{\text{int}}\lambda}\right) &= \frac{1}{3}\Bigg((sP_{\text{int}}\lambda)^{2/3}\Bigg(-2\sqrt{3}\arctan\Bigg(\frac{1-\frac{2w}{\sqrt[3]{sP_{\text{int}}\lambda}}}{\sqrt{3}}\Bigg) \\
&- 2\ln\left(\sqrt[3]{sP_{\text{int}}\lambda}+w\right) + \ln\left((sP_{\text{int}}\lambda)^{2/3} - \sqrt[3]{sP_{\text{int}}\lambda}w + w^2\right)\Bigg)\Bigg)
\end{aligned} \tag{3.13}$$

In addition, assuming a function f(x), it can be shown that the n^{th} derivative of $\exp(f(x))$ is given by:

$$\frac{\partial^n \mathcal{L}_I(s,4)}{\partial^n s} = \exp(f(x)) \sum_{l=0}^{n} \sum_{i=0}^{l} \frac{(-1)^i f(x)^i}{i!(l-i)!} \frac{\partial^n f(x)^{l-i}}{\partial^n s} \tag{3.14}$$

If α is fixed to 4, the following expression can be obtained:

$$\begin{aligned}
\mathcal{L}_I(s,4) &= \exp\left(-\pi\Lambda_{\text{int}}\left[\sqrt{sP_{\text{int}}\lambda}\arctan\left(\frac{w^2}{\sqrt{sP_{\text{int}}\lambda}}\right)\right]_{w=r_{x,y}}^{w=\infty}\right) \\
&= \exp\left(-\pi\Lambda_{\text{int}}\sqrt{sP_{\text{int}}\lambda}\left(\frac{\pi}{2} - \arctan\left(\frac{r_{x,y}^2}{\sqrt{sP_{\text{int}}\lambda}}\right)\right)\right) \\
&\overset{(1)}{=} \exp\left(-\pi\Lambda_{\text{int}}\sqrt{sP_{\text{int}}\lambda}\arctan\left(\frac{\sqrt{sP_{\text{int}}\lambda}}{r_{x,y}^2}\right)\right) \\
&\overset{(2)}{=} \exp\left(-\mathcal{B}(\text{int})\sqrt{s}\arctan\left(\frac{\sqrt{s}}{\mathcal{C}(\text{int})r_{x,y}^2}\right)\right)
\end{aligned} \tag{3.15}$$

where (1) is computed knowing $\frac{\pi}{2} - \arctan(x) = \arctan\left(\frac{1}{x}\right)$ for x > 0 and $\frac{r_{x,y}^2}{\sqrt{sP_{\text{int}}\lambda}}$ always > 0 and (2) is obtained by supposing $\mathcal{B}(\text{int}) = \pi\Lambda_{\text{int}}\sqrt{P_{\text{int}}\lambda}$ and $\mathcal{C}(\text{int}) = \frac{1}{\sqrt{P_{\text{int}}\lambda}}$.

Replacing T by its value, using equations 3.14 and 3.15 and Proposition 3.2.1, the following expression is obtained:

$$P\left(\gamma_{x,y}^t > \xi, 4\right) = \sum_{k=0}^{\infty}\sum_{j=0}^{k}\sum_{l=0}^{k-j}\sum_{i=0}^{l} \mathcal{D}_{iljk}(\text{int},\text{link})\mathcal{F}_{li}(\text{int},\text{link},x,y,k-j)\exp\left(-\pi\mathcal{E}(\text{int},\text{link})r_{x,y}^2\right) r_{x,y}^{2i+4(k-j)} \tag{3.16}$$

where

$$\begin{aligned}
\mathcal{D}_{iljk}(\text{int},\text{link}) &= \mathcal{A}_{jk}(-1)^{k-j+i}\frac{\left(-\pi\Lambda_{\text{int}}\sqrt{\lambda P_{\text{int}}}\arctan\left(\sqrt{\frac{\xi(K+1)P_{\text{int}}}{P_{\text{link}}}}\right)\right)^i}{i!(l-i)!}\left(\frac{\xi(K+1)}{\lambda P_{\text{link}}}\right)^{\frac{i}{2}+k-j} \\
\mathcal{E}(\text{int},\text{link}) &= \Lambda_{\text{int}}\sqrt{\frac{\xi(K+1)P_{\text{int}}}{P_{\text{link}}}}\arctan\left(\sqrt{\frac{\xi(K+1)P_{\text{int}}}{P_{\text{link}}}}\right) \\
\mathcal{F}_{li}(\text{int},\text{link},x,y,n) &= \left.\frac{\partial^n\left(-\mathcal{B}(\text{int})\sqrt{s}\arctan\left(\frac{\sqrt{s}}{\mathcal{C}(\text{int})r_{x,y}^2}\right)\right)^{l-i}}{\partial^n s}\right|_{s=\frac{\xi(K+1)}{\lambda P_{\text{link}}}r_{x,y}^4}
\end{aligned}$$

As it can be seen, no closed-form equation for the n^{th} derivative of the LT under hypothesis 1 can be found and this last expression will have to be solved numerically. This can also be done using Taylor approximations as it will be shown in the following sections.

Proposition 3.2.3 (Laplacian transform under hypothesis 2)**.** Under Rician fading on the studied link, the Laplacian transform of the interference is given by:

$$\mathcal{L}_I(s) = \exp\left(-\mathcal{G}(\text{int})s^{\delta}\right)$$

where

$$\mathcal{G}(\text{int}) = \Lambda_{\text{int}}\pi\lambda^{\delta}P_{\text{int}}^{\delta}sinc^{-1}(\pi\delta)$$

Proposition 3.2.3 (continuation)

$$\delta = \frac{2}{\alpha} \tag{3.17}$$

Proof.

$$\begin{aligned}
\mathcal{L}_I(s) &= \mathbb{E}\left[\prod_{\substack{\text{int}\in\Phi_{\text{int}}\\ \text{int}\neq x}} \exp\left(-s g_{\text{int},y} P_{\text{int}} \lambda ||\text{int}-x||^{-\alpha}\right)\right] \\
&\overset{(1)}{=} \mathbb{E}\left[\prod_{\substack{\text{int}\in\Phi_{\text{int}}\\ \text{int}\neq x}} \exp\left(-s g_{\text{int},y} P_{\text{int}} \lambda ||\text{int}||^{-\alpha}\right)\right] \\
&\overset{(2)}{=} \mathbb{E}\left[\prod_{r\in\Phi_r} \exp\left(-s g_{\text{int},y} P_{\text{int}} \lambda r^{-\alpha}\right)\right] \\
&\overset{(3)}{=} \exp\left(-\int_0^\infty \mathbb{E}_g\left[1-\exp\left(-s g_{\text{int},y} P_{\text{int}} \lambda r^{-\alpha}\right)\right] 2\pi\Lambda_{\text{int}} r dr\right) \\
&\overset{(4)}{=} \exp\left(-\pi\Lambda_{\text{int}} \mathbb{E}\left[g_{\text{int},y}^{\delta}\right] \Gamma\left(1-\delta\right) s^{\delta}\lambda^{\delta} P_{\text{int}}^{\delta}\right) \\
&\overset{(5)}{=} \exp\left(-\pi\Lambda_{\text{int}} \Gamma(1+\delta)\Gamma\left(1-\delta\right) s^{\delta}\lambda^{\delta} P_{\text{int}}^{\delta}\right) \\
&\overset{(6)}{=} \exp\left(-\pi\Lambda_{\text{int}} \lambda^{\delta} P_{\text{int}}^{\delta} sinc^{-1}\left(\pi\delta\right) s^{\delta}\right)
\end{aligned}$$

(1) is obtained by considering x at the origin. Let's $\Phi_r \triangleq \{r = ||\text{int}||\}$ which is an inhomogeneous PPP with intensity $\lambda(r) = \Lambda_{\text{int}} c_d d r^{d-1}$ where c_d is the d-dimensional unit ball. Supposing d=2 in our case, we get $\lambda(r) = 2\pi\Lambda_{\text{int}} r$.(2) follows from this last supposition and from hypothesis 2, (3) comes from Theorem 2.1.1, (4) is proven on page 156 in [SG6]. (5) is explained by the following computations as the interferers are assumed to be Rayleigh-affected.

$$\mathbb{E}\left[g_{\text{int},y}^{\delta}\right] = \int_0^\infty g^{\delta}\exp\left(-g\right) dg = \int_0^\infty g^{(\delta+1)-1}\exp\left(-g\right) dg = \Gamma(\delta+1)$$

(6) comes from the following properties of the Gamma function: $\Gamma(a+1) = a\Gamma(a)$ and $\Gamma(z)\Gamma(1-z) = \frac{\pi}{sin(\pi z)}$. ☐

Using Wolfram Alpha, it can then be shown that the n^{th} derivative of the Laplacian is given by:

$$\frac{\partial^n \mathcal{L}_I(s)}{\partial^n s} = s^{-n}\exp\left(-\mathcal{G}(\text{int})s^{\delta}\right)\sum_{l=0}^{n}\sum_{i=0}^{l}\frac{(-1)^i(-\mathcal{G}(\text{int})s^{\delta})^l\left(1-\delta i+\delta l-n\right)_n}{i!(l-i)!} \tag{3.18}$$

As it can observed, this last expression can be adapted to any value of α>2. To stay is the same vein as for hypothesis 1, α will be assumed to be equal to 4 in the following computations.

As a consequence, replacing T by its value, expression 3.2.1 becomes for $\alpha = 4$:

$$P\left(\gamma_{x,y}^t > \xi, 4\right) = \sum_{k=0}^{\infty}\sum_{j=0}^{k}\sum_{l=0}^{k-j}\sum_{i=0}^{l}\mathcal{H}_{iljk}(\text{link}) r_{x,y}^{2l}\exp\left(-\mathcal{G}(\text{int})\sqrt{\frac{\xi(K+1)}{\lambda P_{\text{link}}}} r_{x,y}^2\right) \tag{3.19}$$

where

$$\mathcal{H}_{iljk}(\text{link}) \quad = \quad \mathcal{A}_{jk}(-1)^{k-j+i}\left(\frac{\xi(K+1)}{\lambda P_{\text{link}}}\right)^{\frac{l}{2}}(-\mathcal{G}(\text{int}))^l\frac{\left(1-\frac{i}{2}+\frac{l}{2}-(k-j)\right)_{k-j}}{i!(l-i)!}$$

A good point of this last expression is the fact that is closed-form unlike its counterpart for far interferers.

3.3 Conventional cellular outage probability

At first, this section disregards the D2D communications in order for the reader to see the impact of adding D2D communications in a given network. The interferers in the UL are then only considered as the co-channel cellular users that are supposed to be distributed following an HPPP of intensity Λ_{cc} defined in $\mathbb{R}^2$. For the DL, the interferers are only considered as the adjacent BSs that are distributed following an HPPP of intensity Λ_{bs} defined in $\mathbb{R}^2$. Proposition 3.2.2 best matches those types of interferers as they are representing inter-cell sources of interference. This explains Table 3.2 that will be used to fill the parameters in the equation 3.16.

t	int	link	$r_{x,y}$	$\gamma_{x,y}^{t}$
UL	CC	CC	$r_{m,n}$	$\gamma_{m,n}^{UL}$
DL	BS	BS	$r_{n,m'}$	$\gamma_{n,m'}^{DL}$

Table 3.2: Parameters to fill in equation 3.16.

Proposition 3.3.1. The outage probability of the CC communication between CC UE m and CC UE m' via their closest BS n is given by :

$$P_{CC,out} = 1 - P\left(\gamma_{m,n}^{UL} > \xi, \alpha\right) P\left(\gamma_{n,m'}^{DL} > \xi, \alpha\right) \tag{3.20}$$

Proof. The proof is trivial. □

Proposition 3.3.2. Let $a = k - j$. The expectation of the outage probability of the CC communication between CC UE m and CC UE m' via their closest BS n for $\alpha = 4$ is given by :

$$\mathbb{E}\left[P_{CC,out}\right] = 1 - \mathbb{E}\left[P\left(\gamma_{m,n}^{UL} > \xi, 4\right)\right] \mathbb{E}\left[P\left(\gamma_{n,m'}^{DL} > \xi, 4\right)\right]$$

where

$$\mathbb{E}\left[P\left(\gamma_{m,n}^{UL} > \xi, 4\right)\right] = \sum_{k=0}^{\infty}\sum_{j=0}^{k}\sum_{l=0}^{k-j}\sum_{i=0}^{l} 2\pi\Lambda_b \mathcal{D}_{iljk}(CC, CC)\mathcal{I}_{iljk}(CC, CC, m, n)$$

$$\mathbb{E}\left[P\left(\gamma_{n,m'}^{DL} > \xi, 4\right)\right] = \sum_{k=0}^{\infty}\sum_{j=0}^{k}\sum_{l=0}^{k-j}\sum_{i=0}^{l} 2\pi\Lambda_b \mathcal{D}_{iljk}(BS, BS)\mathcal{I}_{iljk}(BS, BS, n, m')$$

$$\mathcal{I}_{iljk}(\text{int}, \text{link}, x, y) = \int_0^{\infty} \mathcal{F}_{li}(\text{int}, \text{link}, x, y, a) \exp\left(-\pi(\mathcal{E}(\text{int}, \text{link}) + \Lambda_b) r_{x,y}^2\right) r_{x,y}^{2i+4a+1} dr_{x,y} \tag{3.21}$$

Proof. In the following computations, $\mathbb{E}_{UL}$ will refer to $\mathbb{E}\left[P\left(\gamma_{m,n}^{UL} > \xi, \alpha\right)\right]$, $\mathbb{E}_{DL}$ to $\mathbb{E}\left[P\left(\gamma_{m,n}^{DL} > \xi, \alpha\right)\right]$ and $\sum_{\times 4}$ to $\sum_{k=0}^{\infty}\sum_{j=0}^{k}\sum_{l=0}^{k-j}\sum_{i=0}^{l}$

$$\begin{aligned}\mathbb{E}\left[P_{CC,out}\right] &= \mathbb{E}\left[1 - P\left(\gamma_{m,n}^{UL} > \xi, \alpha\right) P\left(\gamma_{n,m'}^{DL} > \xi, \alpha\right)\right] \\ &\overset{(1)}{=} 1 - \mathbb{E}_{UL}\mathbb{E}_{DL}\end{aligned} \tag{3.22}$$

(1) comes from the fact that $r_{m,n}$ and $r_{n,m'}$ are indepedant random variables. Then, supposing $a = k - j$:

$$\begin{aligned}\mathbb{E}_{UL} &\overset{(2)}{=} \sum_{\times 4} \mathcal{D}_{iljk}(CC, CC)\mathbb{E}\left[\mathcal{F}_{li}(CC, CC, m, n, a) \exp\left(-\pi\mathcal{E}(CC, CC) r_{m,n}^2\right) r_{m,n}^{2i+4a}\right] \\ &\overset{(3)}{=} \sum_{\times 4} 2\pi\Lambda_b \mathcal{D}_{iljk}(CC, CC) \int_0^{\infty} \mathcal{F}_{li}(CC, CC, m, n, a) \exp\left(-\pi(\mathcal{E}(CC, CC) + \Lambda_b) r_{m,n}^2\right) r_{m,n}^{2i+4a+1} dr_{m,n}\end{aligned}$$

$$\mathbb{E}_{UL} \overset{(3)}{=} \sum_{\times 4} 2\pi \Lambda_b \mathcal{D}_{iljk}(CC, CC)\mathcal{I}_{iljk}(CC, CC, m, n) \quad (3.23)$$

(2) comes from equation 3.16 and Table 3.2 , (3) follows from expression 3.1 and (4) arises from the definition of $\mathcal{I}_{iljk}$ (CC,CC,m,n).
The proof is finished by using a similar approach to show that:

$$\mathbb{E}_{DL} = \sum_{\times 4} 2\pi \Lambda_b \mathcal{D}_{iljk}(BS, BS)\mathcal{I}_{iljk}(BS, BS, n, m') \quad (3.24)$$

□

3.4 Integration of device-to-device communications

This section is about integrating D2D communications into the previously studied network. Interfering D2D UEs are here distributed following an HPPP of intensity Λ_{d2d} defined in $\mathbb{R}^2$. As mentioned in [D2D45], the D2D communications underlaying cellular network can be considered as a temporary 2-tier heterogeneous network. In other words, we suppose two independent sources giving respectively rise to interference I_1 and I_2. By definition, I_1 will represent the source of interference potentially closer to receiver than the transmitter itself (see Proposition 3.2.3) and I_2 the source of interference at least at the same distance from the receiver that the transmitter (see Proposition 3.2.2).

Proposition 3.4.1. The coverage probability at the distance $r_{x,y}$ from a transmitting node x of the v^{th} tier (v ∈ {CC,D2D,BS}) in the t-link (t ∈ {UL,DL,D2D}) is given by:

$$P\left(\gamma^t_{v,x,y} > \xi, \alpha, r_{x,y}\right) = \sum_{k=0}^{\infty}\sum_{j=0}^{k}\sum_{p=0}^{k-j} \mathcal{A}_{jk}\left(Tr^{\alpha}_{x,y}\right)^{k-j} \binom{k-j}{p} (-1)^{k-j} \left.\frac{\partial^p \mathcal{L}_{I_1}(s,\alpha)}{\partial^p s}\right|_{Tr^{\alpha}_{x,y}} \left.\frac{\partial^{k-j-p} \mathcal{L}_{I_2}(s,\alpha)}{\partial^{k-j-p} s}\right|_{Tr^{\alpha}_{x,y}} \quad (3.25)$$

Proof. In the following proof, P will refer to $P\left(\gamma^t_{v,x,y} > \xi, \alpha, r_{x,y}\right)$.

$$\begin{aligned}
P &= \sum_{k=0}^{\infty}\sum_{j=0}^{k} \mathcal{A}_{jk}\left(Tr^{\alpha}_{x,y}\right)^{k-j} \mathbb{E}\left[I^{k-j}\exp(-TI)\right] \\
&= \sum_{k=0}^{\infty}\sum_{j=0}^{k} \mathcal{A}_{jk}\left(Tr^{\alpha}_{x,y}\right)^{k-j} \mathbb{E}\left[(I_1+I_2)^{k-j}\exp(-T(I_1+I_2))\right] \\
&\overset{(1)}{=} \sum_{k=0}^{\infty}\sum_{j=0}^{k} \mathcal{A}_{jk}\left(Tr^{\alpha}_{x,y}\right)^{k-j} \mathbb{E}\left[\left[\sum_{p=0}^{\infty} I_1^p I_2^{k-j-p}\binom{k-j}{p}\right]\exp(-T(I_1+I_2))\right] \\
&\overset{(2)}{=} \sum_{k=0}^{\infty}\sum_{j=0}^{k} \mathcal{A}_{jk}\left(Tr^{\alpha}_{x,y}\right)^{k-j} \sum_{p=0}^{\infty}\binom{k-j}{p} \mathbb{E}\left[I_1^p\exp(-TI_1)\right]\mathbb{E}\left[I_2^{k-j-p}\exp(-TI_2)\right] \\
&\overset{(3)}{=} \sum_{k=0}^{\infty}\sum_{j=0}^{k}\sum_{p=0}^{k-j} \mathcal{A}_{jk}\left(Tr^{\alpha}_{x,y}\right)^{k-j}\binom{k-j}{p}(-1)^{k-j} \left.\frac{\partial^p \mathcal{L}_{I_1}(s,\alpha)}{\partial^p s}\right|_{Tr^{\alpha}_{x,y}} \left.\frac{\partial^{k-j-p} \mathcal{L}_{I_2}(s,\alpha)}{\partial^{k-j-p} s}\right|_{Tr^{\alpha}_{x,y}}
\end{aligned} \quad (3.26)$$

(1) is computed by means of the following series representation $(a+b)^c = \sum_{p=0}^{c} a^p b^{c-p}\binom{c}{p}$,(2) comes from the fact that I_1 and I_2 are independent sources of interference, (3) follows from the definition of the Laplace transform. □

A this point, two cases are distinguished to represent both CC communications and D2D communications. Those two cases are given in Propositions 3.4.2 and 3.4.3 and are shown to be mathematically complex. Therefore, this complexity will be discussed in a future section.

Proposition 3.4.2 (Coverage probability for CC UEs and BSs)**.** The expectation of coverage probability at the distance $r_{x,y}$ from a transmitting node x of the v^{th} tier (v ∈ {CC,BS}) in the t-link (t ∈ {UL,DL}) for α=4 is given by:

$$\mathbb{E}_R\left[P\left(\gamma^t_{v,x,y} > \xi, 4, r_{x,y}\right)\right] = 2\pi\Lambda_b \sum_{k=0}^{\infty}\sum_{j=0}^{k}\sum_{p=0}^{k-j}\sum_{l=0}^{p}\sum_{i=0}^{l}\sum_{l'=0}^{k-j-p}\sum_{i'=0}^{l'} \mathcal{J}_{i'l'ilpjk}(v, \text{int}_1, \text{int}_2)\times$$
$$\int_0^{\infty} \exp\left(-r^2_{x,y}\left(\mathcal{E}\left(\text{int}_2, v\right) + \mathcal{G}\left(\text{int}_1\right)\sqrt{\frac{\xi(K+1)}{P_v\lambda}} + \pi\Lambda_b\right)\right)\mathcal{F}_{l'i'}(\text{int}_2, v, x, y, k-j-p)r^b_{x,y}dr_{x,y}$$

where

$$\mathcal{J}_{i'l'ilpjk}(v, \text{int}_1, \text{int}_2) = \mathcal{A}_{jk}\binom{k-j}{p}(-1)^{k-j+i+i'}\frac{\left(-\mathcal{G}(\text{int}_1)\right)^l\left(1-\frac{i}{2}+\frac{l}{2}-p\right)_p}{i!(l-i)!i'!(l'-i')!}\times$$
$$\left(\frac{\xi(K+1)}{\lambda P_v}\right)^{k-j+\frac{l}{2}-p+\frac{i'}{2}}\left(-\pi\Lambda_{\text{int}_2}\arctan\left(\sqrt{\frac{\xi(K+1)P_{\text{int}_2}}{P_v}}\right)\right)^{i'}$$

$$b = 2i' + 2l - 4p + 1 + 4(k-j) \tag{3.27}$$

Proof. This can be proven by means of Propositions 3.2.2, 3.2.3 and 3.4.1 and equations 3.1. The mathematical developments are left to the reader. □

Proposition 3.4.3 (Coverage probability for D2D UEs)**.** The expectation of coverage probability at the distance $r_{x,y}$ from a transmitting node of the D2D tier (v = D2D) to another D2D UE (t=D2D) for α=4 is given by:

$$\mathbb{E}_R\left[P\left(\gamma^{D2D}_{D2D,x,y} > \xi, 4, r_{x,y}\right)\right] = \frac{2}{R^2_{max}}\sum_{k=0}^{\infty}\sum_{j=0}^{k}\sum_{p=0}^{k-j}\sum_{l=0}^{p}\sum_{i=0}^{l}\sum_{l'=0}^{k-j-p}\sum_{i'=0}^{l'} \mathcal{J}_{i'l'ilpjk}(D2D, \text{int}_1, \text{int}_2)\times$$
$$\int_0^{R_{max}} \exp\left(-r^2_{x,y}\left(\mathcal{E}\left(\text{int}_2, v\right) + \mathcal{G}\left(\text{int}_1\right)\sqrt{\frac{\xi(K+1)}{P_v\lambda}}\right)\right)\mathcal{F}_{l'i'}(\text{int}_2, v, x, y, k-j-p)r^b_{x,y}dr_{x,y} \tag{3.28}$$

Proof. This can be proven by means of Propositions 3.2.2, 3.2.3 and 3.4.1 and equation 3.2. The mathematical developments are left to the reader. □

The values for int_1, int_2 and v for a given case can be derived from Table 3.1. However, for the convenience of the the reader, the following table resumes the parameters to be filled in the previous expressions for the different cases.

		v	int_1	int_2
Case 1	CC comm. (modified UL)	CC	D2D	CC
	D2D comm.	D2D	CC	D2D
Case2	CC comm. (modified DL)	BS	D2D	BS
	D2D comm.	D2D	BS	D2D

Table 3.3: Parameters to fill in Proposition 3.4.2.

It can be seen that, when analyzing the modified CC communications, only the UL probability is modified in the first case and the DL probability in the second case.

3.4.1 Device-to-device outage probability

Proposition 3.4.4. The expectation of the outage probability of the D2D communication between D2D UE TX and D2D UE RX for $\alpha = 4$ is given by

$$\mathbb{E}\left[P_{D2D,out}\right] = 1 - \mathbb{E}_R\left[P\left(\gamma^{D2D}_{D2D,TX,RX} > \xi, 4, r_{TX,RX}\right)\right] \tag{3.29}$$

where $\mathbb{E}_R\left[P\left(\gamma_{D2D,TX,RX} > \xi, 4, r_{TX,RX}\right)\right]$ is computed by means of Proposition 3.4.3.

Proof. The proof is trivial. □

3.4.2 Impact on the conventional cellular outage probability

When introducing D2D communications in the previously studied network, either the UL coverage probability or the DL coverage probability is modified depending on the considered case (i.e. 1 or 2).This is due to the introduction of a new source of interference.

Proposition 3.4.5 (CC outage probability in case 1)**.** The modified expectation of the outage probability of the CC communication between CC UE m and CC UE m' via their closest BS n for α = 4 is given by :

$$\mathbb{E}\left[P_{CC,out}\right] = 1 - \mathbb{E}_R\left[P\left(\gamma^{UL}_{CC,m,n} > \xi, 4, r_{m,n}\right)\right]\mathbb{E}\left[P\left(\gamma^{DL}_{n,m'} > \xi, 4\right)\right] \tag{3.30}$$

where the two terms on the right side of the equation are respectively given by Propositions 3.4.2 and 3.3.2.

Proof. In case 1, the UL coverage probability is modified. The rest of the proof is trivial. □

Proposition 3.4.6 (CC outage probability in case 2)**.** The modified expectation of the outage probability of the CC communication between CC UE m and CC UE m' via their closest BS n for α = 4 is given by :

$$\mathbb{E}\left[P_{CC,out}\right] = 1 - \mathbb{E}_R\left[P\left(\gamma^{DL}_{BS,n,m'} > \xi, 4, r_{n,m'}\right)\right]\mathbb{E}\left[P\left(\gamma^{UL}_{m,n} > \xi, 4\right)\right] \tag{3.31}$$

where the two terms on the right side of the equation are respectively given by Propositions 3.4.2 and 3.3.2..

Proof. In case 2, the DL coverage probability is modified. The rest of the proof is trivial. □

3.5 Numerical results

The following results were obtained using the parameters in Table 3.4 unless specified otherwise.

Parameter	Symbol	Value
CC UEs density	Λ_c	50/km^2
D2D UEs density	Λ_d	20/km^2
BSs density	Λ_b	2/km^2
Co-channel CC UEs/D2D UEs/BSs density	$\Lambda_{cc}/\Lambda_{d2d}/\Lambda_{bs}$	1.27/km^2
BSs transmit power	P_{bs}	40W
CC/D2D UEs transmit power	P_{cc} / P_{d2d}	0.1W
pathloss coefficient	α	4
max. D2D link distance	R_{max}	0.1km

Table 3.4: Simulation parameters.

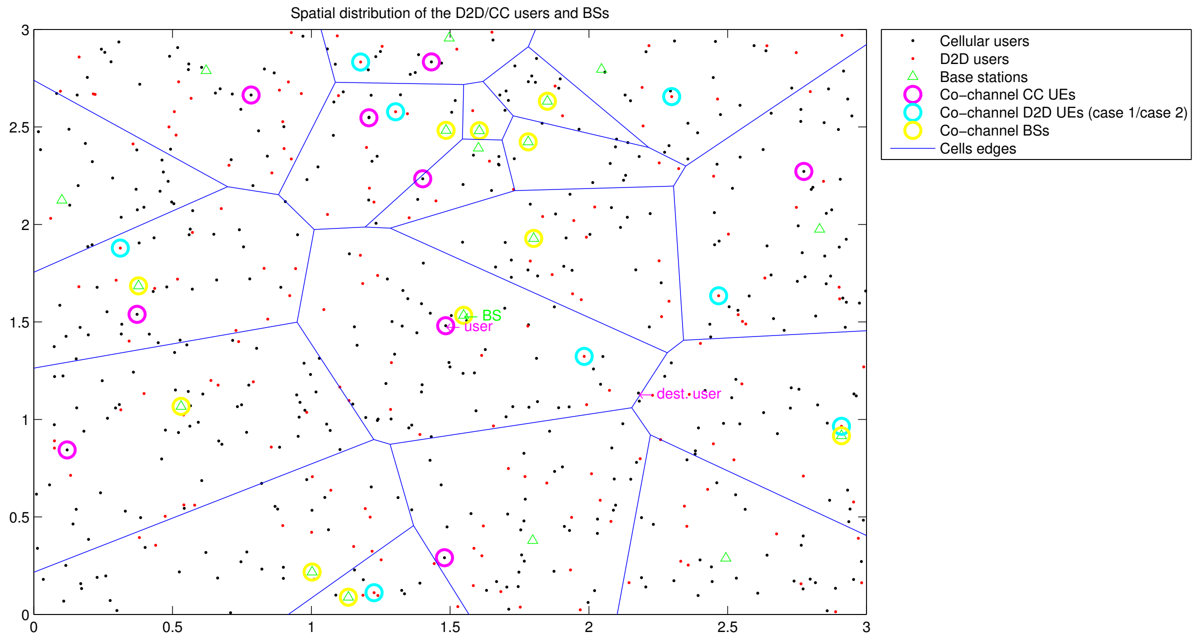

Figure 3.5: Spatial distribution of CC/D2D UEs and BSs over 4 square kilometres.

In our implementation, the respective interferers were randomly chosen among the overall BSs, CC UEs and D2D UEs in order to respect the interferers densities. Thanks to the thinning property, this approach can be said to result in a PPP as the overal BSs, CC UEs and D2D UEs were drawn using PPPs. Figure 3.5 represents a typical snapshot of the studied network. The studied CC UE in each realization of the network is always the most central one. This CC UE as well as its destination CC UE and its associated BS are incidentally higlighted on the picture.

When analyzing D2D communications, the considered user will logically be a D2D UE instead. Again, the most central D2D UE will be studied. As it can be seen in the picture, co-channel D2D UEs are the same for case 1 and case 2. This has no impact on the relevance of the results. In fact, this spatial configuration only respects the D2D density constraint. The difference between the two cases will be made in the computations which are based on that spatial configuration.

Throughout this section, different experiences will be made in order for the network manager to know how to fix different parameters like the BS transmit power and the density of BSs. Other experiences are then realized to help us understand how the studied network behaves in particular situations. When it is necessary, the analysis will be shown for an acceptable value of the SIR around 16 dB. Otherwise, this analysis will be based on smaller values of the SIR to highlight the impact of the different varying parameters. In fact, when going for too high values of the SIR, the problem of complete outage makes it impossible to observe anything, hence the need for further control mechanisms that will be presented in Section 3.5.4.

It is important to mention that the following analysis is done for the parameters fixed as in Table 3.4. Those parameters have been chosen in order to represent a possible network. However, for different parameters, the observations might be a little bit different. A more global analysis is not discussed here and is left for a future work. This is partly due to the program computation time which rendered an intensive study of the parameters prohibitive as discussed in Section 3.5.5.

Finally, it is necessary to insist on the difference between Λ_b and Λ_{bs}. The first one is the density of overall BSs while the second one is the density of interfering BSs.

3.5.1 Cellular outage probability without device-to-device communications

As it can be seen in the previous section, Propositions 3.3.2 and 3.4.2 both require the computation of an infinite sum. As this sum is supposed to converge after some time, the computations are stopped when the contribution of a given element of this sum to the global result becomes negligible. However, one common term of those two propositions, $\mathcal{F}_{li}(\text{int}, \text{link}, x, y, n)$, significantly increases the program computation time as it requires the computation of high-order derivatives of the function $f(x) = \left(-\mathcal{B}(\text{int})\sqrt{s}\arctan\left(\frac{\sqrt{s}}{\mathcal{C}(\text{int})r_{x,y}^2}\right)\right)^{l-i}$. An easy way to derivate this expression multiple times is to use the symbolic toolbox implemented in MATLAB and then to replace s by $\frac{\xi(K+1)}{\lambda P_{\text{link}}} r_{x,y}^4$ as defined in $\mathcal{F}_{li}(\text{int}, \text{link}, x, y, n)$. As this toolbox is not totally optimized, one could wait indefinitely to get any result.

In order to tackle that problem, the proposed mathematical model is simplified by using 6^{th} order Taylor approximations of the function $f(x)$ around the evaluation point $\frac{\xi(K+1)}{\lambda P_{\text{link}}} r_{x,y}^4$. This approach enables us to rewrite $f(x)$ as follows:

$$f(x) = c_6x^6 + c_5x^5 + c_4x^4 + c_3x^3 + c_2x^2 + c_1x + c_0$$

Due to space constraints, the c_i coefficients are not provided in this document but are easily found using the Taylor approximations formula. This trick enables us to only compute the six first derivatives while the higher-order ones are cancelled.

The final results for the average CC outage probability is shown in Figure 3.6. In addition, the contributions of each of the Taylor polynomial derivatives to the CC outage probability expectation are available in Table 3.5. As it can be seen, the studied model is pretty accurate when comparing it to the MC simulations. Nevertheless, it increasingly diverges from those simulations when increasing the Rice K factor and the SINR threshold ξ. This is due to the lack of precision of Taylor approximations as shown in Table 3.5. For example, for K=5 and ξ=1, the contribution of the 6^{th} derivative to the average CC outage derivative is still -0.0102 which is not negligible. This problem might become critical for interesting values of ξ around 16-18 dB. Observing the general trend of the contributions, it is normal to hope a better precision with higher-order Taylor approximations. Unfortunately, this also increases the program computation time to non acceptable waiting times. For this reason, the following results will be drawn despite this small lack of precision.
Moreover, the outage probabilities are already high for small values of the SINR threshold ξ. This does not bode well for acceptable values of this threshold. As a consequence, performance dependencies on a few parameters and particular implementation mechanisms will be studied in the next discussions in order to see how to fix this problem.

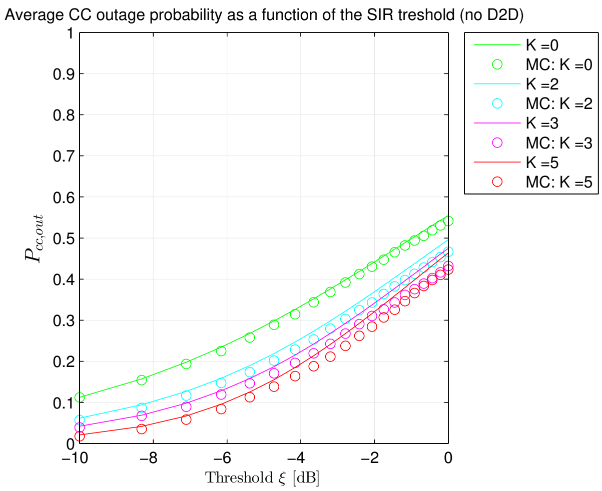

Figure 3.6: Average CC outage probability without D2D.

ξ		der. 4	der. 5	der. 6
0.1947	K = 2	-0.0019	-0.0003	-3.246e-05
	K = 5	-0.0313	-0.0131	-0.005
0.5263	K = 2	-0.0074	-0.0016	-0.0003
	K = 5	-0.0346	-0.018	-0.0089
1	K = 2	-0.008	-0.002	-0.0004
	K = 5	-0.0325	-0.0187	-0.0102

Table 3.5: Taylor polynomial derivatives contributions to the expectation of the CC outage probability.

3.5.2 Integration of device-to-device communications

CC outage probabilities

The final results for the average CC outage probabilities after the integration of D2D communications are shown in Figures 3.7 (case 1) and 3.8 (case 2). To allow the reader to see the impact on conventional cellular networks, the obtained results for both cases are compared to the case without D2D communications.

In case 1, D2D UEs are interfering with the considered CC UE for the UL part of the CC communication between the considered user and its associated BS. As CC UEs and D2D UEs are using the same transmit power (0,1W), the added interference on the cellular link is non-negligible, hence an higher outage probability.

In case 2, D2D UEs are competing with the associated BS for the DL part of the CC communication between the associated BS and the target CC UE. As the transmit power of the BS (40W) is strictly higher than the one of D2D UEs (0,1W), the added interference is negligible, hence a similar outage probability.

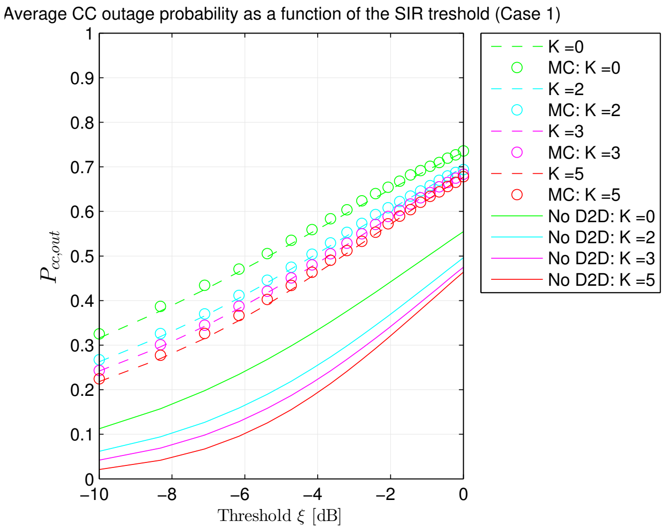

Figure 3.7: CC outage probability with D2D communications (case 1).

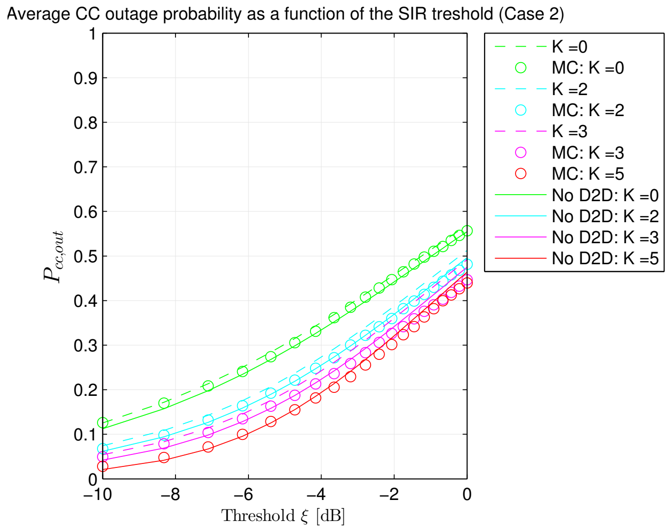

Figure 3.8: CC outage probability with D2D communications (case 2).

D2D outage probabilities

The final results for the average D2D outage probabilities are depicted in Figures 3.9 (case 1) and 3.10 (case 2). The reciprocal of the discussion on CC communications above can be used to justify an higher outage probability in case 2 for D2D communications when compared to case 1.

The outage probabilities values are proven to be highly acceptable especially if case 1 is chosen. This is however the case for a maximum D2D link of 100m as shown in Table 3.4. It will be shown in the future sections that increasing this maximum distance can lead to a completely different situation where the D2D communications are killed by the CC communications. This last observation will be demonstrated to be particularly applicable to case 2.

This brings us to a general trade-off between D2D communications performances and CC communications performances regarding the fixed parameters values. On the one hand, it is preferable for the D2D communications to be done in the DL band for an optimal average CC outage probability. On the other hand, it is better for the D2D communications to be done in the UL band for an optimal average D2D outage probability. Further investigations will be made in the next sections to strike a balance between both types of communications perfomances.

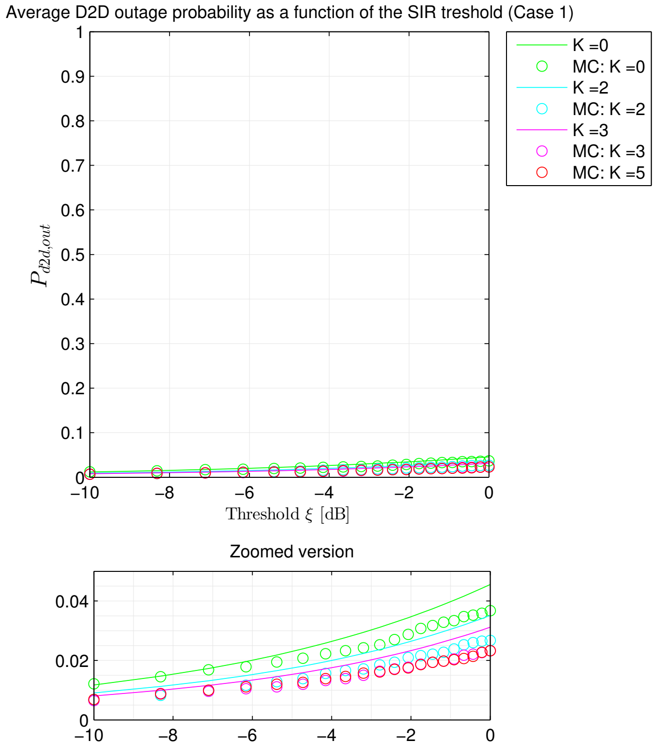

Figure 3.9: D2D outage probability (case 1).

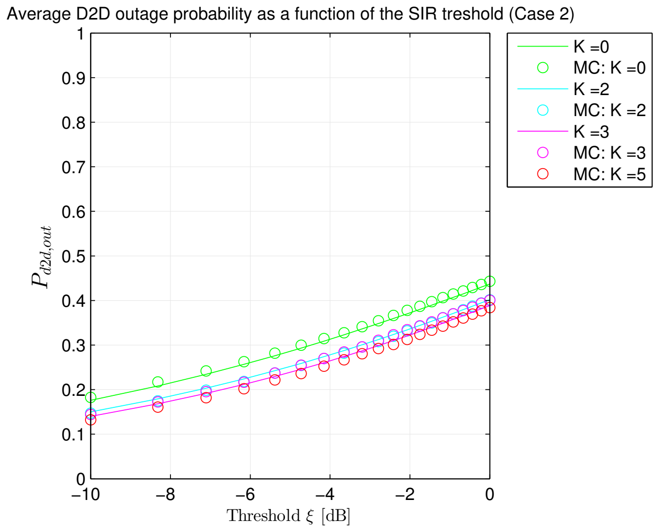

Figure 3.10: D2D outage probability (case 2).

3.5.3 Performance dependencies on different parameters

Reduction of interferers densities

In this section, the simultaneous reduction of the interferers densities (Λ_{cc},Λ_{d2d} and Λ_{bs}) from 1.27/km^2 to 0.1/km^2 will be studied. The goal of this study is just to show if acceptable outage probabilities can be achieved for realistic densities of interferers and for a acceptable value of the SIR (16 dB). It is worth mentioning that a situation where there is only 0.1 interferers per km^2 is very unlikely to happen and is only considered to illustrate to following discussion.

As it can be seen in Figure 3.11, even when reducing the interferers densities to unrealistic values, the average outage probability stays above 60% for CC communications in both cases. This can be explained by the fact that CC communications are always accepted as soon as they are inter-cell. This policy permits CC link distances sometimes going above 1km as it can be seen in Figure 3.5. At such distances, the link is strongly attenuated making it vulnerable to interfering links. In order to improve the average CC outage probability, one solution could be to densify the overall BSs to limit the link distances as it is done in the following subsection.

Regarding D2D communications, the accepted link distance is 100m. This limitation makes the outage probabilities significantly lower than for CC communications in the current configuration. However, D2D communications that are done in the DL band are still suffering from strong interference coming from BS making the outage probability unacceptable for realistic values of interferers densities.

Densification of bases stations under a constant frequency reuse factor

In this section, the densification of BSs under a constant frequency reuse factor is studied. Λ_b is here varied from 1.27/km^2 to 5/km^2 while Λ_{cc}, Λ_{d2d} and Λ_{bs} are kept at 0.635Λ_b.

It was proven by means of this experience that the reduction of the distance between the CC UE and its nearest BS is compensated by the increase of the interference to keep a constant frequency reuse factor. In fact, as BSs are densified, the useful BS and the sources of interference are both potentially moved

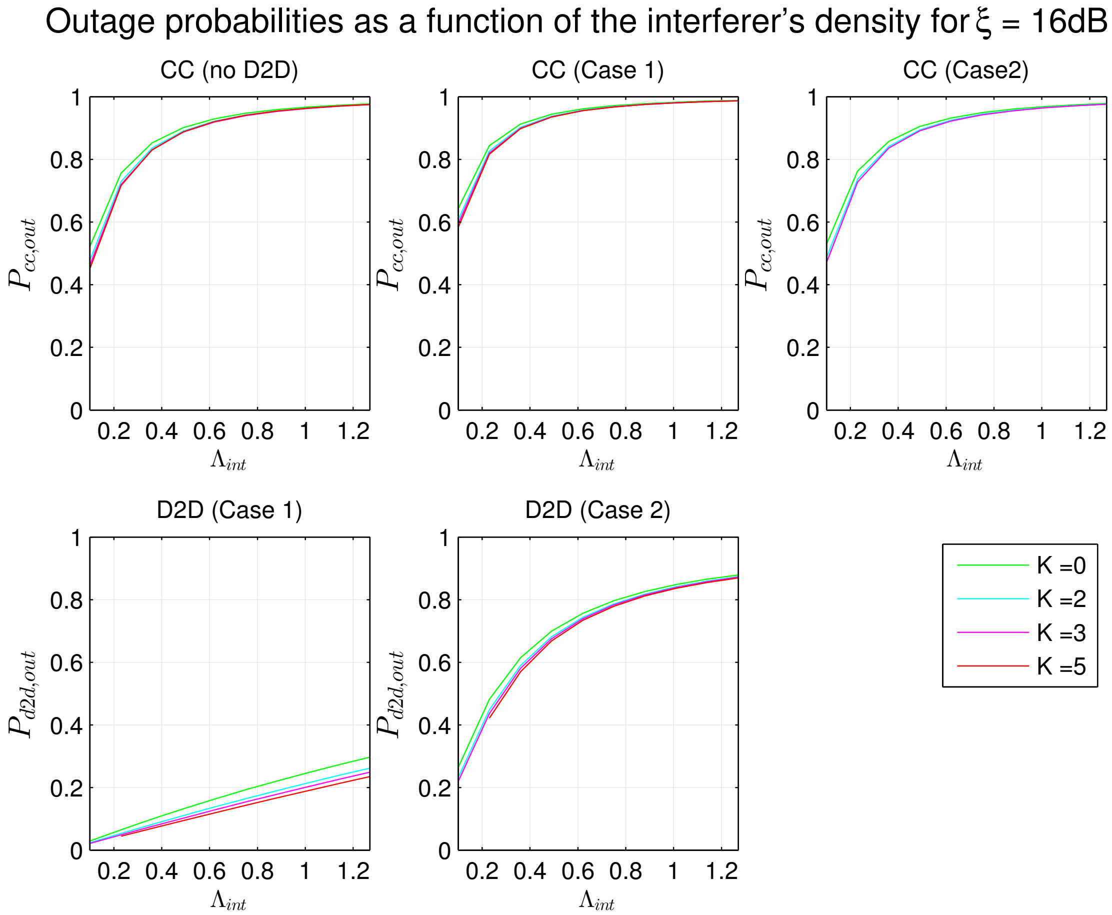

Figure 3.11: Reduction of overall interferers densities for ξ=16dB.

closer. As a consequence, there is no changes in the average CC outage probabilities.

The final average D2D outage probability in case 2 is depicted in Figure 3.12. As it can be observed, densifying BSs has here a negative impact on the average outage probability. This is because the D2D UE only sees the potential sources of interference (BSs) come closer as no BS is included in the D2D link.

The average CC outage probabilities can however be improved by densifying BSs at the condition that the frequency reuse factor is not kept constant as shown in Figure 3.13. This is done by varying only Λ_b, the density of overall BSs, without changing the interferers densities. Of course, this is possible only if there are sufficient spectral ressources to permit a lower frequency reuse factor.

Variation of the base stations transmit power

In this section, the BS transmit power P_{bs} is varied from 0.1W to 50W. It is important to mention that the typical macro BS transmit power generally goes from 20W to 69W [Misc66].

The variation of P_{bs} has logically no impact on D2D communications using the UL band as the BSs are not source of interference. As a consequence, the average D2D outage probability in case 1 stays constant when varying P_{bs}. For a different reason, the same observation can be made on the CC average outage probability in case 1. This is due to the fact that the transmit power of the BS involved in the useful link and the transmit powers of interfering BSs are equally changed. Of course, this last statement is only true if the noise is neglected. Without this assumption, increasing P_{bs} should result in a decrease of the outage probability.

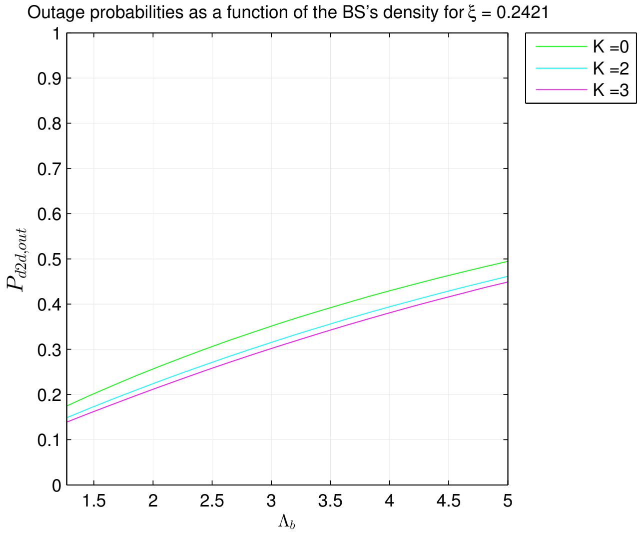

Figure 3.12: Average D2D outage probability in case 2 under a fixed frequency reuse factor.

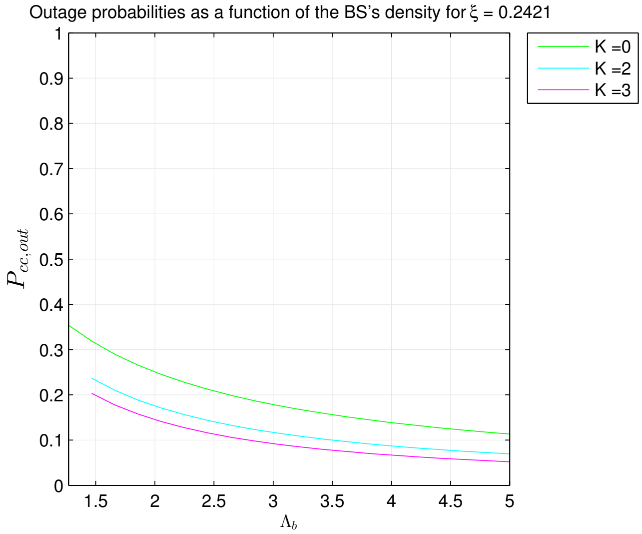

Figure 3.13: Average CC outage probability in case 2 under a varying frequency reuse factor.

The interesting results are shown in Figure 3.14 and 3.15 which respectively represent the average outage probability for $\xi = 0.2421$ for CC communications in case 2 and D2D communications in case 2. Those two figures highlight the trade-off between D2D communications and CC communications when D2D communications are done in the DL band. Starting from the right side of the figures (50W) and progressively decreasing P_{bs}, it can be observed that the D2D average outage probability (resp. CC) sligthly decreases (resp. increases) until it reaches a threshold where the reduction becomes more important. This threshold can be identified as the CC UE transmit power $P_{cc} = 0.1W$ meaning that P_{cc} and P_{bs} are equal. This point is also considered as the fairest point for both communications. Further reducing the BS transmit power then gives the advantage to D2D links. With those fixed parameters, one could say that the outage probability on D2D communications seems pretty acceptable even when $P_{bs} = 50W$. However, when increasing the maximum D2D link distance, this trade-off is proven to be of the utmost importance to avoid complete outage on D2D communications.

Variation of the device-to-device maximum link distance

In this section, the maximum D2D link distance is varied from 8m to 1,5km. The D2D average outage probability in both cases in analyzed for ξ=16dB. The final results are depicted in Figure 3.16. In the following discussion, an outage probability below 0,3 is already considered interesting.

It is important to keep in mind that accepting too large link distances has no sense as D2D communications are generally used for short-range applications and are intended to exploit proximity between two users. If the network is correctly handled to achieve acceptable values of the outage probabilities for both CC and D2D communications on the desired distances, it is then not a problem if the outage probability is very high for undesired distances. In this case, if a maximum link distance above approximately 500m is accepted, D2D communications are almost ensured to be unsuccessful. Unfortunately, the outage probability also remains high even for smaller distances.

If D2D communications are done in the UL band, the outage probability becomes interesting below R_{max}=10m regarding the fixed parameters. Needless to say, such a value is far from the expected distances as it restricts D2D communications to a very local region of the space.

If D2D communications are done in the DL band, an unsuccessful transmission is almost inevitable. This shows the importance to tune the BS transmit power carefully in order to prevent complete D2D outage.

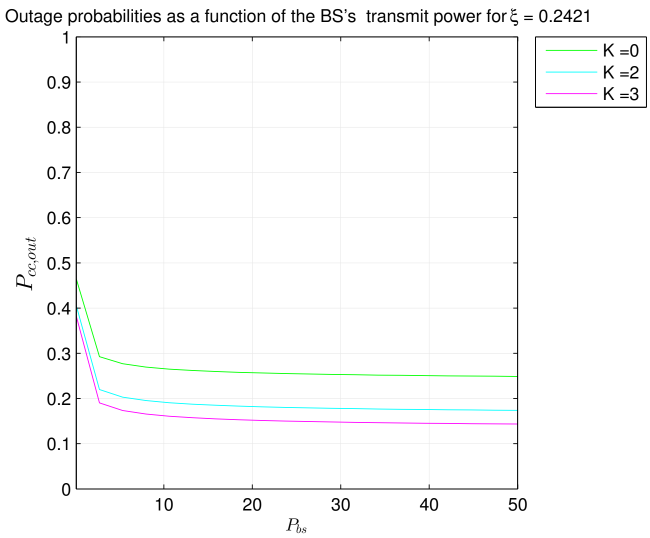

Figure 3.14: CC outage probability as a function of the BS transmit power [W] (case 2).

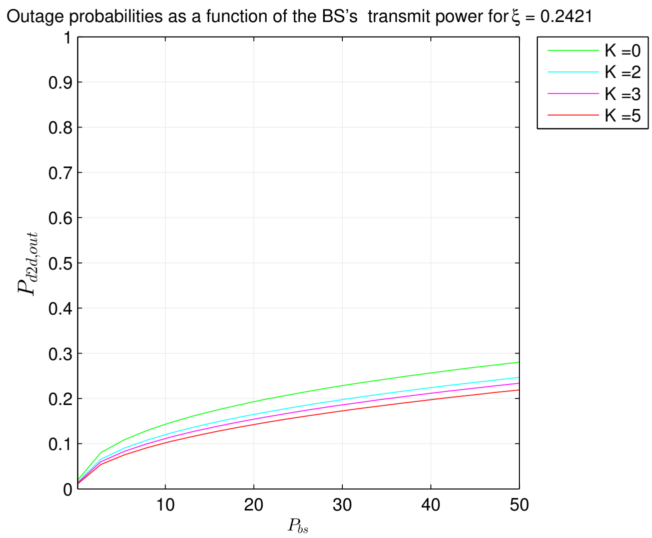

Figure 3.15: D2D outage probability as a function of the BS transmit power [W] (case 2).

Thanks to this last analysis, the importance to add more control mechanisms in the studied network is demonstrated.

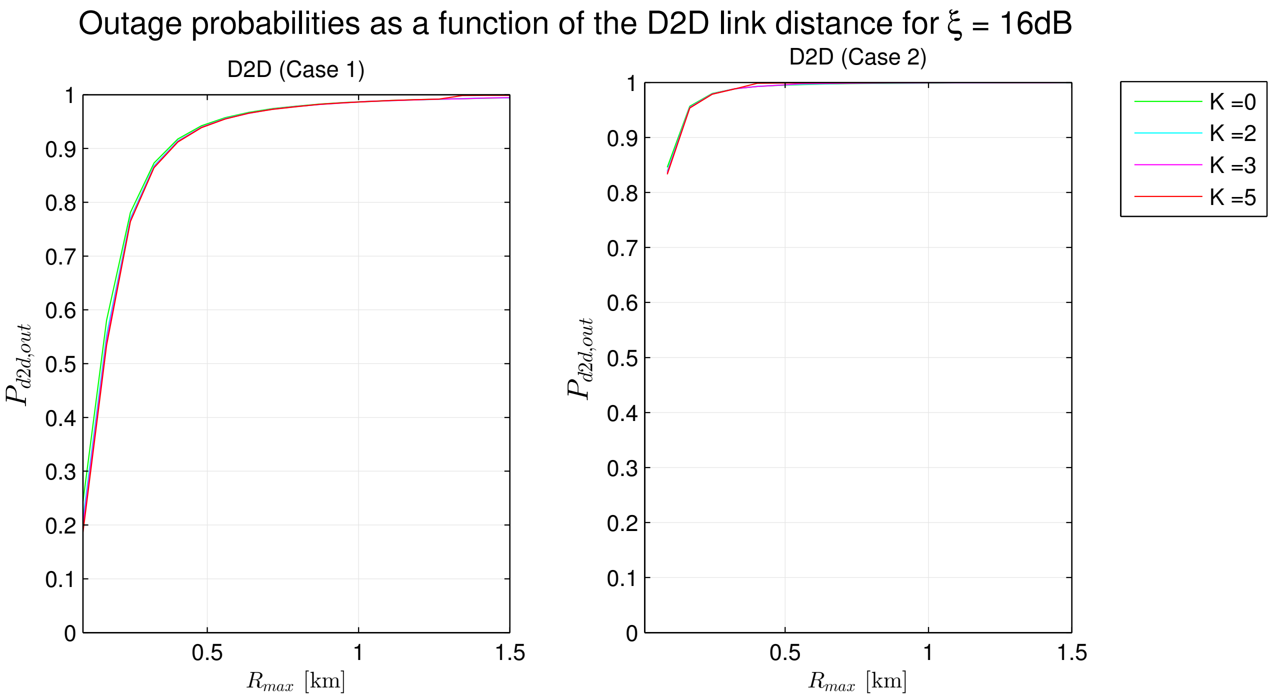

Figure 3.16: Impact of the maximum D2D link distance on the D2D average outage probability for ξ=16dB.

Impact of noise

In order to validate the studied model, the impact of the noise is analyzed for K=2 as shown in Figure 3.17. Unlike an SIR-based analysis, including noise requires to take the UL and DL frequencies into account. The following values will be used in the next analysis: f_{DL}=1805MHz and f_{UL}=1710MHz. The frequency dependent pathlosses are then λ_{DL}=1.75·10^{-4} and λ_{UL}=1.95·10^{-4} which means that the signal is strongly attenuated.

Noise is demonstrated to have a more important proportional impact on CC communications than on D2D communications. This is due to the fact that noise has detrimental effects on both the UL and DL coverage probability while it only affects a single link for D2D communications. It can be observed that values of noise power around -70dBm (10^{-10}W) already induce total outage. This observation might become less critical if lower frequencies are used. A typical thermal noise power value for the GSM band and for a bandwidth of 200kHz is generally taken around -121dBm [Misc68]. At this level of noise, the effect might become problematic for CC communications while it has almost no impact on D2D communciations. This shows the importance to take noise into account when it is possible.

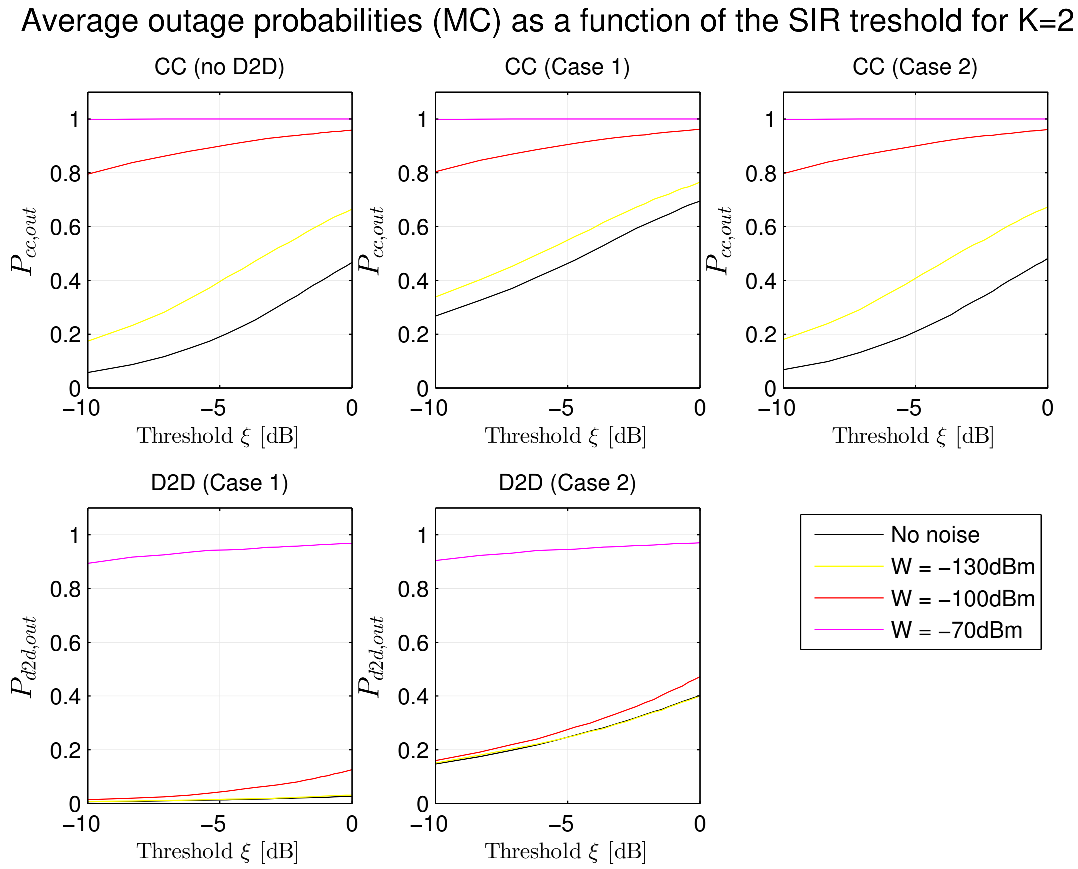

Figure 3.17: Impact of the noise for K = 2,f_{DL}=1805MHz and f_{UL}=1710MHz.

In order to include noise in the studied model, a mathematical development similar to equation 2.4 has to be done. Equation 3.9 then becomes:

$$P\left(\gamma_{x,y}^{t} > \xi, \alpha\right) = \sum_{k=0}^{\infty}\sum_{j=0}^{k} \mathcal{A}_{jk}\left(Tr_{x,y}^{\alpha}\right)^{k-j}\mathbb{E}\left[(I+W)^{k-j}\exp(-Tr_{x,y}^{\alpha}(I+W))\right] \tag{3.32}$$

As it can be seen, introducing noise further complicates the mathematical expression, hence the fact that it was neglected in our analysis. However, the equality $(a+b)^c = \sum_{p=0}^{c} a^p b^{c-p}\binom{c}{p}$ could be used to simplify this expression but at the cost of an additional sum.

3.5.4 Further improvements and analyses of the studied network

Guard zones

Increasing the maximum D2D link distance appears to be critical for the D2D communications in terms of outage probability and even fatal when they are done in the DL band following the current disposition.

As a consequence, additional considerations have to be taken into account to limit the interference coming from the BS. This is where the idea of guard zones (GZ) around BSs came from [D2D20]. The main principle behind GZ is to enable coordination of D2D communications by the cellular network itself. When a D2D UE wants to communicate with another D2D UE in the DL band, he first asks the neighbouring BSs if the D2D is eligible. If a neighbouring BS is using the same DL frequency, the D2D UE as well as its target D2D UE have to be at a given distance R_g from this same BS to get a positive answer. If it is not the case, the D2D UE is not constrained. If the D2D UE receives only positive answers, the D2D link is activated. Of course, if a given BS then wants to communicate in a particular frequency, it has to remember if a D2D was already scheduled inside the GZ for that frequency. This is shown in Figure 3.18 where GZ are depicted as brown circles around BSs and D2D are indeed outside GZ. Even if guard zones are here implemented to tackle the problem of D2D outage in case 2, the impact on CC and D2D in case 1 is also analyzed. Ideally, a similar approach would be used for case 1 by placing GZ around CC UEs instead.

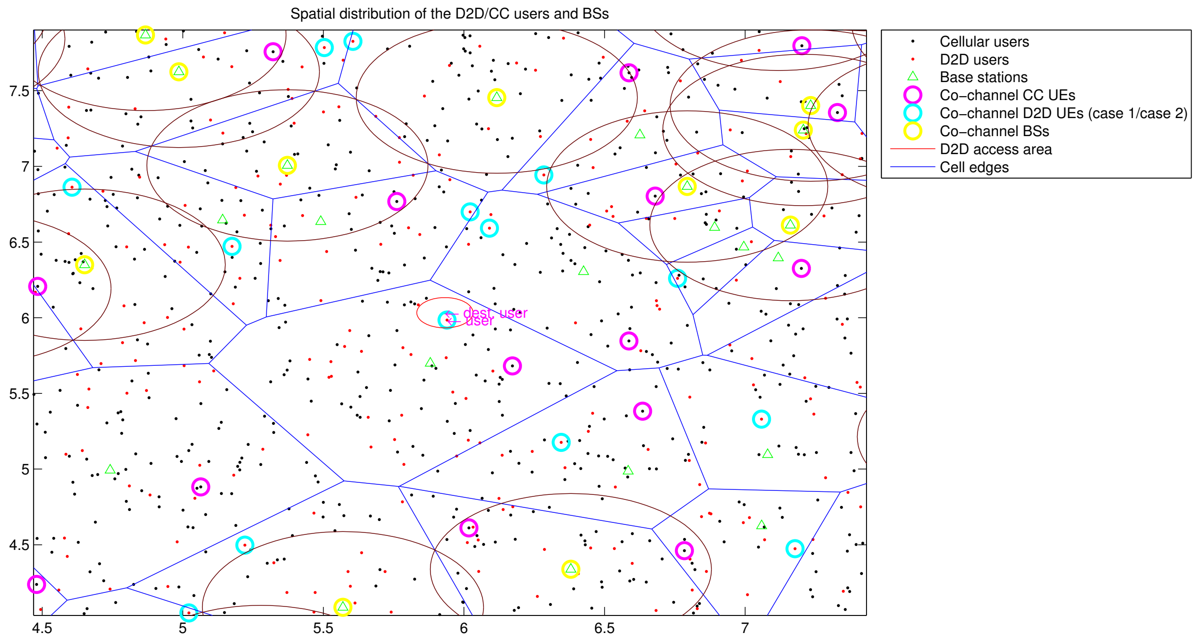

Figure 3.18: Network snapshot after the introduction of guard zones around BSs.

The new perfomances for the CC communications (case 1) and D2D communications (case 2) are respectively depicted in Figures 3.19 and 3.20 for GZ zones of radius 300m and 500m. The network performance is shown to be improved in both cases. For D2D communications in case 2, the interference coming from BSs is in fact limited.

For CC communications in case 1, the interference comes from the inter-cell CC UEs and from the intra-cell and inter-cell D2D UEs as mentioned in Table 3.1. As D2D UEs are using the same power as CC UEs, the impact of introducing D2D communications was proven to be non negligible. By imposing GZ, the D2D links are more and more repelled to the edges of the cell when increasing the guard zone radius. As a consequence, CC UEs trying to communicate inside the GZ are better protected against the harmful interference caused by D2D UEs.

The impact on CC communications (case 2) and D2D communications (case 1) are intentionally not shown. In the first case, the main contributions to the interference was proven to be due to BSs. Including GZ only slightly improves the perfomance by reducing the interference coming from D2D UEs but do not reduce the contribution from BSs. In the second case, the outage probabilities were already very low as shown in Figure 3.9 and showing the new curves was then decided not to be relevant.

Nevertheless, GZ also have a big disadvantage: they limit the number of eligible D2D links and restricts their deployment to the edges of the cell if the GZ radius is supposed too high. The studied network was even run with R_g=1km and no network respecting the parameters in Table 3.4 was successfully generated. This is because GZ are almost covering the entire space which gives no space for D2D links.

The intoduction of GZ in our model is made possible by adapting hypothesis 2 as following:

- **Hypothesis 2bis:** interferers are at least at a distance R_g from the receiver

The LT for this new kind of interferers is then similar to the one of hypothesis 1 (Proposition 3.10) and is given as follows:

$$\mathcal{L}_I(s,\alpha) = \exp\left(-2\pi\Lambda_{\text{int}}\left[\frac{1}{2}t^2{}_2F_1\left(1,\frac{2}{\alpha};\frac{\alpha+2}{\alpha};\frac{-t^\alpha}{sP_{\text{int}}\lambda}\right)\right]_{t=R_g}^{t=\infty}\right) \tag{3.33}$$

The remaining computations can be done following the approach presented in the previous sections. Unfortunately, adding this new LT in the final outage probability formula also includes a second term involving higher-order derivatives that was proven to dramatically increase the program computation time. For this reason, the presented results were drawn using MC simulations.

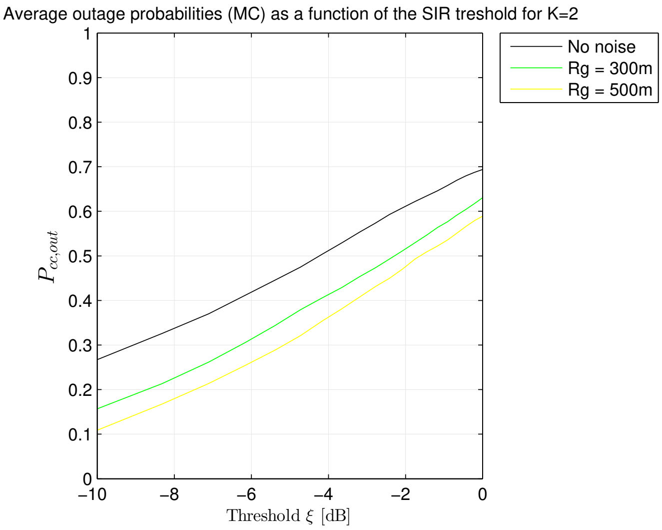

Figure 3.19: Average CC outage probability (case 1) after the integration of guard zones around BSs.

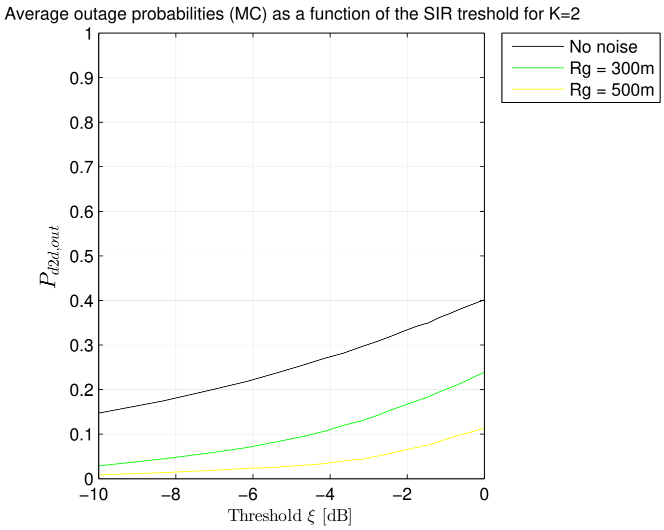

Figure 3.20: Average D2D outage probability (case 2) after the integration of guard zones around BSs.

Rejection principle

In this section, the well known rejection principle will be integrated in the network and studied. This principle prevent two BS that are too close to each other to use the same frequency in the DL to avoid harmful interference to the served CC UEs. For this mechanism to work, it has to rely on communications between neighbouring base stations. With the fixed frequency reuse factor, the maximum possible rejection distance is about 400m. This distance is used in the following study. This method is known for years and has been proven to be beneficial for CC communications. Figure 3.21 confirms this last statement.

However, this method is also proven not to be beneficial for D2D communications as depicted in Figure 3.22. The reason for this comes from the fact that D2D links do not need any BSs as the two D2D UEs are directly connected with each other. Unlike for the analysis of a given CC UE, the nearest BS is not ensured to use the considered DL frequency. As a consequence, the rejection might have a negative impact as it can force close BSs to communicate in this particular frequency as shown in Figure 3.23. With the fixed parameters, about 65% of the BS are interfering with each other meaning that, when BS already interfering include other BS in their rejection zone, the BSs not included in their rejection zones are almost sure to communicate in that frequency. This last observation is certainly not positive for D2D communications. In addition, the rejection can also be done symetrically with respect to the considered D2D UE inducing no reduction of the interference. The only positive case happens when a neighbouring BS is already using the DL frequency but this also means that the interference coming from that BS is strong.

One step further, using the rejection principle together with the GZ principle might become interesting. However, this is almost impossible with the fixed parameters.

Integrating this repulsion principle makes the choice of a PPP to model interfering BSs not coherent anymore. There is here a need for adapting the model by using a different PP like the Hard Core Point Process (HCPP) which imposes a certain distance between the different points of the PP. This would however result in an increased mathematical complexity as several theorems specific to the PPP were used to set up the model.

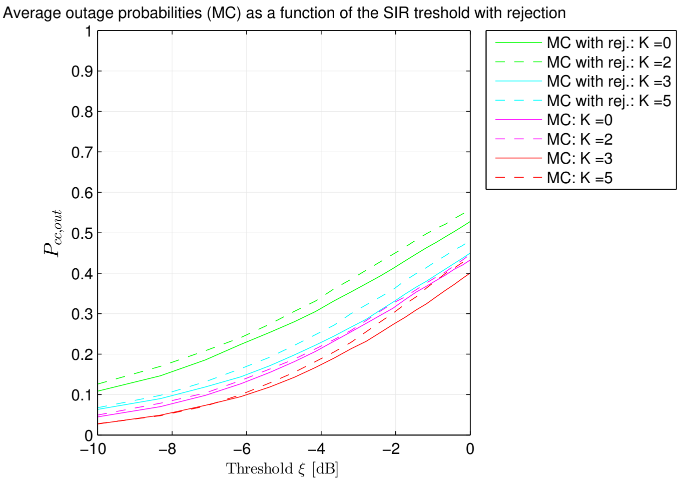

Figure 3.21: Average CC outage probability (case 2) after the integration of the rejection principle for a rejection distance of 400m.

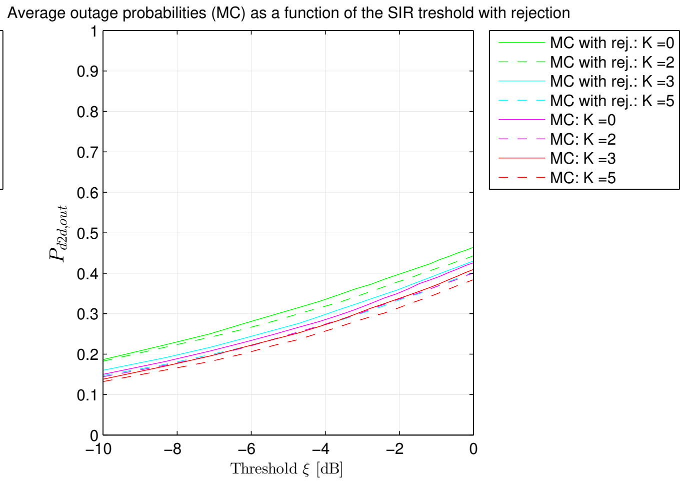

Figure 3.22: Average D2D outage probability (case 2) after the integration of the rejection principle for a rejection distance of 400m.

3.5.5 Computation time

This program computation time analysis is based on the analytical and numerical curves presented in Figures 3.6,3.7 and 3.8. Table 3.6 resumes the average computation time per point of the curve for the different values of the Rice K factor. As each of the different curves are composed by 20 points, those times have to be multiplied by 20 and added to get the total computation time. As it can be seen, the model was stopped after 5 days for K=5. This is the reason why the case K=5 is not appearing in Figure 3.8 and in many other figures throughout this last section. Table 3.7 summarizes the required time for the generation and analysis of 8000 networks.

The model is shown to outperfom the MC simulations for K=0 in terms of computation time. This can be concluded as the most important part of the MC simulations computation time is due to the network generation which is independent of the fact that K=0. However, when increasing K, one of the biggest advantages of modeling networks using SG is lost. In fact, besides the mathematical insight, SG is generally used to avoid testing all possible spatial configurations with MC simulations in order not to waste time. In this case, MC simulations become however more interesting. In addition, the fact that the model is capable to outperfom MC simulations for K=0 is not really of interest as a simplier analysis based on the Rayleigh fading model would have been sufficient.

The reason for this comes again from the term for which we had to resort to Taylor approximations. More precisely, the studied model requires the computation of numerical integrals that are involving this

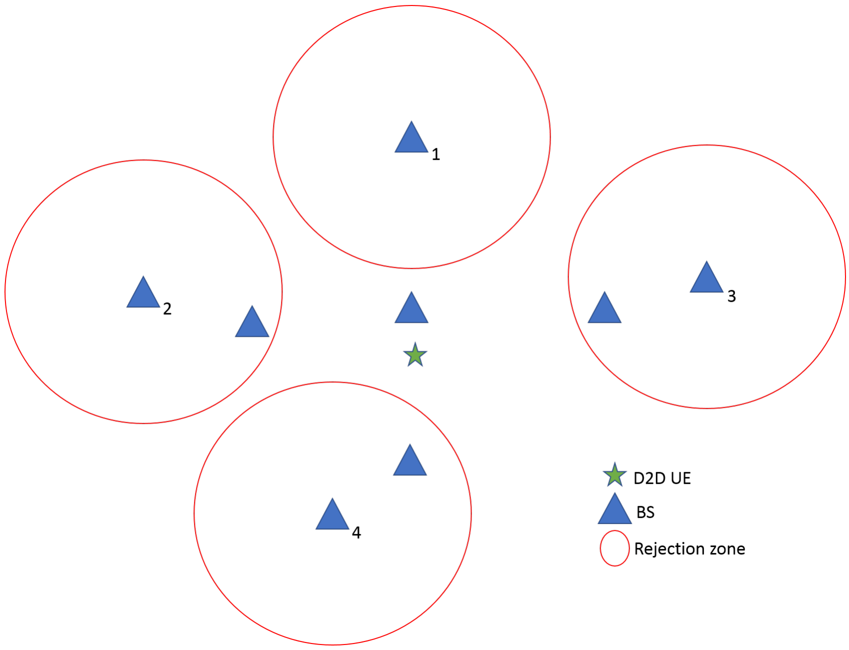

Figure 3.23: Bad scenario for D2D communications after the integration of the rejection principle. BS labels corresponds to the order of those BSs. The order is based on the moments at which each BS started to communicate in this particular frequency.

term. The Taylor coefficient being very long and the number of integrals to be computed being high, this increases significantly the program computation time. In fact, the integral function implemented in MATLAB tries to increase the number of intervals until it reaches the desired precision. When this precision is too demanding, the function continues to run until it has reached the maximum number of intervals. Apart from the fact that the desired precision is possibly not reached, reaching the maximum number of intervals takes a lot of time. One solution could be to decrease this precision but then the accuracy of the final results is possibly affected.

	K=0	K=2	K=3	K=5
CC-average time/point	0.116	5.156	18.419	>120
D2D-average time/point	0.106	6.997	21.088	>120

Table 3.6: Model computation time in hours.

	Network Generation	Probabilities Computations
CC-MC time	74.616	0.188
D2D-MC time	80.286	0.094

Table 3.7: MC computation time in hours (8000 networks).

3.6 Model weaknesses

This section aims to identify the main weaknesses of this model. Two different topics are addressed: the choice of the interferers fading model and the mathematical complexity.

3.6.1 Interferers fading model

For mathematical tractability, the Rayleigh fading model was preferred to the Rician fading model to model both close (hypothesis 2) and far (hypothesis 1) interferers. Nevertheless, this choice of the fading model is inconsistent for close interferers as there might also be a strong LOS component in zone 1 as shown in Figure 3.24. It is even more incoherent knowing that the useful link was supposed to be affected by Rician fading.

Opting for the Rician fading model for close interferers instead is possible but makes it incoherent for close interferers of zone 2. In fact, interferers entering in the close interferers category can be closer to the TX than the RX itself but can also be far away. However, if such a choice is made, Proposition 3.2.3 can be modified using the following expression instead:

$$\mathcal{G}_{bis}(\text{int}) = \Lambda_{int}\pi\lambda^{\delta}P_{int}^{\delta}e^{-K}sinc^{-1}(\pi\delta)\sum_{k'=0}^{\infty}\frac{K^{k'}}{(k'!)^2}(1+\delta)_{k'} \tag{3.34}$$

A general comment would be to say that using the Rayleigh fading model or the Rician fading model leads respectively to a lower bound and an upper bound of the interference caused by close interferers. The final average outage probability computed by the model is then respectively lower and higher than the real one.

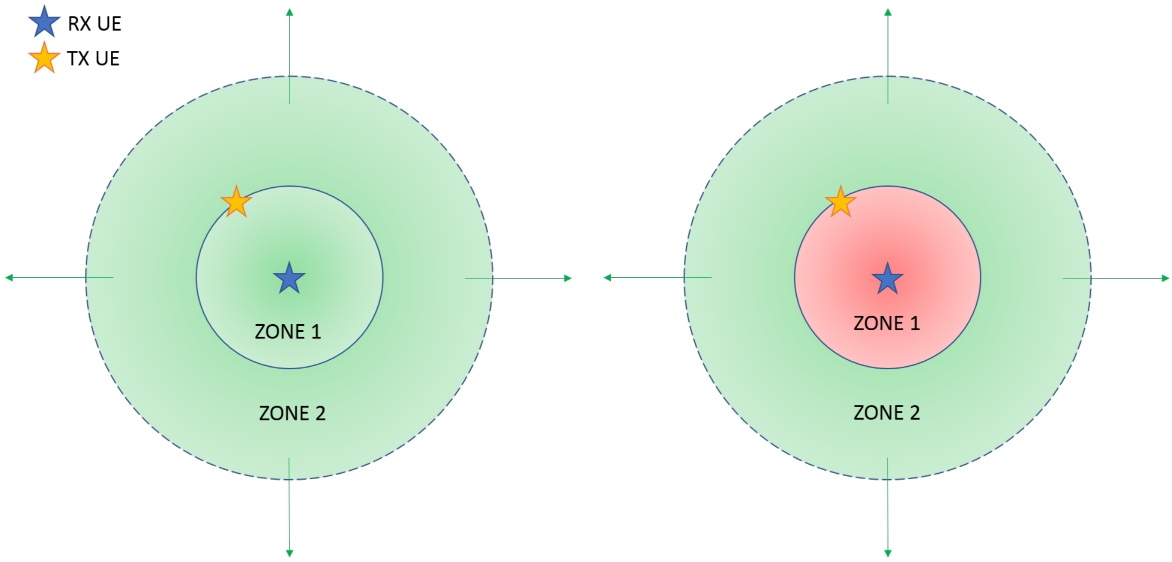

Figure 3.24: Different sorts of interferers. Left: Close interferers (hypothesis 2). Right: Far interferers (hypotehsis 1).

3.6.2 Mathematical complexity

This section aims to take a more critical look at the so-called benefits of stochastic geometry. One of the reasons often cited is certainly the gain of mathematical insight by means of mathematical expressions arising from a stochastic geometry-based analysis of wireless networks. Another reason concerns the gain of time in the analysis but this benefit was already shown not to be the strength of the presented model.

As it can be seen in several expressions of this section, the mathematical complexity is relatively high. This last statement can be illustrated by the presence of multiple sums, high-order partial derivatives or integrals that have to be solved numerically. More precisely, this shows that, when going for other fading distibutions than the Rayleigh fading, the mathematical complexity increases significantly. Such a strong mathematical complexity has rendered the intensive analysis of the impact of different network parameters time-consuming especially for high values of the Rice K factor. If the model is tested for values of K greater than 5, the waiting times might become prohibitive as higher order Taylor approximations should be used in order to provide appropriate results. This last discussion questions the relevance of using stochastic geometry in any case especially as no completely closed-form expressions can be proposed in the studied model.

3.7 Chapter summary

As the BS transmit power is generally higher than the CC UE tranmit power in nowadays networks, Table 3.8 illustrates the trade-off between CC communications and D2D communications.

	CC communications	D2D communications
Case 1	Less favourable	More favourable
Case 2	More favourable	Less favourable

Table 3.8: Trade-off between CC and D2D communications.

A summary of all discussions of this chapter is available in Table 3.9. Some of the observations are only valid for the studied parameters. When one of those observations is strongly related to the model setup, the critical parameter is intentionally highlighted in order for the reader to keep in mind that the observation could change with another value of this parameter.

	CC communications Case 1	CC communications Case 2	D2D communications Case 1	D2D communications Case 2
Realistic interferers density	Outage probability still high	Outage probability still high	Acceptable outage probability for R_{max}=100m	Outage probability still high for P_{bs}=40W
BS transmit power	Unsensitive	Sensitive when $P_{bs}<P_{cc}$	Unsensitive	Highly sensitive when $P_{bs}>P_{cc}$
Maximum D2D link distance	Irrelevant	Irrelevant	Sensitive	Highly sensitive for P_{bs}=40W
Realistic noise power	Sensitive	Sensitive	Slightly sensitive	Slightly sensitive
Integration of GZs	Positive impact	Positive impact	Very positive impact	Very positive impact
Integration of the rejection principle	Slight positive impact for a rejection distance of 400m	Slight positive impact for a rejection distance of 400m	Slight negative impact for a rejection distance of 400m	Slight negative impact for a rejection distance of 400m

Table 3.9: Chapter summary.

Chapter 4

Energy harvesting-aided device-to-device communications

Due to the ever-growing wireless applications, the amount of devices powered by batteries has been constantly increasing in the last few years. This constitutes an important problem as replacing those batteries as they die has become more costly and particularly complex in some cases. To be persuaded of this, it suffices to put ourselves in the shoes of the manager of a big hotel that has equipped his 400 rooms with 4 battery-powered sensors as suggested in [EH50]. Each two or three years, he would then have to replace his 1600 batteries. This is certainly undesirable as the hotel customers might be disturbed and even more if the sensors are hard to access.

Energy harvesting technologies have been widely studied in the past few years in an attempt to overcome that problem by increasing batteries lifespans or even replacing them. From big satellite stations to a simple CC UE, ambient energy sources are multiple and are not limited by time or space which makes this technology even more interesting. In addition, scientists also see in EH the possibility to decrease battery wastes which is undoubtly beneficial for the environment.

Therefore, the following chapter aims to propose a general analysis of D2D-aided communications where D2D UE are equipped with infinite capacity rechargeable batteries. This chapter can be seen as an extension of the network studied in Chapter 3. For sake of simplicity, the Rayleigh fading model will be considered on CC and D2D communications in this chapter but the presented model could be easily adapted to Rician fading. This choice was made as our main interest is here foccussed on the EH technology. Closed-form expressions are derived.

High frequencies around 2.45GHz or 5.8GHz are generally preferred for long-range power transfer (MPT) as mentioned in [EH61]. This comes together with a strong atmospheric attenuation, hence the potential benefit of beamforming techniques. Three different beamforming methods are compared to the isotropic case namely isotropic uniform linear array (ULA) beamforming, best antenna (BA) beamforming and optimal vector (OV) beamforming [Misc69, EH53].

The given model draws heavily on articles [EH55] and [EH56] and can be seen as an extension of those two works. Some of the results presented in this chapter are even directly taken from them. In [EH56], the harvested powers are analyzed for the isotropic and directed cases and for both infinite and finite capacity batteries. In this same article, the model is established for a general UE (not necessarily a D2D UE) which harvests power from all PBs while neglecting the fading. Finally, the directed case is not given any name and is just represented by a main lobe gain z_m and a secondary lobe gain z_s. [EH55] can be seen as the theoretical background of [EH56]. The improvements relative to those two publications as well as the contributions of this chapter are the following:

- Rician fading model is included in the analysis of power transfer for the power harvesting strategy adopted in [EH56]. Rayleigh fading model is then used to examine another power harvesting strategy where only the nearest PB is assumed to power the D2D UEs.

- A more detailed approach based on ULAs is proposed for PBs using directed beamforming as presented in [EH56]. The idea of antenna arrays is then generalized to the D2D UE itself in order to propose more efficient beamforming techniques.
- The power harvesting system presented in [EH56] is also integrated into a real network and used to power D2D communications. The trade-off between the transmission probability and the outage probability on D2D communications is then studied. The transmission probability is defined as the probability that a sufficient amount of power has been harvested for a message to be transmitted.

4.1 System model

The system model is exactly the same as the one presented in Chapter 3 except for the choice of the fading model which will rather be assumed to be Rayleigh for CC and D2D communications. This change has an impact on several mathematical expressions presented in this same Chapter 3. Due to place restrictions, not all of them will be rewritten but the two most important modifications will be identified instead. This should enable the reader to find all the corresponding equalities proposed until now by following the same approach.

4.1.1 Mathematical modifications

First, knowing it has to be evaluated in $\frac{\xi r_{x,y}^{\alpha}}{\lambda P_{\text{link}}}$, the LT under hypothesis 1 can be further simplified as there is no need for partial derivative computation. This simplification is shown in Proposition 4.1.1.

Proposition 4.1.1 (Laplacian transform under hypothesis 1)**.** Under Rayleigh fading on the studied link, the Laplacian transform of the interference is given by:

$$\mathcal{L}_I(s,\alpha)\Big|_{s=\frac{\xi r_{x,y}^{\alpha}}{\lambda P_{\text{link}}}} = \exp\left(-\pi\Lambda_{\text{int}} r_{x,y}^2 \mathcal{K}(\alpha,\xi,\text{int},\text{link})\right)$$

where

$$\mathcal{K}(\alpha,\xi,\text{int},\text{link}) = \int_{\left(\frac{\xi P_{\text{int}}}{P_{\text{link}}}\right)^{-\frac{2}{\alpha}}}^{\infty} \frac{\left(\frac{\xi P_{\text{int}}}{P_{\text{link}}}\right)^{\frac{2}{\alpha}}}{1+u^{\frac{\alpha}{2}}} du \tag{4.1}$$

Proof. This equality is proven in the Appendices of [SG10]. □

As a remark, it can be shown that, when neglecting the noise power, the average final outage probability expression is closed-form [D2D45]. However, noise will be taken into account in this analysis in order to propose a more general model as noise was shown to have a big impact on CC communications in the previous chapter.

Under Rayleigh fading model, Proposition 3.4.1 can be modified as follows

Proposition 4.1.2. The coverage probability at the distance $r_{x,y}$ from a transmitting node x of the v^{th} tier (v ∈ {CC,D2D,BS}) in the t-link (t ∈ {UL,DL,D2D}) is given by:

$$P\left(\gamma_{v,x,y}^{t} > \xi,\alpha,r_{x,y}\right) = e^{-W\frac{\xi r_{x,y}^{\alpha}}{\lambda P_{\text{link}}}} \mathcal{L}_{I_1}(s,\alpha)\Big|_{s=\frac{\xi r_{x,y}^{\alpha}}{\lambda P_{\text{link}}}} \mathcal{L}_{I_2}(s,\alpha)\Big|_{s=\frac{\xi r_{x,y}^{\alpha}}{\lambda P_{\text{link}}}} \tag{4.2}$$

Proof. This equality is easily found by means of equation 2.4 □

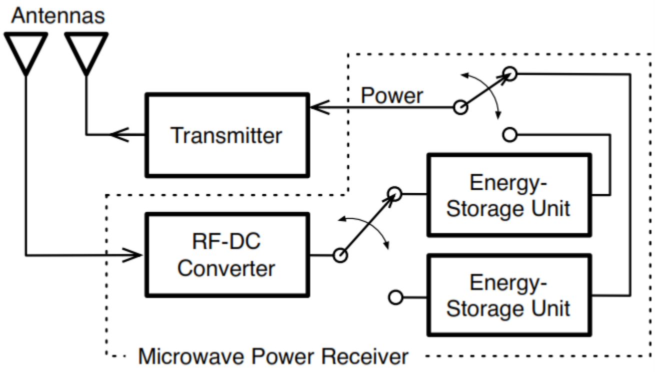

Figure 4.1: D2D UE architecture (Source:[EH57]).

4.1.2 Energy harvesting model

The considered model focusses on the MPT technology. Each D2D UE is assumed to be able to simultaneously harvest energy from PBs and send information to another D2D UE thanks to the architecture depicted in Figure 4.1.

As it can be seen, each of them has two energy storage units. At any given time, one of them is filled thanks to the extracted power while the other is used to provide the required power for the eventual transmission of a message to another D2D UE. More importantly, the D2D UE is only allowed to transmit when he has harvested a sufficient amount P_{thres} of power. The general battery level C_t at a given time t is then expressed as in [EH55]:

$$C_t = C_{t-1} + H_t - P_{\text{thres}} I \left(C_{t-1} \geq P_{\text{thres}} \right) \tag{4.3}$$

where H_t is the harvested power during time slot t and I($\cdot$) equals 1 if the condition inside is respected and 0 otherwise.

Based on this system setup, the probability that a D2D UE is transmitting is given by :

$$\rho = \lim_{n \to \infty} \frac{1}{n} \sum_{t=1}^{n} \mathbb{E} \left[I \left(C_t \geq P_{\text{thres}} \right) \right] = \begin{cases} 1, & E_a \geq P_{\text{thres}} \\ \frac{E_a}{P_{\text{thres}}}, & E_a < P_{\text{thres}} \end{cases} \tag{4.4}$$

where E_a is the energy arrival rate often defined as $\mathbb{E}\left[H_t\right]$.

As already mentioned, the harvested power comes from PBs. We will refer to the PBs frequency as f_{pb} or indirectly as $\lambda_{pb} = \left(\frac{c}{4\pi f_{pb}}\right)^2$. Those PBs are supposed to use a dedicated band which is not overlapping with the UL and DL bands to avoid harmful interference to CC and D2D communications. However, this also implies that the D2D can only harvest power coming from the PBs. The PBs are further supposed to be distributed following an homogeneous Poisson point process (HPPP) of intensity Λ_{pb} defined in $\mathbb{R}^2$. Also, they are assumed to be able to isotropically emit with a power P_{pb}.

In addition, two different harvesting strategies are considered.

- **Strategy 1:** D2D UEs are harvesting power from all PBs
- **Strategy 2:** D2D UEs are only harvesting power from the nearest PB.

The harvester itself generally needs a certain amount of power for the activation of its circuit. This activation power will be neglected in our analysis but could be easily added. Also, harvesters are known not to be able to perfectly extract the ambient power. This non-ideality is represented by a RF-to-DC power conversion efficiency factor ϵ.

Unlike for D2D and CC communications, Rician fading model will be assumed for the power harvesting model under the first strategy. Using Rician fading for all signals coming from all PBs might seem very optimistic. This is partially true as the main contribution of ambient power generally comes from the nearest PB. This last observation together with the fact that MPT is operated at high frequencies can convince us that this assumption is not too restrictive. However, the reader has to keep in mind that the computed harvested power might still be a little bit lower in reality. For mathematical tractability, Rayleigh fading model will then be considered under the second strategy. The same discussion can be used to say that the computed harvested power might, in this case, be a little bit higher in reality.

Under both strategies, a short-range propagation model will be adopted on power transfer links in order to avoid infinite harvested powers. Assuming unitary time intervals and supposing $U_0 \in \mathbb{R}^2$ is a typical D2D user, this model is expressed as follows:

$$H_t = \epsilon P_{pb} \textstyle\sum_{pb \in \Phi_{pb}} g_{pb,U_0} \max\left(|pb - U_0|, \nu\right)^{-\gamma} \quad \text{(first strategy)} \tag{4.5}$$

$$H_t = \epsilon P_{pb} g_{pb_0,U_0} \max\left(|pb_0 - U_0|, \nu\right)^{-\gamma} \quad \text{(second strategy)} \tag{4.6}$$

where $\nu>1$, γ is the power transfer path loss coefficient and $pb_0 \in \mathbb{R}^2$ is defined as the nearest PB.

Those expressions will be adapted in the corresponding sections to match with the studied model. As the main contributions in terms of ambient power come from the nearest PBs, it is logical to consider a small value for γ. This explains why the path loss coefficient on D2D and CC communications and the path loss coefficient on power transfer links are generally supposed to have different values.

One particular term of interest is $\mathbb{E}[H_t]$ as shown in equation 4.4. This term will be derived in the next sections for both strategies and for different cases.

4.1.3 Power harvesting from all power beacons

Isotropic case

In this case, each PB is supposed to be equipped with a single antenna that emits isotropically with power P_{pb}.

Proposition 4.1.3 (Isotropic case under strategy 1)**.** The average harvested power under strategy 1 in the isotropic case supposing Rician fading is given by :

$$\mathbb{E}_{\text{iso},1} = \frac{\exp(-K)}{K+1} \frac{\pi\gamma\nu^{2-\gamma}\epsilon P_{pb}\Lambda_{pb}\lambda_{pb}}{\gamma - 2} \sum_{k=0}^{\infty} K^k (k+1) \tag{4.7}$$

Proof. This expression is proven by means of the following equalities:

$$\begin{aligned}
\mathbb{E}_{\text{iso},1} &= \mathbb{E}[H_t] \\
&= \mathbb{E}\left[\epsilon P_{pb} \sum_{pb \in \Phi_{pb}} g_{pb,U_0} \max\left(|pb - U_0|, \nu\right)^{-\gamma}\right] \\
&\overset{(1)}{=} \epsilon P_{pb}\Lambda_{pb} \int_{x \in \mathbb{R}^2} \mathbb{E}_g[g] \max\left(|x - U*|, \nu\right)^{-\gamma} dx \\
&\overset{(2)}{=} 2\pi\epsilon P_{pb}\Lambda_{pb}\mathbb{E}_g[g] \int_r \max(r, \nu)^{-\gamma} r dr
\end{aligned} \tag{4.8}$$

where (1) comes from Theorem 2.1.2 and (2) follows from the stationarity property of PPPs and the transition to the polar coordinates system.

By means of expression 3.5, the expectation of the fading power gain is then given by

$$\mathbb{E}[g] = \frac{\exp(-K)}{K+1} \sum_{k=0}^{\infty} K^k (k+1) \tag{4.9}$$

In addition, the right side integral is computed as follows

$$\begin{aligned} \int_r \max(r,\nu)^{-\gamma} r dr &= \nu^{-\gamma} \int_0^{\nu} r dr + \int_{\nu}^{\infty} r^{1-\gamma} dr \\ &= \frac{\nu^{2-\gamma}}{2} + \frac{\nu^{2-\gamma}}{\gamma-2} \end{aligned} \tag{4.10}$$

Combining expressions 4.8, 4.9 and 4.10 finally gives the desired result.

□

Isotropic uniform linear array

Each D2D UE is here assumed to be mainly served by its nearest PB thanks to directed beamforming using isotropic ULAs with N antennas as depicted in Figure 4.2. The term beamforming is here taken from an antenna standpoint. In addition to that, it also receives the secondary contributions of all other PBs. This model also supposes each PB has the necessary tools to know exactly where the D2D UE it has to serve is located.

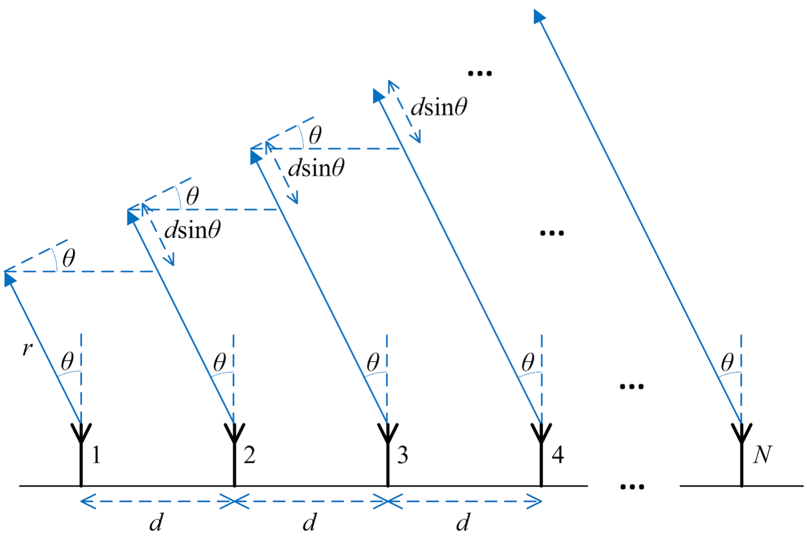

Figure 4.2: Isotropic ULA (Source:[Misc65]).

Those assumptions might seem very simplistic. In fact, nothing ensures that several D2D UEs are not associated to the same PB leading to situations where the PB is not able to satisfy all users at the same time in terms of directed beamforming. This situation is very likely to happen. However, the analysis is based on one single frequency for each generated network making this last observation less critical. In reality, satisfying all D2D UEs might indeed need some kind of scheduling. Furthermore, as power transfer systems are still in the early stages of their development, it is difficult to say how those PBs will be equipped in reality. In the worst case scenario, it is possible that those PBs are just plugged somewhere without any means of communications with their surrounding environment. It would then be impossible for the PB to know in which direction the beamforming has to be done. However, those assumptions are considered sufficient to gain insight on the performances of such a system.

As mentionned in [Misc69], the array factor representing the far-field radiation of an isotropic ULA is:

$$F(\theta) = w \cdot v \tag{4.11}$$

where w is the weighting vector and v is the array propagation vector.

Using simple trigonometric developments, the array propagation vector is computed as:

$$v = \left[1, e^{j\frac{2\pi d}{\lambda}\sin(\theta)}, \ldots, e^{j(N-1)\frac{2\pi d}{\lambda}\sin(\theta)}\right]^{\mathrm{T}} \tag{4.12}$$

where d is the distance between antennas as shown in Figure 4.2 and λ is the signal wavelength not to be mixed up with the frequency dependent pathloss here.

In order to achieve correct beamforming in the direction θ_0, the following weighting vector is used:

$$w = \left[1, e^{-j\frac{2\pi d}{\lambda}\sin(\theta_0)}, \ldots, e^{-j(N-1)\frac{2\pi d}{\lambda}\sin(\theta_0)}\right] \tag{4.13}$$

Using these two expressions for the respective vectors, equation 4.11 simplifies to:

$$F_{\theta_0}(\theta) = \begin{cases} \frac{\sin\left(\sin\left(\frac{\pi N d}{\lambda}\right)(sin(\theta)-sin(\theta_0))\right)}{\sin\left(\sin\left(\frac{\pi d}{\lambda}\right)(sin(\theta)-sin(\theta_0))\right)}, & \theta \neq \theta_0 \\ N, & \theta = \theta_0 \end{cases} \tag{4.14}$$

An example of the normalized isotropic ULA power pattern for $\theta_0 = 45°$ and for different values of N is shown in Figure 4.3.

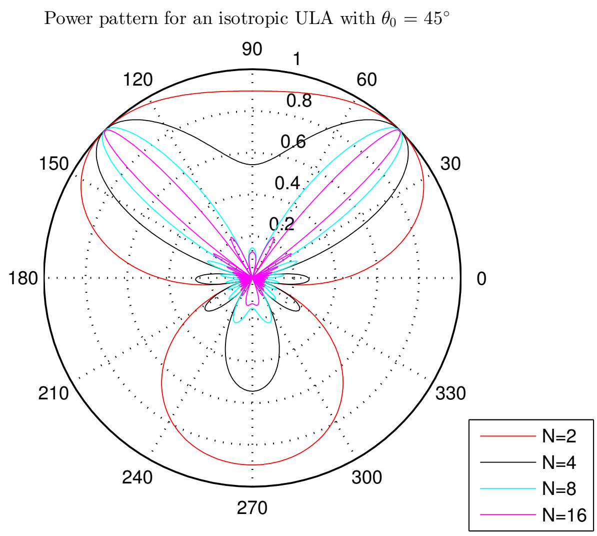

Figure 4.3: Isotropic ULA power pattern for $\theta_0 = 45°$.

The short-range propagation model in case of directed beamforming is slightly modified. Assuming the available power P_{pb} is shared among the N antennas, equation 4.5 becomes:

$$H_t = \epsilon P_{pb} g_{pb_0,U_0} \max\left(|pb_0 - U_0|, \nu\right)^{-\gamma} + \epsilon \frac{P_{pb}}{N} \sum_{\substack{pb\in\Phi_{pb} \\ pb\neq pb_0}} F_{\theta_{0,pb}}(\theta_{pb}) g_{pb,U_0} \max\left(|pb - U_0|, \nu\right)^{-\gamma} \tag{4.15}$$

where $\theta_{0,pb}$ denotes the beamforming direction of a secondary PB pb and θ_{pb} is the angle between the D2D harvester and the secondary PB pb.

Proposition 4.1.4 (ULA case under strategy 1)**.** The average harvested power under strategy 1 in the ULA case supposing Rician fading is given by :

$$\mathbb{E}_{\mathrm{ULA},1} = \frac{\exp(-K)}{K+1}\epsilon P_{pb}\lambda_{pb}\left(\psi + \frac{1}{N}\mathbb{E}_{\theta,\theta_0}\left[F_{\theta_0}(\theta)\right]\left(\frac{\pi\gamma\Lambda_{pb}\nu^{2-\gamma}}{\gamma-2} - \psi\right)\right)\sum_{k=0}^{\infty} K^k(k+1)$$

where

$$\mathbb{E}_{\theta,\theta_0}\left[F(\theta)\right] = \frac{1}{4\pi^2}\int_0^{2\pi}\int_0^{2\pi} F_{\theta_0}(\theta)d\theta d\theta_0$$
$$\psi = \nu^{-\gamma}\left[1-e^{-\pi\Lambda_{pb}\nu^2}\right] + (\pi\Lambda_{pb})^{\frac{\gamma}{2}}\cdot\Gamma\left(\pi\Lambda_{pb}\nu^2, 1-\frac{\gamma}{2}\right) \tag{4.16}$$

where $\Gamma(\cdot,\cdot)$ is th upper incomplete gamma function.

Proof. In the following computations, F_{pb} will refer to $F_{\theta_{0,pb}}(\theta_{pb})$. This desired result is demonstrated by means of the following equalities:

$$\begin{aligned}
\mathbb{E}_{\text{ULA},1} &= \mathbb{E}\left[H_t\right] \\
&= \mathbb{E}\left[\epsilon P_{pb} g_{pb_0,U_0}\max\left(|pb_0-U_0|,\nu\right)^{-\gamma} + \epsilon\frac{P_{pb}}{N}\sum_{\substack{pb\in\Phi_{pb}\\ pb\neq pb_0}} F_{pb}g_{pb,U_0}\max\left(|pb-U_0|,\nu\right)^{-\gamma}\right] \\
&= \mathbb{E}\left[\epsilon P_{pb}(1-F_{pb_0})g_{pb_0,U_0}\max\left(|pb_0-U_0|,\nu\right)^{-\gamma} + \epsilon\frac{P_{pb}}{N}\sum_{pb\in\Phi_{pb}} F_{pb}g_{pb,U_0}\max\left(|pb-U_0|,\nu\right)^{-\gamma}\right] \\
&\overset{(1)}{=} \epsilon P_{pb}\left(1-\mathbb{E}_{\theta,\theta_0}\left[F_{pb_0}\right]\right)\mathbb{E}_g\left[g_{pb_0,U_0}\right]\mathbb{E}\left[\max\left(|pb_0-U_0|,\nu\right)^{-\gamma}\right] \\
&\quad + 2\pi\epsilon\frac{P_{pb}}{N}\Lambda_{pb}\mathbb{E}_g\left[g\right]\mathbb{E}_{\theta,\theta_0}\left[F\right]\int_r \max\left(r,\nu\right)^{-\gamma} rdr
\end{aligned} \tag{4.17}$$

where (1) comes from the fact that all different RVs are independent and from expression 4.8.

$\mathbb{E}_{\theta,\theta_0}\left[F_{pb_0}\right]$ is found using the definition of the expectation on expression 4.14. By means of expression 3.1, it can also be shown that:

$$\begin{aligned}
\mathbb{E}\left[\max\left(|pb_0-U_0|,\nu\right)^{-\gamma}\right] &\overset{(1)}{=} 2\pi\Lambda_{pb}\int_0^\infty \max\left(D,\nu\right)^{-\gamma} De^{-\pi\Lambda_{pb}D^2}dD \\
&= 2\pi\Lambda_{pb}\int_0^\nu \nu^{-\gamma}De^{-\pi\Lambda_{pb}D^2}dD + 2\pi\Lambda_{pb}\int_\nu^\infty \max\left(D,\nu\right)^{-\gamma} De^{-\pi\Lambda_{pb}D^2}dD \\
&\overset{(2)}{=} \nu^{-\gamma}\left[1-e^{-\pi\Lambda_{pb}\nu^2}\right] + (\pi\Lambda_{pb})^{\frac{\gamma}{2}}\,\Gamma\left(\pi\Lambda_{pb}\nu^2, 1-\frac{\gamma}{2}\right)
\end{aligned} \tag{4.18}$$

where (1) is obtained by supposing $D = |pb_0 - U_0|$ and (2) follows from the definition of the upper incomplete gamma function. Combining expressions 4.9, 4.10, 4.17 and 4.18 finishes the proof. □

4.1.4 Power harvesting from the nearest power beacon

In this section, multiple antennas are also considered at the D2D UE itself. This means that the D2D UE has potentially more antennas to harvest energy as shown in Figure 4.4. We will refer to the number of antennas at the PB as N_{pb} and to the number of antennas at the D2D UE as N_{d2d} in this section. In addition, the channel matrix between the PB and the D2D UE is named $\text{H} \in \mathbb{C}^{N_{pb}\times N_{d2d}}$. Equation 4.6 is then shown to represent the harvested power from one antenna of the PB at one of the antennas of the D2D UE unless the power P_{pb} is multiplied by a certain coefficient c_i. Those coefficients are gathered in the vector $c = \left[c_1, \ldots, c_{N_{pb}}\right] \in \mathbb{C}^{N_{pb}\times 1}$ with $\|c\|^2 = 1$. In the isotropic case, the PB will always be equipped with one single antenna. Also, remember that Rayleigh fading will be considered in this section and thus $\mathbb{E}\left[g\right] = 1$ as g$\sim$exp(1).

Using multiple antennas on both sides of the link gives the opportunity for more efficient beamforming techniques in terms of signal processing. In fact, the best antenna beamforming technique and the optimal vector technique are investigated. Those methods both require information on the channel, hence the need for a feedback from the D2D UE. This feedback generally induces a small overhead especially if the channel state has to be updated on a very regular basis. Nevertheless, this overhead is neglected in the proposed analysis as the channel update is supposed immediate.

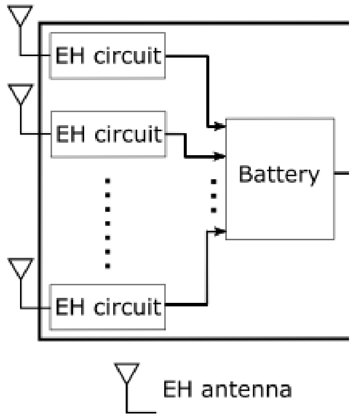

Figure 4.4: New D2D UE architecture (Source:[EH53]).

Isotropic case

Proposition 4.1.5 (Isotropic case under strategy 2)**.** The average harvested power under strategy 2 in the isotropic case supposing Rayleigh fading is given by :

$$\mathbb{E}_{\text{iso},2} = N_{d2d}\epsilon P_{pb}\lambda_{pb}\psi \tag{4.19}$$

Proof. This result is easily obtained using equations 4.18 and 4.6. Also, it comes from the addition of the signals received at each of the D2D UE antennas. As all power fading gains are following the same distribution, it can be shown that:

$$\mathbb{E}\left[\sum_{i=1}^{N_{d2d}} g_i\right] = N_{d2d}\mathbb{E}\left[g\right] = N_{d2d} \tag{4.20}$$

□

Uniform linear array

Under strategy 2, the average harvested power at the D2D UE is exactly the same in the ULA case and the isotropic case. The difference with strategy 1 is that the second term disappears.

Proposition 4.1.6 (ULA case under strategy 2)**.** The average harvested power under strategy 2 in the ULA case supposing Rayleigh fading is given by :

$$\mathbb{E}_{\text{ULA},2} = N_{d2d}\epsilon P_{pb}\lambda_{pb}\psi \tag{4.21}$$

Proof. This result is proven by means of equations 4.18 and 4.20. □

Best antenna

The principle of the best antenna beamforming technique is to benefit from the feedback coming from the D2D UE on the channel state to use only the best antenna. Unlike in the ULA case, the best antenna is then given the entire power while the others are left inactive. The index of the best antenna is determined as follows:

$$i^* = \arg\max_{i=1,\ldots,N_{pb}} \sum_{j=1}^{N_{d2d}} \left|h_{pb_{0,i},U_{0,j}}\right|^2 \tag{4.22}$$

where $h_{pb_{0,i},U_{0,j}}$ is the (i,j)-th element of H corresponding to the channel between the i-th antenna of the nearest PB and the j-th antenna of the considered D2D UE.

As a consequence, using 4.6, the average harvested power in this particular case is given by:

$$H_t = \epsilon P_{pb} \max\left(|pb_0 - U_0|, \nu\right)^{-\gamma} \sum_{j=1}^{N_{d2d}} g_{pb_{0,i^*},U_{0,j}} \tag{4.23}$$

where $g_{pb_{0,i^*},U_{0,j}} = \left|h_{pb_{0,i^*},U_{0,j}}\right|^2$.

The vector c is here given by the i^*-th column of the identity matrix $\mathbb{I}^{N_{pb}\times N_{pb}}$.

Proposition 4.1.7 (BA case under strategy 2)**.** The average harvested power under strategy 2 in the BA case supposing Rayleigh fading is given by :

$$\mathbb{E}_{\text{BA},2} = \epsilon P_{pb}\lambda_{pb}\psi\mathbb{E}\left[\sum_{j=1}^{N_{d2d}} g_{pb_{0,i^*},U_{0,j}}\right]$$

where

$$\mathbb{E}\left[\sum_{j=1}^{N_{d2d}} g_{pb_{0,i^*},U_{0,j}}\right] = \mathbb{E}[X] = \int_0^\infty x \sum_{m=0}^{N_{pb}} (-1)^m \binom{N_{pb}}{m} \frac{-me^{-x}x^{N_{d2d}-1}\left(\frac{\Gamma(N_{d2d},x)}{\Gamma(N_{d2d})}\right)^m}{\Gamma\left(N_{d2d},x\right)} dx \tag{4.24}$$

Proof. The CDF of $X = \sum_{j=1}^{N_{d2d}} g_{pb_{0,i^*},U_{0,j}} = \max_{i=1,\ldots,N_{pb}} \sum_{j=1}^{N_{d2d}} g_{pb_{0,i},U_{0,j}}$ is given by:

$$\begin{aligned} P\left(X < x\right) &\overset{(1)}{=} P\left(\sum_{j=1}^{N_{d2d}} g_{pb_{0,i},U_{0,j}} < x\right)^{N_{pb}} \\ &\overset{(2)}{=} \left(1 - \sum_{n=0}^{N_{d2d}-1} \frac{x^n}{n!}\exp(-x)\right)^{N_{pb}} \\ &\overset{(3)}{=} \sum_{m=0}^{N_{pb}} (-1)^m \binom{N_{pb}}{m} \left(\frac{\Gamma\left(N_{d2d},x\right)}{\Gamma\left(N_{d2d}\right)}\right)^m \end{aligned} \tag{4.25}$$

$$\tag{4.26}$$

where (1) is obtained because the probability that the maximum value is lower than x is equal to the product of the probabilities that each element is separatly lower than x. (2) follows from the distribution of $g_{pb_{0,i},U_{0,j}}$. In fact, it is shown that the sum of N_{d2d} RVs following an exponential distibution with mean μ gives a gamma-distribution $\gamma\left(N_{d2d},\mu\right)$ for which the CDF corresponds to $1-\sum_{n=0}^{N_{d2d}-1}\frac{x^n}{n!}\exp(-x)$ when $\mu = 1$. (3) comes from the properties of the upper incomplete gamma function.

The PDF of X is then found as the derivative of the CDF:

$$f_X(x) = \sum_{m=0}^{N_{pb}} (-1)^m \binom{N_{pb}}{m} \frac{-me^{-x}x^{N_{d2d}-1}\left(\frac{\Gamma(N_{d2d},x)}{\Gamma(N_{d2d})}\right)^m}{\Gamma\left(N_{d2d},x\right)} \tag{4.27}$$

The final result is obtained with the help of equations 4.18 and 4.27. □

Optimal vector

As its name suggests, the optimal vector beamforming technique proposes optimal values for the vector c using the channel state information. The optimal vector is defined as follows:

$$c^* = \arg\max_{c\in\mathbb{C}^{N_{pb}\times 1}} \|Hc\|^2 = \arg\max_{c\in\mathbb{C}^{N_{pb}\times 1}} c^{\mathrm{H}}HH^{\mathrm{H}}c \tag{4.28}$$

It can be demonstrated that the vector c satisfying this condition is the eigenvector correponding to the largest eigenvalue e_{max} of the Wishart matrix HH^{H} [EH53].

Therefore, using 4.6, the average harvested power in this particular case is given by:

$$H_t = \epsilon P_{pb} \max\left(|pb_0 - U_0|, \nu\right)^{-\gamma} e_{max} \tag{4.29}$$

Proposition 4.1.8 (OV case under strategy 2)**.** Let $N_{min} = min\left(N_{pb}, N_{d2d}\right)$. The average harvested power under strategy 2 in the OV case supposing Rayleigh fading is given by :

$$\mathbb{E}_{\mathrm{OV},2} = \epsilon P_{pb} \lambda_{pb} \psi \mathbb{E}\left[e_{max}\right]$$

where

$$\mathbb{E}\left[e_{max}\right] = \mathbb{E}[X] = \int_0^\infty x \frac{\sum_{i=1}^{N_{min}} \sum_{m=\left|N_{pb}-N_{d2d}\right|}^{\left(N_{pb}+N_{d2d}\right)i-2i^2} a_{i,m} e^{-ix} x^m}{\prod_{k=1}^{N_{min}} \left(N_{d2d}-k\right)! \left(N_{pb}-k\right)!} dx \tag{4.30}$$

and $a_{i,m}$ can be identified by means of equation 4.31.

Proof. The PDF of $X = e_{max}$ is given in [Misc64] as follows :

$$\begin{aligned} f_X(x) &\overset{(1)}{=} \frac{\frac{d}{dx}\left(det\left(\Psi(x)\right)\right)}{\prod_{k=1}^{N_{min}} \left(N_{d2d}-k\right)! \left(N_{pb}-k\right)!} \\ &= \frac{\sum_{i=1}^{N_{min}} \sum_{m=\left|N_{pb}-N_{d2d}\right|}^{\left(N_{pb}+N_{d2d}\right)i-2i^2} a_{i,m} e^{-ix} x^m}{\prod_{k=1}^{N_{min}} \left(N_{d2d}-k\right)! \left(N_{pb}-k\right)!} \end{aligned} \tag{4.31}$$

where $\Psi(x) \in \mathbb{R}^{N_{min} \times N_{min}}$ and $\Psi(x)_{ij} = \left(\left|N_{pb} - N_{d2d}\right| + i + j - 2\right)! \sum_{k=0}^{\left|N_{pb}-N_{d2d}\right|+i+j-2} \frac{\exp(-x)x^k}{k!}$. The coefficients $a_{i,m}$ are numerically identified as the coefficient of $e^{-ix}x^m$ when developping (1) and are not shown in this document due to space constraints.

The final result is obtained by combining equations 4.18 and 4.31. □

4.2 Numerical results

The following results were obtained using the parameters in Table 4.1 unless specified otherwise.

The RF-to-DC power conversion efficiency factor was here expressly artificially increased to limit the temporal analysis to a smaller number of time slots. Using such a value makes the harvested powers higher and thus the probability of transmission higher. This choice was made to quickly show the differences between the model and MC simulations in order to validate the model. A smaller and more realistic value of 0.3 is used in the experiences that come after the model validation.

4.2.1 Model validation

Power harvesting from all power beacons

The final results in terms of harvested power for strategy 1 are shown in Figure 4.5. The PB density Λ_{pb} is here varied from 5/km^2 to 1000/km^2.

It can be observed that the harvested powers in the isotropic and ULA cases are pretty similar for a PB density smaller than 100/km^2. This comes from the fact that the main contribution to the harvested power comes in that case comes from the nearest PB. In the ULA case, the available power is shared among the N antennas constituing the array and the received power in the beamforming direction is N

Parameter	Symbol	Value
CC UEs density	Λ_c	50/km^2
PBSs density	Λ_{pb}	50/km^2
D2D UEs density	Λ_d	20/km^2
BSs density	Λ_b	2/km^2
Co-channel CC UEs/D2D UEs/BSs density	$\Lambda_{cc}/\Lambda_{d2d}/\Lambda_{bs}$	1.27/km^2
BSs transmit power	P_{bs}	40W
CC transmit power	P_{cc}	0.1W
D2D threshold transmit power	P_{thres}	0.005W
Pathloss coefficient on D2D and CC links	α	4
Pathloss coefficient on power transfer links	β	2.5
Short-range model parameter	ν	1.1
Max. D2D link distance	R_{max}	0.1km
Power transfer links frequency	f_{pb}	2.45 GHz
DL frequency	f_{DL}	1805 MHz
UL frequency	f_{UL}	1710 MHz
Noise power	W	-130dBm
RF-to-DC power conversion efficiency factor	ϵ	0.8
Rice K factor on power transfer links	K	3

Table 4.1: Simulation parameters.

times the power of one antenna which is exactly equal to the available power. As a consequence, the received powers coming from the nearest PB at the considered D2D UE are exactly the same for both the isotropic and the ULA cases.

As the PB density further increases, the harvested power in the isotropic case becomes more important than the one in the ULA case. In case of high density, the probability to have several close PBs is higher. In the isotropic case, the D2D can harvest from all those close PBs. On the contrary, due to beamforming in the ULA case, the D2D receives only secondary contributions from the PBs that are not the nearest one making the harvested power smaller.

This last discussion makes the isotropic case more interesting when the power transfer is done in an orthogonal band. However, in terms of spectral efficiency, the designers might opt for a situation where power transfer technologies are done in the CC and D2D communications bands. In that particular case, the ULA case becomes more interesting in order to limit the interference inflicted on CC and D2D communications but at the cost of a lower harvested power.

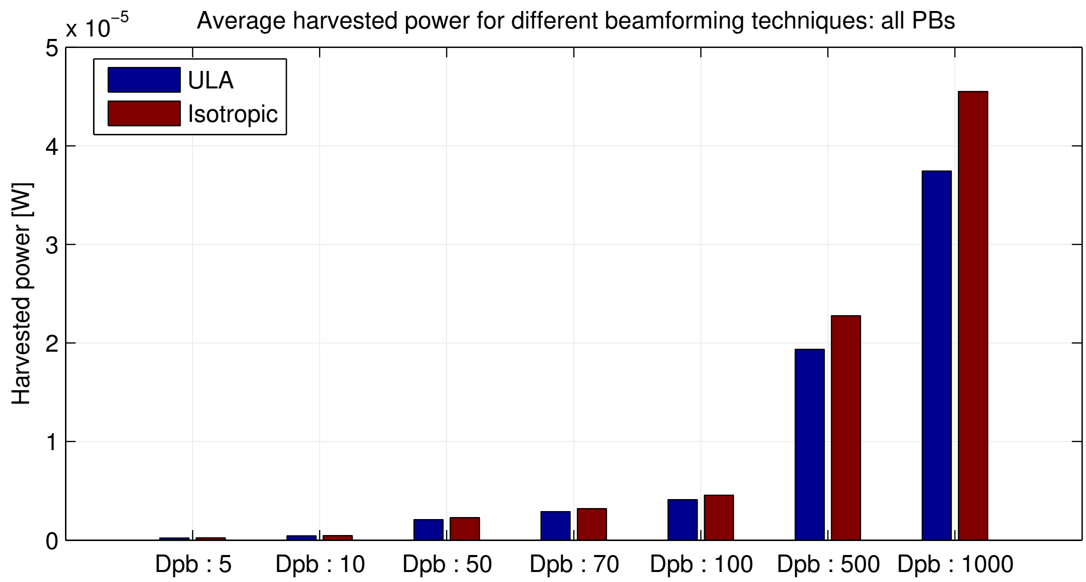

Figure 4.5: Harvested energy for different densities of PBs (Dpb corresponds to Λ_{pb}).

Power harvesting from the nearest power beacon

The final results in terms of harvested power for strategy 2 are shown in Figure 4.6. The PB density is here kept as in Table 4.1. Also, the number of antennas at the PB and at the D2D RX are varied from 1 to 8. Thinking about an higher number of antennas seems unreasonable as the antennas have to match the PB and D2D design dimensions.

Under strategy 2, the ULA and isotropic cases are equivalent in terms of harvested power as explained in the previous section. The OV case is proven to outperform the BA case which outperforms itself the two last cases.

In the BA case, an increase of the number of antennas on both sides (PB and D2D) has always a positive impact on the harvested powers for the considered values. If the number of antennas is increased on the PB side, a more attractive best antenna can potentially be chosen. This effect should fade for a fixed number of antennas at the D2D while increasing the number of antennas at the PB as the probability to find a more attractive antenna will become lower and lower. If the number of antennas is increased on the D2D side, the harvesting capacity of the D2D UE is also increased.

In the OV case, the harvested power is always limited by the minimum number of antennas between the PB and the D2D UE. In fact, choosing $N_{pb} = a$ and $N_{d2d} = b$ or $N_{pb} = b$ and $N_{d2d} = a$ leads to the same harvested power as it is limited by min(a,b).

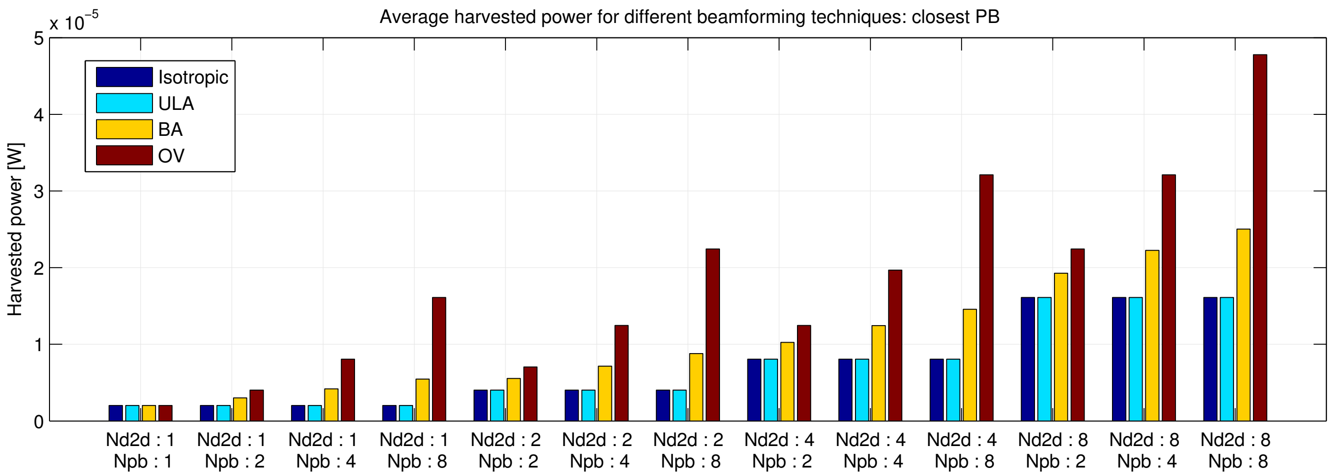

Figure 4.6: Harvested energy for different beamforming techniques as a function of the number of antennas at the PB and at the D2D UE.

Monte Carlo simulations

The final average outage probabilities are respectively shown in Figures 4.7 and 4.8 for CC and D2D communications. The analytical results are proven to be coherent with the numerical results. However, a small difference can be observed for CC communications. This difference will be explained in a future section. Only strategy 1 is analyzed here but similar results are obtained for strategy 2 as the transmission probabilities are small in both cases.

Regarding CC communications, all curves are demonstrated to be confused. More precisely, all curves are very close to the average outage probability without D2D communications. This is explained by a very small probability of transmission in all cases for the current parameters and by a small D2D UE transmit power in case of tranmission.

The same observation can be made for D2D communications except that there is here a difference between case 1 and case 2 as the interference coming from BSs is higher than the interference coming from CC UEs.

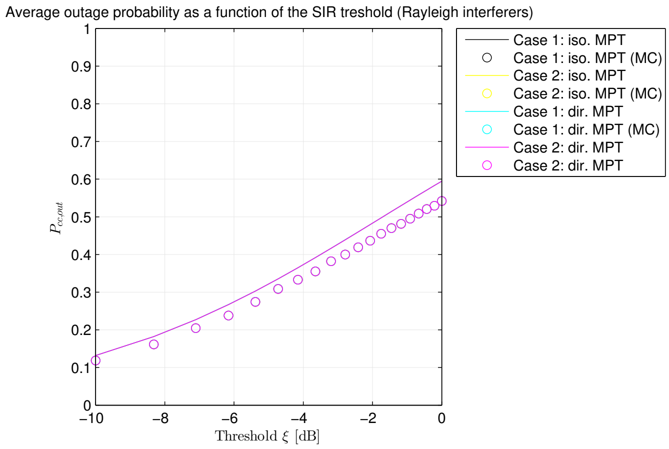

Figure 4.7: Average CC outage probabilities. All curves are here confused.

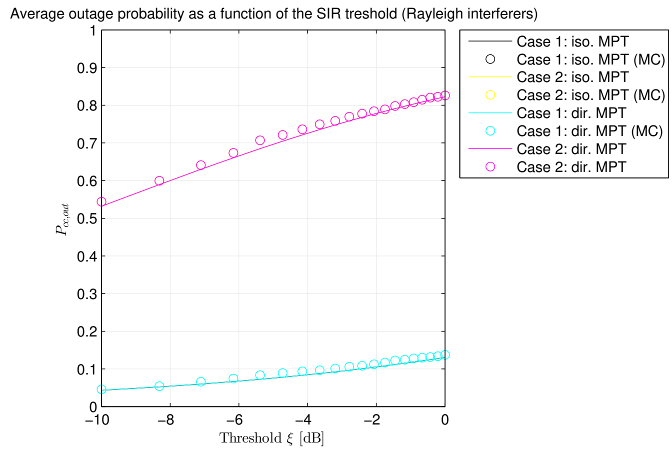

Figure 4.8: Average D2D outage probabilities. The curves for case 1 and case 2 are respectively confused.

4.2.2 Trade-off between the transmission probability and the maximum D2D link distance

This section aims to evaluate the trade-off between the transmission probability and the maximum D2D link distance. As already mentioned, it is assumed from here that ϵ=0,3. Also, two different values for the PBs density will be assumed: 50/km^2 and 100/km^2.

The transmission probabilities for different cases are shown in Figures 4.9, 4.10, 4.11, 4.12 and 4.13. In any case, the transmission probabilities increase when the threshold transmit power decreases.

The benefits of MIMO systems are more and more highlighted as we decrease the threshold probability. In fact, as the harvested powers are very small, a too demanding threshold transmit power results in a very small transmission probability regardless of the beamforming method and the order of the MIMO sytem. Indicatively, using a 1×1 system is proven not to advantage any of the beamforming techniques. When increasing the order of the MIMO system, the different methods induce different curves except for the isotropic and ULA cases that are always confused. The curves are also demonstrated to saturate earlier at 1 as the harvested powers are higher for an higher order MIMO system.

In the following analysis, a good outage probability on D2D communications is considered as 0.3 for a SINR threshold of 16 dB. The maximum D2D link distances in order to respect that last condition are respectively shown in Figures 4.14 and 4.15 for case 1 and case 2.

As a general remark, the interference coming from inter-cell D2D UES is almost negligible. This can be explained by means of two different situations. In the first case, the considered threshold transmit powers are quite low in order to achieve a high transmission probability. In the second case, a higher threshold transmit power is desired at the cost of a lower transmission probability. As a consequence, no difference can be observed between the different studied beamforming methods for different orders of the MIMO system and a general curve representing all cases is depicted instead.

It is demonstrated that decreasing the threshold transmit probability also makes the maximum D2D link distance smaller. This can be explained by the fact that the power on the useful link is decreased making it more vulnerable to the interference coming from CC UEs in case 1 and from BSs in case 2. As a result, in order to achieve an acceptable SINR, the maximum permitted D2D link distance has to be decreased.

For the considered threshold transmit powers, the D2D link can be established on distances varying from 10m to 63m for case 1 and from 2m to 14m for case 2. Those link distances are shown to be quite small especially if a high transmission probability is desired, hence the need for further control mechanisms as presented in section 3.5.4.

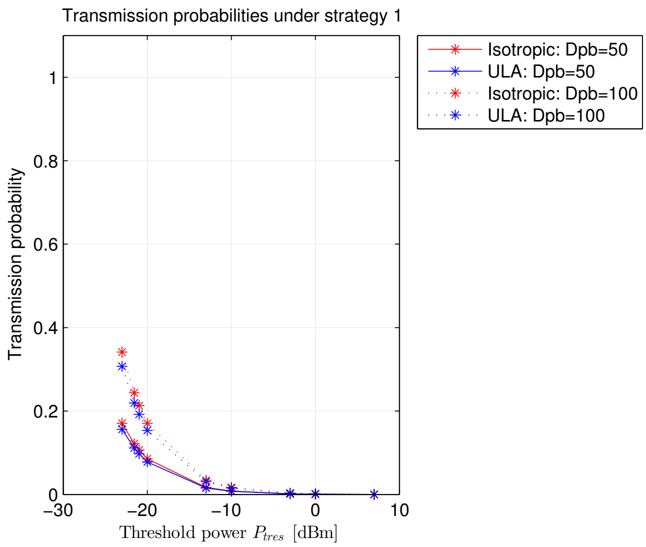

Figure 4.9: Transmission probabilities under strategy 1.

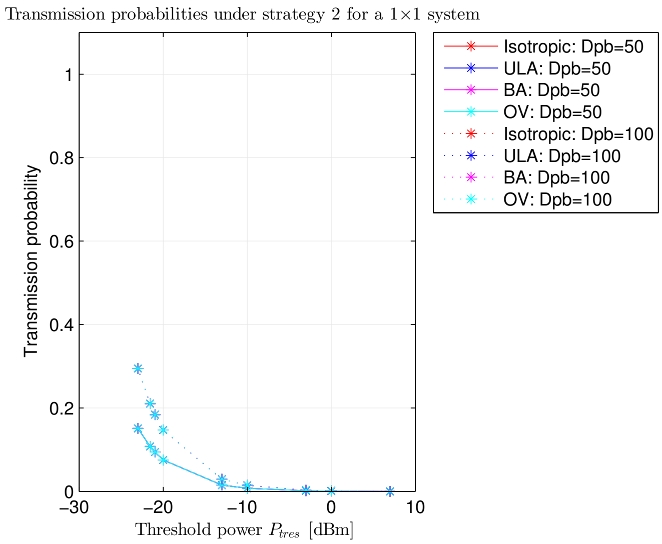

Figure 4.10: Transmission probabilities under strategy 2 for a 1×1 system. All curves are here confused.

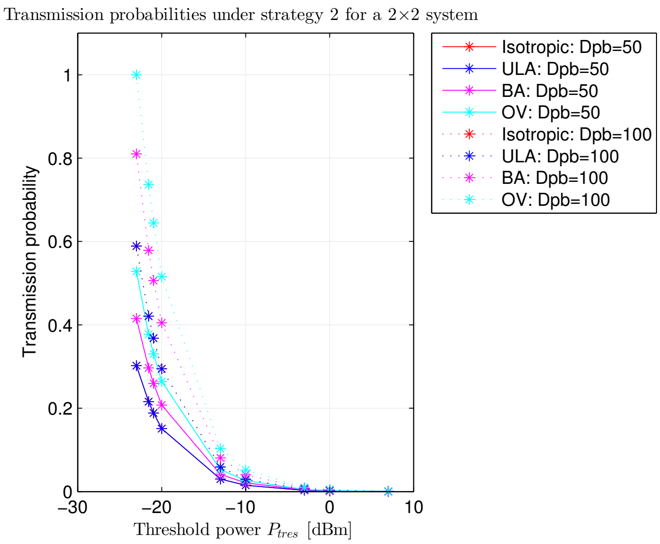

Figure 4.11: Transmission probabilities under strategy 2 for a 2×2 system.

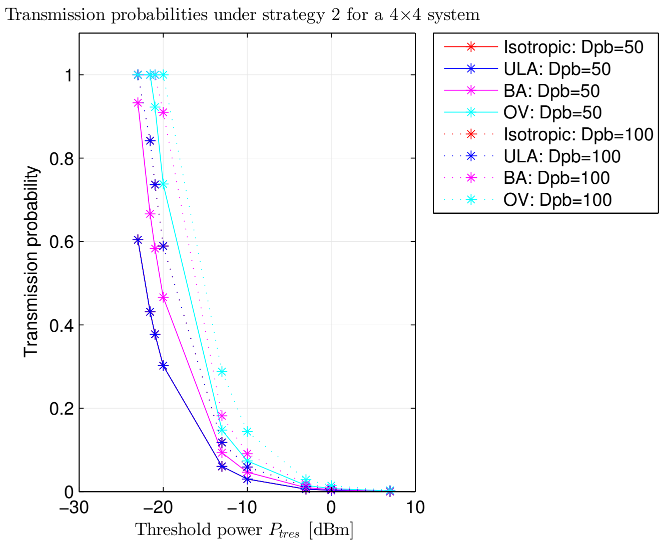

Figure 4.12: Transmission probabilities under strategy 2 for a 4×4 system.

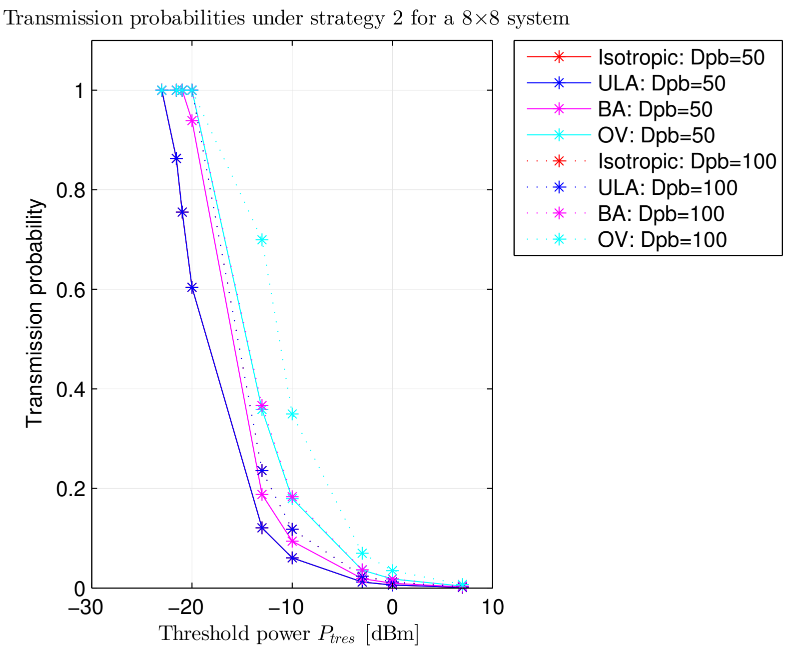

Figure 4.13: Transmission probabilities under strategy 2 for a 8×8 system.

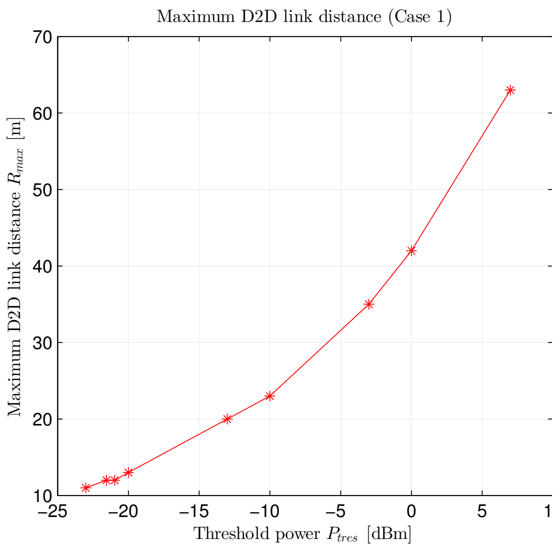

Figure 4.14: Maximum D2D link distance (case 1) for both strategies and for all beamforming techniques.

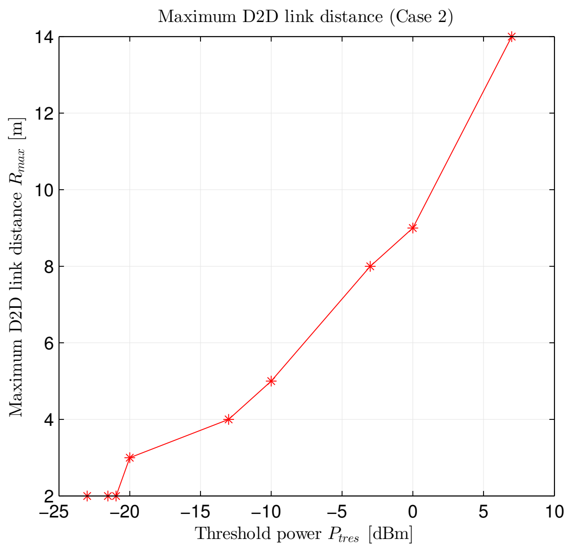

Figure 4.15: Maximum D2D link distance (case 2) for both strategies and for all beamforming techniques.

4.2.3 Model innaccuracies

In this section, a closer look is taken at the model inaccuracies in order to explain the differences between the analytical and numerical results.

To prevent intensive computations, CC UEs and D2D UEs were assumed to have a fixed position all along the temporal analysis. Using such a strategy makes the computation of the harvested powers coming from all PBs at each D2D UE one-shot. Otherwise, they would have had to be computed again at each time slot. But this strategy also creates disparities between D2D UEs in terms of harvested power. In fact, some of them are in a region where the power received from PBs is negligible while others are right next to several PBs. This last observation makes the average harvested power not representative of all UEs as depicted in Figure 4.16 because some UEs artificially increase the value. As a consequence, the transmission probability proposed by the model is generally higher than the real one.

Enabling D2D UEs to move would have made the average harvested powers of each D2D UE more similar and the model would have more closely reflected reality.

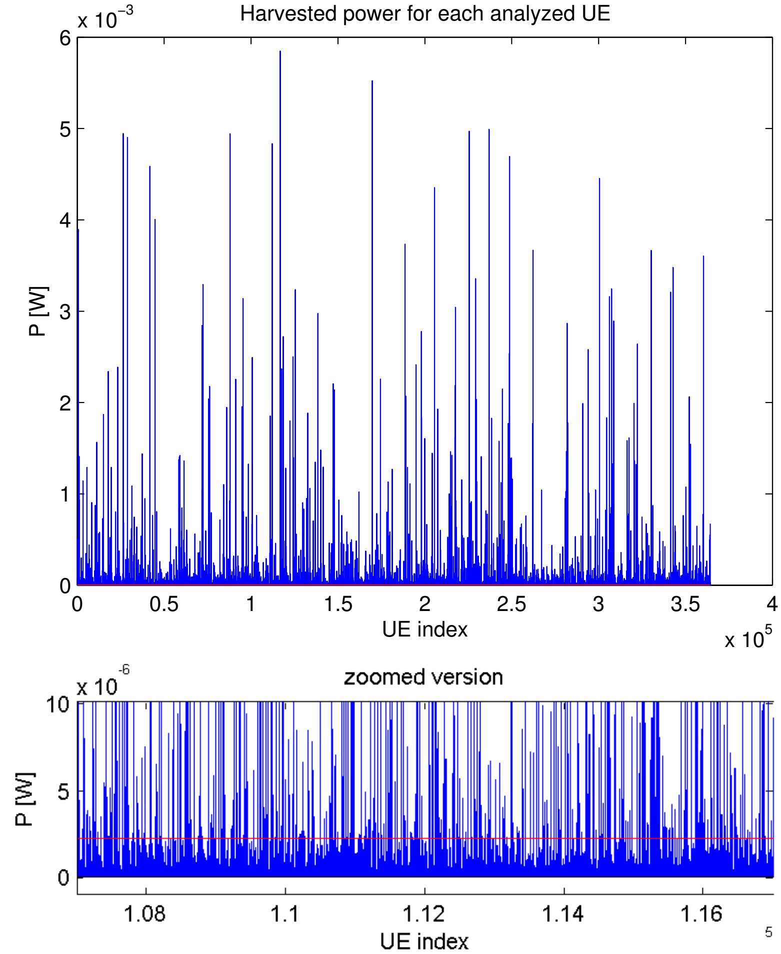

Figure 4.16: Harvested powers of all analyzed D2D UEs. The red line is representing the average harvested power.

Another remark would be to say that infinite capacity batteries are a little bit unreal and that this might thus lead to biased results. However, the D2D UEs are harvesting very low powers. If the transmit threshold power is assumed low, those harvested powers are always below this threshold power and as soon as enough power is harvested, it is directly used for transmission. That way the batteries capacities are regulated thanks to the regular transmissions.

Unfortunately, if the threshold transmit power is lowered to achieve a higher transmission probability, the batteries capacity might increase indefinitely. Also, if a low duty cycle is assumed, the harvested power might not be used as soon as the battery capacity reaches the threshold transmit power. To be able to correctly handle those situations, it would then be preferable to opt for finite battery capacities. This generalization is left for a future work.

4.3 Introduction to another strategy using energy harvesting

Another interesting approach would have been to transmit at each time slot thanks to the power harvested at the previous time slot. Such an approach requires a mathematical expression of the PDF of the harvested power if a mathematical model of the network is to be proposed. As the harvested powers are generally low, this approach might restricts D2D links to very small distances unless PBs are extremely densified.

4.4 Chapter summary

The results obtained in this chapter are concisely summarized in Table 4.2.

Threshold transmit probability	Transmission probability	Maximum D2D link distance
Low	High	Low
High	Low	High

Table 4.2: Trade-off between the transmission probability and the maximum D2D link distance.

In addition, the densification of PBs is only shown to increase the transmission probability. This transmission probability is increasing with the progressive densification of PBs until it saturates at 1. Further densifying PBs might cause trouble as the infinite capacity battery assumption becomes too restrictive. As the harvested powers are very small, the threshold transmit power has to be sufficiently low to achieve an acceptable transmission probability. As a consequence, even if the transmission probability is increased thanks to densification of PBs, the interference caused to CC communications by D2D communications is in this case negligible. The same discussion can be used to evaluate the impact of increasing the PB transmit power, of using MIMO systems and of implementing better beamforming techniques.

Finally, the implementation of better beamforming techniques and the possibility to have multiple antennas at the PB and at the D2D UE are proven to increase the harvested power at each time slot. Thererfore, under a fixed transmission probability, the threshold transmit power can be increased to successfully reach higher distances for D2D links.

Chapter 5

Conclusions

5.1 Summary of contributions

In this master thesis, new SG-based models have been proposed in order to integrate up-and-coming technologies into CC wireless networks.

First of all, the D2D technology has been integrated into a CC wireless network under an underlaid policy as it was done in [D2D45]. Both D2D communications in the UL band and in the DL band have been studied and compared. A new mathematical framework has been established using Rician fading in order to account for strong LOS components on CC and D2D links. A new expression of the Laplace transform for far interferers has particularly been computed. Average outage probabilities formulas have been derived taking into account the added interference caused by the underlaying D2D network. The success of D2D transmissions using the DL band has been proven to be strongly dependent on the BS transmit power. Finally, the average outage probabilities on CC links have been shown to be relatively high, hence the need for additional control mechanisms. Some of them have been already studied while others will be presented in the next section.

Then, the EH technology has been integrated into the already developed D2D wireless network in order to power D2D UEs. Infinite capacity batteries have been assumed at the D2D UE and the MPT technology has been used. A fixed threshold transmit power at the D2D UE has been assumed in order for the D2D UE to be allowed to transmit. This threshold transmit power has been proven to promote either an acceptable transmission probability or a better maximum D2D link distance in order to respect an average outage probability of 0,3. Different beamforming techniques have been compared in terms of harvested power. Also, the possibility to have several antennas on both sides of the power transfer link has been added and its impact on the harvested power has been studied. A mathematical expression for the transmission probability has been proposed for different cases by extending the work done in [EH56].

5.2 Further research directions

5.2.1 Analytical models

Chapter 3

The main drawback of the proposed model has been shown to concern CC communications. The average CC outage probabilities have been proven to be relatively high even with several improvements. Therefore, the presented model could be extended in several directions:

- It could be possible to make the model SIR-based. Under that strategy, a particular CC link would be accepted only if the SIR is above a certain threshold. This should prevent impossible CC links to be permitted but could further increase the mathematical complexity. Assuming the channel is varying sufficiently fast for that particular UE, this strategy only delays the intended communication for the UE to have a good quality of service.

- The D2D technology could be used as a relay to complement bad CC transmissions as presented in [D2D32] for the UL extension and in [D2D33] for the DL extension.

Once this last problem has been tackled, it could be interesting to generalize the model to inter-cell CC communications. A particular challenge is then to derive new PDFs for the link distances.

Regardless of the mathematical complexity, expressions for other metrics of interest could be derived under the studied network setup. In particular, an expression of the average throughput on D2D links seems relatively interesting.

Then, other PPs could be used to model the different network elements as the PPP sometimes fails to represent particular network topologies. It would then be useful to find other ways to account for strong LOS components than Rician fading to limit the initial mathematical complexity.

Also, a general optimization problem regrouping all considered macroparameters could be established and solved under different constraints.

Finally, one of the concerns of the D2D underlaid scheme is certainly power control. Several papers have already proposed approaches to tackle that problem [D2D29, D2D35]. As only a few methods have been presented, it could be of interest to further find new algorithms to better handle the integration of D2D communications into CC networks.

Chapter 4

First, the network could be further generalized to the second power harvesting strategy presented in Section 4.3. As a reminder, this technique supposes that the harvested power at one time slot is directly used at the next time slot. A generalization of the expressions of the power outage probability and the transmission outage probability proposed for one single PB in [EH54] could be extended to both strategies presented in this document. As only upper bounds were computed, deriving closed-form expressions could be of particular interest.

Secondly, the proposed model could be generalized to finite capacity batteries. In this particular case, deriving closed-form expressions represents a big challenge as shown in [EH56].

5.2.2 Beyond the framework of this document

The biggest part of the available literature is generally dedicated to the analysis and optimization of a single service like data transfer, power transfer, etc... However, optimizing each service separately might lead to a rather inneficient use of the network infrastructure. Until now, this has not been considered as a big deal but with the arrival of a whole bunch of new services, the need to set up a more general approach becomes more and more relevant.

To the best of the author's knowledge, such an approach has not been proposed yet. A SG-based model could help us understand the different performance trade-offs for supporting the different services. Also, the establishment of more general performance metrics than the usual ones might be of particular interest.

Bibliography

Stochastic Geometry

[SG1] J. G. Andrews, A. K. Gupta, and H. S. Dhillon. A primer on cellular network analysis using stochastic geometry. *arXiv preprint arXiv:1604.03183*, 2016.

[SG2] Y. J. Chun, S. L. Cotton, H. S. Dhillon, F. J. Lopez-Martinez, J. F. Paris, and S. K. Yoo. A comprehensive analysis of 5g heterogeneous cellular systems operating over $\kappa - \mu$ shadowed fading channels. *IEEE Transactions on Wireless Communications*, 16(11):6995–7010, 2017.

[SG3] H. ElSawy, A. Sultan-Salem, M.-S. Alouini, and M. Z. Win. Modeling and analysis of cellular networks using stochastic geometry: A tutorial. *IEEE Communications Surveys & Tutorials*, 19(1):167–203, 2017.

[SG4] H. M. M. M. Elsawy. Modeling, analysis, and optimization of random wireless networks: Stochastic geometry approach. 2014.

[SG5] M. Haenggi, J.G. Andrews, F. Bacceli, O. Dousse, and Franceschetti. Stochastic geometry and random graphs for the analysis and design of wireless networks. *IEEE Journal on Selected Areas in Communications*, 27(7), Sept. 2009.

[SG6] M. Haenggi, R.K. Ganti, et al. Interference in large wireless networks. *Foundations and Trends® in Networking*, 3(2):127–248, 2009.

[SG7] N. Miyoshi and T. Shirai. Spatial modeling and analysis of cellular networks using the ginibre point process: A tutorial. *IEICE Transactions on Communications*, 99(11):2247–2255, 2016.

[SG8] C. Saha, M. Afshang, and H. S. Dhillon. Poisson cluster process: Bridging the gap between ppp and 3gpp hetnet models. In *Information Theory and Applications Workshop (ITA), 2017*, pages 1–9. IEEE, 2017.

[SG9] S. Wang, W. Guo, and M. D. McDonnell. Distance distributions for real cellular networks. In *Computer Communications Workshops (INFOCOM WKSHPS), 2014 IEEE Conference on*, pages 181–182. IEEE, 2014.

[SG10] S. Wang, W Guo, and T. O'Farrell. Two-tier cellular networks with frequency selective surface. *IEEE International Conference on High Performance Computing and Communication (HPCC)*, pages 740–747, Jun. 2012.

[SG11] C. Wiame. Stochastic geometry-based analysis of wireless communication networks. Master's thesis, Ecole polytechnique de Louvain, 2017.

Device to device

[D2D12] M. Afshang, H. S. Dhillon, and P. H. J. Chong. Coverage and area spectral efficiency of clustered device-to-device networks. In *Global Communications Conference (GLOBECOM), 2015 IEEE*, pages 1–6. IEEE, 2015.

[D2D13] A. Afzal, S. A. R. Zaidi, D. McLernon, and M. Ghogho. On the analysis of device-to-device overlaid cellular networks in the uplink under 3gpp propagation model. In *Wireless Communications and Networking Conference (WCNC), 2016 IEEE*, pages 1–6. IEEE, 2016.

[D2D14] A. Al-Hourani, S. Kandeepan, and A. Jamalipour. Stochastic geometry study on device-to-device communication as a disaster relief solution. *IEEE Transactions on Vehicular Technology*, 65(5):3005–3017, 2016.

[D2D15] K. S. Ali, H. ElSawy, and M.-S. Alouini. Modeling cellular networks with full-duplex d2d communication: A stochastic geometry approach. *IEEE Transactions on Communications*, 64(10):4409–4424, 2016.

[D2D16] A. Altieri, P. Piantanida, L. R. Vega, and C. G. Galarza. On fundamental trade-offs of device-to-device communications in large wireless networks. *IEEE Transactions on Wireless Communications*, 14(9):4958–4971, 2015.

[D2D17] S. Andreev, O. Galinina, A. Pyattaev, K. Johnsson, and Y. Koucheryavy. Analyzing assisted offloading of cellular user sessions onto d2d links in unlicensed bands. *IEEE Journal on Selected Areas in Communications*, 33(1):67–80, 2015.

[D2D18] A. Asadi, Q. Wang, and V. Mancuso. A survey on device-to-device communication in cellular networks. *IEEE Communications Surveys & Tutorials*, 16(4):1801–1819, 2014.

[D2D19] Z. Chen and M. Kountouris. Guard zone based d2d underlaid cellular networks with two-tier dependence. In *Communication Workshop (ICCW), 2015 IEEE International Conference on*, pages 222–227. IEEE, 2015.

[D2D20] Z. Chen and M. Kountouris. Decentralized opportunistic access for d2d underlaid cellular networks. *arXiv preprint arXiv:1607.05543*, 2016.

[D2D21] Z. Chen, N. Pappas, and M. Kountouris. Probabilistic caching in wireless d2d networks: Cache hit optimal versus throughput optimal. *IEEE Communications Letters*, 21(3):584–587, 2017.

[D2D22] Y. J. Chun, S. L. Cotton, H. S. Dhillon, A. Ghrayeb, and M. O. Hasna. A stochastic geometric analysis of device-to-device communications operating over generalized fading channels. *IEEE Transactions on Wireless Communications*, 16(7):4151–4165, 2017.

[D2D23] G. Fodor, E. Dahlman, G. Mildh, S. Parkvall, Norbert Reider, G. Miklos, and Z. Turanyi. Design aspects of network assisted device-to-device communications. *IEEE Communications Magazine*, 50(3), 2012.

[D2D24] G. George, R. K. Mungara, and A. Lozano. Overlaid device-to-device communication in cellular networks. In *Global Communications Conference (GLOBECOM), 2014 IEEE*, pages 3659–3664. IEEE, 2014.

[D2D25] G. George, R. K Mungara, and A. Lozano. An analytical framework for device-to-device communication in cellular networks. *IEEE Transactions on Wireless Communications*, 14(11):6297–6310, 2015.

[D2D26] J. Guo, S. Durrani, X. Zhou, and H. Yanikomeroglu. Device-to-device communication underlaying a finite cellular network region. *IEEE Transactions on Wireless Communications*, 16(1):332–347, 2017.

[D2D27] M. Hicham, N. Abghour, and M. Ouzzif. Device-to-device (d2d) communication under lte-advanced networks. *Int. J. Wirel. Mob. Networks*, 8(1):11–22, 2016.

[D2D28] S. Krishnan and H. S. Dhillon. Distributed caching in device-to-device networks: A stochastic geometry perspective. In *Signals, Systems and Computers, 2015 49th Asilomar Conference on*, pages 1280–1284. IEEE, 2015.

[D2D29] N. Lee, X. Lin, J. G. Andrews, and R. W. Heath. Power control for d2d underlaid cellular networks: Modeling, algorithms, and analysis. *IEEE Journal on Selected Areas in Communications*, 33(1):1–13, 2015.

[D2D30] X. Lin, J. G. Andrews, and A. Ghosh. A comprehensive framework for device-to-device communications in cellular networks. *submitted to IEEE Journal on Selected Areas in Communications*, 2013.

[D2D31] X. Lin, J. G. Andrews, and A. Ghosh. Spectrum sharing for device-to-device communication in cellular networks. *IEEE Transactions on Wireless Communications*, 13(12):6727–6740, 2014.

[D2D32] J. Liu and N. Kato. Device-to-device communication overlaying two-hop multi-channel uplink cellular networks. In *Proceedings of the 16th ACM International Symposium on Mobile Ad Hoc Networking and Computing*, pages 307–316. ACM, 2015.

[D2D33] J. Liu, S. Zhang, H. Nishiyama, N. Kato, and J. Guo. A stochastic geometry analysis of d2d overlaying multi-channel downlink cellular networks. In *Computer Communications (INFOCOM), 2015 IEEE Conference on*, pages 46–54. IEEE, 2015.

[D2D34] D. Marshall, S. Durrani, J. Guo, and N. Yang. Performance comparison of device-to-device mode selection schemes. In *Personal, Indoor, and Mobile Radio Communications (PIMRC), 2015 IEEE 26th Annual International Symposium on*, pages 1536–1541. IEEE, 2015.

[D2D35] A. Memmi, Z. Rezki, and M.-S. Alouini. Power control for d2d underlay cellular networks with imperfect csi. In *Globecom Workshops (GC Wkshps), 2016 IEEE*, pages 1–6. IEEE, 2016.

[D2D36] R. K Mungara, X. Zhang, A. Lozano, and R. W. Heath. Performance evaluation of itlinq and flashlinq for overlaid device-to-device communication. In *Communication Workshop (ICCW), 2015 IEEE International Conference on*, pages 596–601. IEEE, 2015.

[D2D37] M. Naslcheraghi, L. Marandi, and S. A. Ghorashi. A novel device-to-device discovery scheme for underlay cellular networks. In *Electrical Engineering (ICEE), 2017 Iranian Conference on*, pages 2106–2110. IEEE, 2017.

[D2D38] M. Peng, Y. Li, T.Q.S. Quck, and C. Wang. Device-to-device underlaid cellular networks under rician fading channels. *IEEE Transactions on Wireless Communications*, 13(8):4247 – 4259, Aug. 2014.

[D2D39] G. A. Safdar, M. Ur-Rehman, M. Muhammad, M. A. Imran, and R. Tafazolli. Interference mitigation in d2d communication underlaying lte-a network. *IEEE Access*, 4:7967–7987, 2016.

[D2D40] J. F. Schmidt, M. K. Atiq, U. Schilcher, and C. Bettstetter. Underlay device-to-device communications in lte-a: uplink or downlink? In *Personal, Indoor, and Mobile Radio Communications (PIMRC), 2015 IEEE 26th Annual International Symposium on*, pages 1542–1546. IEEE, 2015.

[D2D41] S. Stefanatos, A. G. Gotsis, and A. Alexiou. Analytical assessment of coordinated overlay d2d communications. In *European Wireless 2014; 20th European Wireless Conference; Proceedings of*, pages 1–6. VDE, 2014.

[D2D42] M. Tanha, D. Sajjadi, F. Tong, and J. Pan. Disaster management and response for modern cellular networks using flow-based multi-hop device-to-device communications. In *Vehicular Technology Conference (VTC-Fall), 2016 IEEE 84th*, pages 1–7. IEEE, 2016.

[D2D43] F. Tong, Y. Wan, L. Zheng, J. Pan, and L. Cai. A probabilistic distance-based modeling and analysis for cellular networks with underlaying device-to-device communications. *IEEE Transactions on Wireless Communications*, 16(1):451–463, 2017.

[D2D44] M. Wang and Z. Yan. Security in d2d communications: A review. In *Trustcom/BigDataSE/ISPA, 2015 IEEE*, volume 1, pages 1199–1204. IEEE, 2015.

[D2D45] S. Wang, W Guo, Z. Zhou, and X. Chu. Outage probability for multi-hop d2d communications with shortest path routing. *IEEE Communications Letters*, 19(11):1997 – 2000, Nov. 2015.

[D2D46] L. Wei, R. Hu, Y. Qian, and G. Wu. Enable device-to-device communications underlaying cellular networks: challenges and research aspects. *IEEE Communications Magazine*, 52(6):90–96, 2014.

[D2D47] H. Yuan, W. Guo, and S. Wang. Emergency route selection for d2d cellular communications during an urban terrorist attack. In *Communications Workshops (ICC), 2014 IEEE International Conference on*, pages 237–242. IEEE, 2014.

[D2D48] S. Zhang, J. Liu, N. Kato, H. Ujikawa, and K. Suzuki. Average rate analysis for a d2d overlaying two-tier downlink cellular network. In *Communications (ICC), 2015 IEEE International Conference on*, pages 3376–3381. IEEE, 2015.

[D2D49] Y. Zhang, C.-Y. Wang, and H.-Y. Wei. Incentive compatible mode selection and spectrum partitioning in overlay d2d-enabled network. In *Globecom Workshops (GC Wkshps), 2015 IEEE*, pages 1–6. IEEE, 2015.

Energy harvesting and Energy harvesting-aided D2D communications

[EH50] The true cost of batteries – why energy harvesting is the best power solution for wireless sensors. *EnOcean*, 2015.

[EH51] R. Atat, L. Liu, N. Mastronarde, and Y. Yi. Energy harvesting-based d2d-assisted machine-type communications. *IEEE Transactions on Communications*, 65(3):1289–1302, 2017.

[EH52] W. C. Brown. The history of power transmission by radio waves. *IEEE Transactions on microwave theory and techniques*, 32(9):1230–1242, 1984.

[EH53] T. X. Doan, T. M. Hoang, T. Q. Duong, and H. Q. Ngo. Energy harvesting-based d2d communications in the presence of interference and ambient rf sources. *IEEE Access*, 5:5224–5234, 2017.

[EH54] I. Flint, X. Lu, N. Privault, D. Niyato, and P. Wang. Performance analysis of ambient rf energy harvesting: A stochastic geometry approach. In *Global Communications Conference (GLOBECOM), 2014 IEEE*, pages 1448–1453. IEEE, 2014.

[EH55] K. Huang. Spatial throughput of mobile ad hoc networks powered by energy harvesting. *IEEE Transactions on Information Theory*, 59(11):7597–7612, 2013.

[EH56] K. Huang and V. K.N. Lau. Enabling wireless power transfer in cellular networks: Architecture, modeling and deployment. *IEEE Transactions on Wireless Communications*, 13(2):902–912, 2014.

[EH57] K. Huang and X. Zhou. Cutting the last wires for mobile communications by microwave power transfer. *IEEE Communications Magazine*, 53(6):86–93, 2015.

[EH58] A. Kurs, A. Karalis, R. Moffatt, J. D. Joannopoulos, P. Fisher, and M. Soljacic. Wireless power transfer via strongly coupled magnetic resonances. *science*, 317(5834):83–86, 2007.

[EH59] Y. Liu, L. Wang, S. A. R. Zaidi, M. Elkashlan, and T. Q. Duong. Secure d2d communication in large-scale cognitive cellular networks: A wireless power transfer model. *IEEE Transactions on Communications*, 64(1):329–342, 2016.

[EH60] D. Mishra, S. De, G. C. Alexandropoulos, and D. Krishnaswamy. Energy-aware mode selection for throughput maximization in rf-powered d2d communications. *arXiv preprint arXiv:1709.01755*, 2017.

[EH61] L.-G. Tran, H.-K. Cha, and W.-T. Park. Rf power harvesting: a review on designing methodologies and applications. *Micro and Nano Systems Letters*, 5(1):14, 2017.

[EH62] R. Want. An introduction to rfid technology. *IEEE pervasive computing*, 5(1):25–33, 2006.

[EH63] H. H. Yang, J. Lee, and T. Q.S. Quek. Heterogeneous cellular network with energy harvesting-based d2d communication. *IEEE Transactions on Wireless communications*, 15(2):1406–1419, 2016.

Miscellaneous

[Misc64] P. A. Dighe, R. K. Mallik, and S. S. Jamuar. Analysis of transmit-receive diversity in rayleigh fading. *IEEE Transactions on Communications*, 51(4):694–703, 2003.

[Misc65] easyRF. Antenna array factor calculator. Accessed: 2018-06-29. URL: `http://antennaarraycalculator.blogspot.be/p/help.html`.

[Misc66] Lte Encyclopedia. Lte radio link budgeting and rf planning. Accessed: 2018-06-29. URL: `https://sites.google.com/site/lteencyclopedia/lte-radio-link-budgeting-and-rf-planning`.

[Misc67] A. Jeffrey and D. Zwillinger. *Table of integrals, series, and products.* Academic Press, 2007.

[Misc68] Radio-Electronics.com. Thermal noise calculator formulae equations. Accessed: 2018-06-27. URL: `http://www.radio-electronics.com/info/rf-technology-design/noise/thermal-calculations.php`.

[Misc69] X. Su and K. Chang. Polarized uniform linear array system: beam radiation pattern, beamforming diversity order, and channel capacity. *International Journal of Antennas and Propagation*, 2015, 2015.

[Misc70] S. Sun, T. S. Rappaport, S. Rangan, T. A. Thomas, A. Ghosh, I. Z. Kovacs, I. Rodriguez, O. Koymen, A. Partyka, and J. Jarvelainen. Propagation path loss models for 5g urban micro-and macro-cellular scenarios. In *Vehicular Technology Conference (VTC Spring), 2016 IEEE 83rd*, pages 1–6. IEEE, 2016.

[Misc71] A. D. Wyner. Shannon-theoretic approach to a gaussian cellular multiple-access channel. *IEEE Transactions on Information Theory*, 40(6):1713–1727, 1994.

[Misc72] J. Xu, J. Zhang, and J. G. Andrews. On the accuracy of the wyner model in cellular networks. *IEEE Transactions on Wireless Communications*, 10(9):3098–3109, 2011.

Rue Archimède, 1 bte L6.11.01, 1348 Louvain-la-Neuve www.uclouvain.be/epl